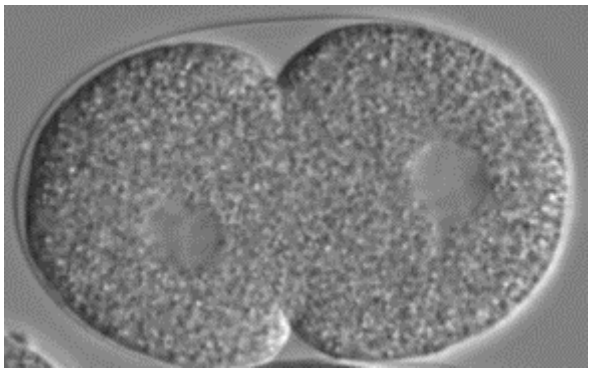

# Functional Characterization of Dynein Cofactors in the One-Cell *C. elegans* Embryo

Patrícia Alexandra Carvalho Simões
Biologia Celular e Molecular
Departamento de Biologia da Faculdade de Ciências do Porto
2014

**Orientador**
Reto Gassmann, Group Leader,
Instituto de Biologia Molecular e Celular, Porto

IBMC
INSTITUTO DE BIOLOGIA MOLECULAR E CELULAR
INSTITUTE FOR MOLECULAR AND CELL BIOLOGY

U.PORTO
FACULDADE DE CIÊNCIAS
UNIVERSIDADE DO PORTO

Todas as correções determinadas pelo júri, e só essas, foram efetuadas.

O Presidente do Júri,

Porto. / /

# Acknowledgements/Agradecimentos

I would like to thank my supervisor, Dr. Reto Gassmann, for giving me the opportunity to develop my dissertation in his laboratory. I thank him for his scientific orientation, support and availability, and for all his words of motivation.

Aos meus colegas de laboratório, do grupo Cell Division Mechanisms e Cytoskeletal Dynamics, por me ajudarem sempre que necessitei. Em particular, agradeço às minhas amigas e colegas, Cláudia Pereira e Elaine Chan. Obrigada pelo companheirismo, ajuda, cafés, jantares, e os estímulos nas alturas de desânimo!

Agradeço à Paula Magalhães. Depois de 3 anos, mantenho a minha opinião: é uma das melhores pessoas que conheço. Sem a sua ajuda e conselhos, não estaria onde estou, e agradeço-lhe muito.

Agradeço muito à Helena Pires. A tua ajuda e amizade foram imprescíndiveis. E o resto tu sabes, mas não convém escrever. Desejo-te toda a sorte e sucesso aí no país das tulipas, para ti e a tua família.

Aos meus pais, pelo incentivo e ajuda na superação de obstáculos. Agradeço também pela grande paciência.

“Para tu” Luis, batatas e um agradecimento muito especial por me apoiares, pela grande paciência e por toda a ajuda e confiança, em tudo e em todos os momentos.

Agradeço em particular às minhas amigas Çagla Sen e Paula Cardoso. Às “meneinas”, Joana Requeijo, Leandra Neto, Ana Matos, Eunice Ferreira, Paula Costa.

Agradeço também à Sara Rocha Joana Gomes, Sofia Costa, Tânia Medeiros, e Francisco Morinha. Desejo-vos tudo de bom, e muito sucesso.

# Abstract

Cytoplasmic dynein is a large microtubule minus-end directed motor protein with multiple functions during cell division. It is known that dynein is subjected to a tight regulation that modulates localization, interaction with cargo and motor activity, but the underlying molecular mechanisms are still unclear. The dynein co-factor Dynactin is an adaptor between Dynein and its cargo, and enhances the processivity of the motor. The dynein co-factor Nuclear Distribution Protein E (NudE) binds Lissencephaly gene 1 (Lis1) and helps to recruit it to dynein. It is thought that the complex formed between Lis1 and NudE regulates the motor activity of dynein to adapt it for movement under high load.

Here, I describe how the Dynactin complex, NudE, and Lis1 contribute to Dynein function throughout the first mitotic division of the *Caernohabditis elegans* embryo. In this study, I confirm that NUD-2 (the *C. elegans* NudE homolog) and LIS-1 (the Lis1 homolog) co-localize with Dynein and Dynactin, except in the Centrosomes. I discover that NUD-2 is a gene that contributes to embryogenesis, shown by embryonic lethality tests that indicate a 10% lethality in animals with a genetic knockout of the *nud-2* gene. In one-cell embryos lacking NUD-2, the migration of the female pronucleus is slower, and the male pronucleus is also affected, travelling less towards the center of the embryo. Lowering LIS-1 levels in animals that lack NUD-2 results in enhanced embryonic lethality and causes a phenotype similar to depletion of dynein, namely a severe defect in pronuclear migration. This synthetic lethal relationship is consistent with a role of NUD-2 in targeting LIS-1 to dynein for transport under high load conditions.

Testing for synthetic lethality between NUD-2 and other dynein co-factors revealed a relationship between NUD-2 with SPDL-1, which is required for dynein recruitment to kinetochores, the structures on chromosomes that interact with the microtubules of the mitotic spindle to drive chromosome segregation. I show that the synthetic lethal interaction between NUD-2 and SPDL-1 is not due to a defect in pronuclear migration. Instead, NUD-2 functions with SPDL-1 at the mitotic kinetochore and is required for the fidelity of chromosome segregation. In embryos lacking NUD-2, kinetochores are defective in establishing stable attachments to microtubules. This results in lagging anaphase chromosome in 65% of one-cell embryos. The resulting aneuploidy is likely to account for the 10% embryonic lethality observed in animals lacking NUD-2. Localization dependency analysis shows that Dynein at the kinetochores is decreased by 3-fold in the absence of NUD-2. My results therefore

suggest that both SPDL-1 and NUD-2 contribute to the recruitment of Dynein to kinetochores, which is essential for the fidelity of chromosome segregation.

I also determined how individual subunits of the Dynactin complex contribute to the first embryonic division. Depletion of the subunits ARP-1, ARP-11 and p62 leads to a dynein-null phenotype, where pronuclear meeting never occurs, ultimately leading to 100% embryonic lethality. By contrast, depleting the dynactin subunits p27 only results in 35% embryonic lethality. Female and male pronuclear migration is not affected in p27-depleted embryos. Instead, the loss-of-function phenotype of p27 is consistent with a specific role at kinetochores.

In summary, my functional characterization of dynein cofactors in the first embryonic division of *C. elegans* mitosis revealed that distinct mitotic functions of dynein are differentially regulated.

## Key Words

Cytoplasmic Dynein; Dynactin; Lissencephaly (Lis1), Nuclear Distribution Protein E (NudE), *Caernohabditis elegans,* Interference RNA, Pointed-end complex, Mitosis, Spindly, Bicaudal D, Rough Deal (Rod), RZZ Complex.

# Sumário

A dineína citoplasmática é uma proteína motora com várias funções durante a divisão celular. É altamente regulada, sendo que esta regulação define a sua localização, interação com a carga e atividade motora, mas os mecanismos subjacentes ainda são desconhecidos. O co-factor dinactina é um adaptador entre a dineína e a carga, e melhora a processabilidade do motor. O co-fator da dineína, a proteína de distribuição nuclear E (NudE), liga-se ao gene da Lissencefalia 1 (Lis1) ajudando a recruitar Lis1 para a dineína. Pensa-se que o complexo formado entre Lis1 e NudE regula a actividade motora da dineína de forma a adaptá-la para aos movimentos sob cargas pesadas.

Nesta dissertação descrevo como o complexo dinactina, NudE e Lis1 contribuem para a função da dineína durante a primeira divisão mitótica do embrião de *Caernohabditis elegans.* Neste estudo, confirmo que NUD-2 (em *C. elegans* o homólogo é NudE) e LIS-1 (o homólogo de Lis1) se colocalizam nos mesmos locais que a dineína e dinactina, excepto nos centrosomas. Descubro que NUD-2 é um gene que contribui para a embriogénese, o que é demonstrado pelos testes de letalidade embrionária que indicam uma letalidade de 10% em animais com o knockout genético do gene *nud-2.* Na primeira divisão mitótica de embriões depletados de NUD-2, a migração do pronúcleo feminino é mais lenta, e a do pronúcleo masculino também é afectada, deslocando-se menos para o centro do embrião. Diminuir os níveis de LIS-1 em animais que não possuam NUD-2 resulta numa acrescida letalidade embrionária, e leva a um fenótipo similar à depleção da dineína, nomeadamente, um defeito grave na migração pronuclear. Esta relação de letalidade sintética é consistente com um papel em que o NUD-2 direcciona LIS-1 para a dineína de forma a transportarem cargas pesadas.

Ao testar a letalidade sintética entre NUD-2 e outros co-factores da dineína revelou uma relação entre NUD-2 e SPDL-1, que é requerido para o recrutamento da dineína para os cinetocóros, as estruturas presentes nos cromosomas, que interagem com os microtúbulos do fuso mitótico de forma a dirigir a segregação cromossómica. Demonstro que a interação sintética letal entre NUD-2 e SPDL-1 não é devida a um defeito na migração pronuclear. Em vez disso, NUD-2 functiona com SPDL-1 nos cinetocóros mitóticos e é requerido para a fidelidade da segregação cromossómica. Em embriões sem NUD-2, os cinetocóros são incapazes de estabelecer ligações estáveis nos microtúbulos. Isto leva a que, na anafase existam cromosomas em atraso em 65% dos embriões da primeira divisão mitótica. A resultante aneuploidia é

provavelmente responsável pela letalidade embrionária de 10% observada em animais sem NUD-2. A análise da dependência da localização mostra que a dineína nos cinetocóros é diminuída cerca de 3 vezes na ausência de NUD-2. Os meus resultados sugerem portanto que tanto SPDL-1 e NUD-2 contribuem para o recrutamento de dineína para os cinetocóros, o que é essencial para a fidelidade da segregação cromossómica.

Também determinei que subunidades individuais do complexo dinactina contribuem para a primeira divisão embrionária. Depletar as subunidades ARP-1, ARP-11, ou p62 leva a um fenótipo semelhante ao sem dineína, onde a junção dos pronúleos nunca ocorre, levando a uma letalidade embrionária de 100%. Contrariamente, depletar a subunidade p27 da dinactina apenas leva a uma letalidade embrionária de 35%. A migração dos pronúcleos feminino e masculino não é afetada em embriões sem p27. Pelo contrário, a perda de fenótipo de p27 é consistente com um papel específico nos cinetocóros.

Concluindo, a minha caracterização funcional dos co-factores da dineína na primeira divisão embrionária da mitose de *C. elegans* revela que as diferentes funções mitóticas da dineína são diferencialmente reguladas.

## Palavras-Chave

Dineína Citoplasmática; Dinactina; Lissencefalia (Lis1), Proteina E de Distribuição Nuclear (NudE), *Caernohabditis elegans,* RNA Interferencia, Complexo Pointed-end, Mitose, Spindly, Bicaudal D, Rough Deal (Rod), Complexo RZZ.

# Table of Contents

# List of Figures

# List of Tables

# List of Abbreviations

| | |
|---|---|
| Actin-related Protein 1 | ARP-1 |
| Adenosine Triphosphate | ATP |
| Anaphase Onset | AO |
| Anaphase Promoting Complex | APC |
| Anaphase Promoting Complex / Cyclosome | APC/C |
| Bicaudal D | Bic-D |
| Bicaudal D homolog in *C. elegans* | BICD-1 |
| *Caenorhabditis elegans* | *C. elegans* |
| Cytoskeleton-Associated Protein-Glycine-Rich | CAP-Gly |
| Deoxyribonucleic Acid | DNA |
| Double-Stranded Ribonucleic Acid | dsRNA |
| Dynamitin | DMN |
| Dynein Heavy Chain | DHC |
| Green Fluorescent Protein | GFP |
| Growth 1 / Gap 1 Phase | G1 |
| Growth 2 / Gap 2 Phase | G2 |
| Heavy Chain | HC |
| Intermediate Chain | IC |
| Kinetochore | KT |
| Kinetochore-Microtubule | kMT |
| Knockout | KO |
| Light Chain | LC |
| Light Intermediate Chain | LIC |
| Lissencephaly 1 homolog in *C. elegans* | LIS1 |
| Messenger Ribonucleic Acid | mRNA |
| Microtubule | MT |
| Microtubule Binding Domain | MTBD |
| Microtubule Organizing Center | MTOC |
| Microtubules-Associated Proteins | MAPs |
| Mitotic Phase | M-Phase |
| Mos1-mediated Single Copy Insertion | MosSCI |
| Nuclear Distribution Protein E | NudE (NUD-2 homologue) |
| Nuclear Envelope Breakdown | NEBD |
| Plus-end Tracking Proteins | + TIPs |

| | |
|---|---|
| Polo-like kinase 1 | Plk1 |
| Polymerase Chain Reaction | PCR |
| Pronuclear Meeting | PM |
| Ribonucleic Acid | RNA |
| Ribonucleic Acid Interference | RNAi |
| Rod / Zwilch / ZW10 Complex | RZZ Complex |
| Rough Deal (ROD) homolog in *C. elegans* | ROD-1 |
| Single-Stranded Ribonucleic Acid | ssRNA |
| Spindle Assembly Checkpoint | SAC |
| Spindly homolog in *C. elegans* | SPDL-1 |
| Synthesis Phase | S |
| WD Repeat | Beta-Transducin Repeat |
| Wild-Type | WT |

# Introduction

## 1. General Introduction

### 1.1. Cell Division

The cell cycle is a series of events that lead to the division and duplication of the cells. In multicellular organisms, somatic cell division occurs in two distinct phases: interphase, during which the cell grows and replicates its DNA, followed by mitosis in which the cell divides to produce two daughter cells (**Figure 1**).

Interphase consists of 3 phases; Gap phase 1 (G1), S-phase and Gap phase 2 (G2). Both G phases ensure that the cell is in favorable conditions to undergo division, gathering nutrients and checking for replication errors. The cell can pause its progress and enter a resting state known as G0 (G zero), where it can remain for years before resuming proliferation. During S phase, DNA is replicated to produce exactly two identical sets of chromosomes, and by the end of S phase, all of the chromosomes have been replicated. After DNA replication, the chromosomes consist of pairs of sister chromatids held together by complexes of proteins known as cohesins [1]. The components responsible for induction of these phases are the Cyclin-dependent protein kinases (Cdks), and their regulatory subunits called Cyclins. Different Cyclins are produced in each stage of the cell cycle, resulting in the formation of a series of Cyclin-Cdk complexes that regulate progression through each stage. The regulation of Cdks is one of the ways checkpoints work (which I will describe further down).

In interphase the G2 stage of interphase precedes the beginning of mitosis and follows chromosomal DNA replication during the S phase. The chromosomes (each containing a sister chromatid) are still dispersed and not visible as distinct structures. During interphase, the centrioles are replicated, forming small daughter centrioles. Mitosis comprises two distinct stages: nuclear division, also called mitosis, and cytoplasmic division or cytokinesis. Together, they define the M-phase. Mitosis is divided into five consecutive phases: prophase, prometaphase, metaphase, anaphase, and telophase. Then, in early prophase the centrosomes, each with a daughter centriole, begin moving toward opposite poles of the cell. The chromosomes can be seen as long threads, and the nuclear membrane begins to disaggregate into small vesicles. During middle and late prophase chromosome condensation is completed; each visible chromosome structure is composed of two chromatids held together at their centromeres – a physical structure that mediates and supports the interaction between the microtubules of the mitotic spindle and the chromosomes. The microtubular spindle fibers begin to radiate from the regions just adjacent to the centrosomes, which are moving closer to their poles. Some spindle fibers reach from

pole to pole; most go to chromatids and attach at kinetochores. Then, at pro-metaphase the chromosomes move towards the equator of the cell, where they become aligned in the equatorial plane (metaphase). The sister chromatids have not yet separated. After metaphase, anaphase follows. Here, the two sister chromatids separate into independent chromosomes. Each contains a centromere that is linked by a spindle fiber to one pole, to which it moves. Simultaneously, the cell elongates, as do the pole-to-pole spindles. Cytokinesis begins as the cleavage furrow starts to form. The last phase of mitosis is telophase, where new nuclear membranes form around the daughter nuclei; the chromosomes uncoil and become less distinct; and the nucleolus becomes visible again. Cytokinesis is nearly complete, and the spindle disappears as the microtubules and other fibers depolymerize. Throughout mitosis the "daughter" centriole at each pole grows, so that by telophase each of the emerging daughter cells has two full-length centrioles. Upon the completion of cytokinesis, each daughter cell enters the G1 phase of the cell cycle and proceeds again around the cycle.

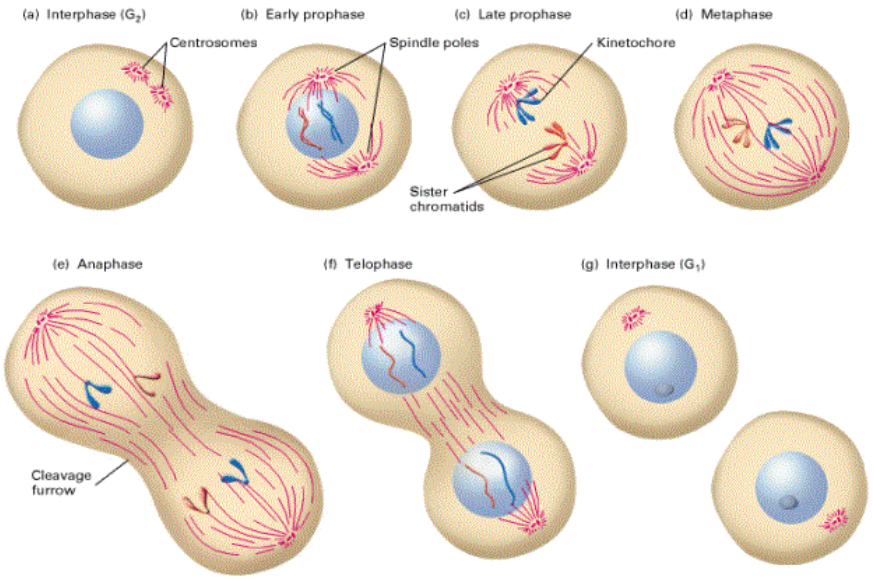


**Figure 1:** The phases of the cell cycle**:** (a) Interphase, (b) Early prophase, (c) Middle and late prophase; (d) Metaphase, (e) Anaphase, (f) Telophase. Upon the completion of cytokinesis, each daughter cell enters the G1 phase. Adapted from [88].

Another strategy that ensures the fidelity of chromosome segregation is the construction of a physical structure on the centromeres. This proteinaceous structure is known as kinetochore. The kinetochore forms in eukaryotes, assembles on the centromere and links the chromosome to microtubule polymers from the mitotic spindle during mitosis. If its formation fails, chromosomes are not able to congress to the spindle equator and aberrant segregation occurs. Extended metaphase delay is also thought to be an outcome of uncoordinated loss of chromatin cohesion [2].

Therefore, the centromere plays an important role in cell cycle as it ensures that kinetochores assembles only in one single site.

### 1.2. The Spindle and the Spindle Checkpoint in Mitosis

To ensure the fidelity of chromosome segregation the spindle assembly checkpoint (SAC) mechanism works through the inhibition of APC/C (anaphase promoting complex/cyclosome) in order to delay the metaphase-anaphase transition. This mechanism is initiated in the presence of unattached chromosomes and therefore can prevent abnormal chromosome segregation. The mitotic spindle is a bipolar, self-organizing microtubule-based machine that uses energy liberated from nucleotide hydrolysis to segregate sister chromatids accurately into the daughter cells during cell division. This critical distribution of the genetic material takes place during anaphase of mitosis, when sister chromatids separate and move to opposite poles of the spindle.

To congress to the spindle equator, a chromosome must biorient, attach to spindle microtubule with each kinetochore interacting with microtubules derived from one of the two spindle poles. Once near the spindle pole the kinetochore captures multiple microtubules plus-ends and builds a kinetochore fiber. These monooriented chromosomes are positioned with their kinetochores pulled away from the spindle pole and with their arms pushed away from the pole and oscillate towards and away from their attached pole. During these oscillations, changes in kinetochores fiber length coincide with chromosome movement toward and away from the spindle pole. Eventually, a microtubule from the opposite pole will contact the unattached sister kinetochore establishing biorientation. The newly bioriented chromosome then moves in a directed manner to the spindle equator. This orients the sister chromatids towards opposite poles and guarantees the equal segregation of genetic material (**Figure 2**).

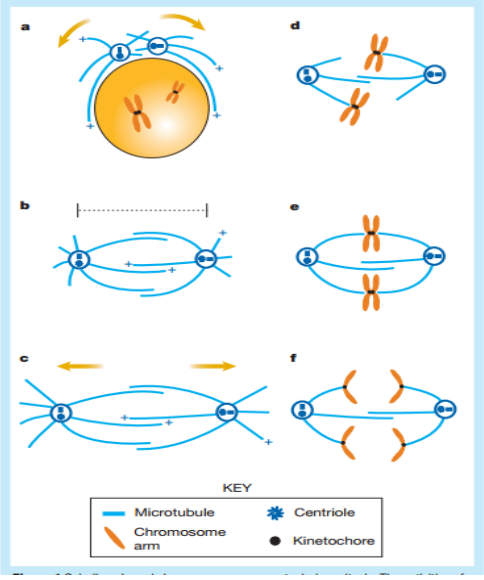


**Figure 2:** Spindle pole and chromosome movements during mitosis. The activities of microtubules and their associated motors are responsible for the sequence of movements that underlie mitosis. Early in mitosis (prophase and prometaphase) the bipolar spindle assembles (a) and condensed chromosomes are captured by spindle microtubules and congress at the spindle equator (d) By metaphase, the spindle consists of two partially interdigitating arrays of MTs emanating from the duplicated centrosomes that form the two spindle poles (b). Chromosomes lie on the equator with pairs of identical sister chromatids facing opposite spindle poles (e).Chromatid segregation involves both the movement of sister chromatids to opposite spindle poles (f; anaphase A) and the elongation of the spindle itself (c; anaphase B). Mechanistically it is convenient to think of these events in terms of spindle assembly, maintenance and elongation (left), and chromosome capture, congression and segregation (right). Adapted from [84].

Chromosome movement proceeds by two distinct mechanisms, referred to as anaphase A and anaphase B, which involve different types of spindle microtubules and associated motor proteins. Anaphase A consists of the movement of chromosomes toward the spindle poles along the KT-MT, which shorten as chromosome movement proceeds. This type of chromosome movement appears to be driven principally by kinetochores-associated motor proteins that translocate chromosomes along the spindle microtubules in the minus-end direction, toward the centrosomes.

Acquiring bipolar attachments for every chromosome can become a prolonged process, which makes prometaphase one of the longest stages of mitosis. However, the spindle checkpoint ensures that the cell cycle will not progress to anaphase until all chromosomes attain appropriate bipolar attachments [3]. Errors in chromosome segregation are linked to the development of human cancers [4] and occur more frequently in cancer cells that non-cancer cells. Regulatory proteins at the kinetochore safeguard against erroneous segregation, and hence, increase the fidelity of mitosis, in two ways: first, attachments on bioriented kinetochore pairs are selectively stabilized, while erroneous attachment configurations are destabilized and eliminated, allowing for another opportunity for biorientation; second, unattached kinetochores are the primary signal to launch the spindle assembly checkpoint (SAC), a cell cycle surveillance pathway that delays exit from mitosis (**Figure 3**).

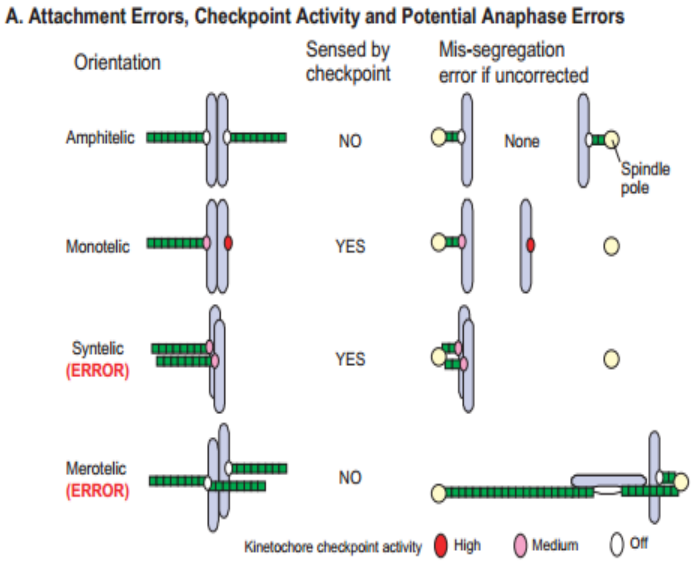


**Figure 3**: Checkpoint controls (also known as surveillance mechanisms) ensure the dependency of cell-cycle transitions on the completion of earlier events. They consist of three distinct sets of functions: sensors (which look out for defects and emit a signal); signal-transduction cascades (checkpoint signals need to be transmitted throughout the nucleus or cell); and effectors (a target is regulated to delay cell-cycle progression) (Adapted from [85]).

### 1.3. Kinetochores Contribution for Chromosome Segregation

In eukaryotes, chromosome segregation during cell division is facilitated by the kinetochore, an assembly of proteins built on centromeric DNA. Kinetochores form on the surface of the chromosome around the time of nuclear envelope breakdown [5]. At metaphase, chromosomes appear as pairs of sister chromatids linked together only at major constriction or centromere. They align along the metaphase plate and are attached to spindle microtubules by kinetochores. The kinetochores attach chromosomes to spindle microtubules modulates the stability of these attachments, and relays MT-binding status to the spindle assemble checkpoint.

The kinetochore is composed of several layers that were first observed by conventional fixation and staining methods for electron microscopy [5]. Innermost is an inner plate, a chromatin structure containing nucleosomes with at least one specialized histone, auxiliary proteins and DNA. The vertebrate kinetochore is composed by the inner plate, the outer plate and the fibrous corona. The inner kinetochore normally forms on highly repetitive DNA sequence and assembles into a specialized form of chromatin that persists throughout the cell cycle. The outer kinetochore is a proteinaceous structure with many dynamic components that assembles and functions only during mitosis. The outer plate of vertebrate kinetochores has about 20 end-on attachment sites for the plus-ends of KT-MT, while the outer plate of budding yeast has only one end-one attachment site. The outermost regions of the kinetochore form a fibrous corona that can be visualized by conventional electron microscopy, and usually only in the absence of microtubules.

Eukaryotes can be divided into two groups based on the architecture of their mitotic chromosomes. Monocentric organisms assemble kinetochores on a single localized chromosomal site defined by the presence of dedicated centromeric chromatin. In contrast, holocentric organisms, including *C. elegans*, assemble diffuse kinetochores along the entire poleward face of each sister chromatid (**Figure 4**). Despite differences in the extent of the chromosomal length occupied by the kinetochore, the molecular composition of kinetochores in *C. elegans* and monocentric organisms is very similar.

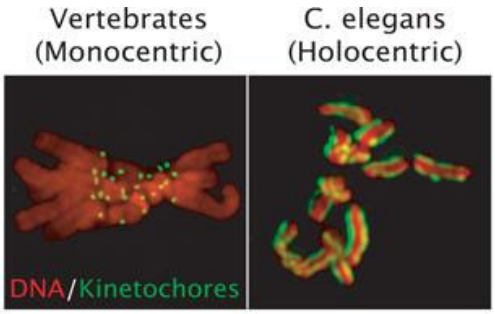


**Figure 4**: Kinetochores in monocentric and in holocentric organisms. Adapted from [86].

### 1.4. Centrosomes Importance for Microtubule Nucleation

Centrosomes are responsible for microtubule nucleation and act as microtubule organizing centers [3]. Each spindle pole contains a centrosome and they dictate the number and orientation of microtubules in the spindle. During the G1 phase of the cell cycle, each cell contains a single centrosome, which acts as the sole microtubule organizing center by nucleating microtubules. Centrosomes duplicate along with the genomic DNA during S phase so that cells enter G2 and subsequent mitosis, with two functional centrosomes [3].

The centrosome is generally positioned at the cell center. The central positioning of the centrosome is critical for proper microtubules-dependent cellular activities such as cell division and organelle distribution [6]. Centrosome centration is an active process in which centrosomes move toward the cell center. In many species, the centrosomes associated with the male pronucleus migrate from the cell periphery toward the cell center. Centrosome centration is achieved by forces that act through the microtubules [7].

Thus, two modifications of microtubule behavior in animal cells are critical to spindle assembly, and both occur at or just prior to the onset of mitosis. Microtubule organization shifts from a single microtubules organizing center in interphase to two microtubule organizing center in mitosis, and the stable interphase microtubule population is replaced by an unstable, highly dynamic microtubules population. Two microtubule-dependent forces, namely, the pushing force and pulling force, are thought to position the centrosome to the cell center. The plus-ends of the growing microtubules can push the cell cortex to move the centrosome away from the cortex. The major driving force for centrosome centration in animal cells is microtubule pulling forces through the action of a motor protein called cytoplasmic dynein [8], which I will explain in detail further down.

### 1.5. Microtubules Role in Mitosis

Microtubules are metastable polymers of α and β-tubulin that switch between phases of growth and shrinkage, a phenomenon known as “dynamic instability” [9]. Microtubules are regulated so that their plus-ends grow from centrosomes towards the cell cortex and reside there briefly before undergoing catastrophe and shrinkage through plus-end depolymerization (**Figure 5**).

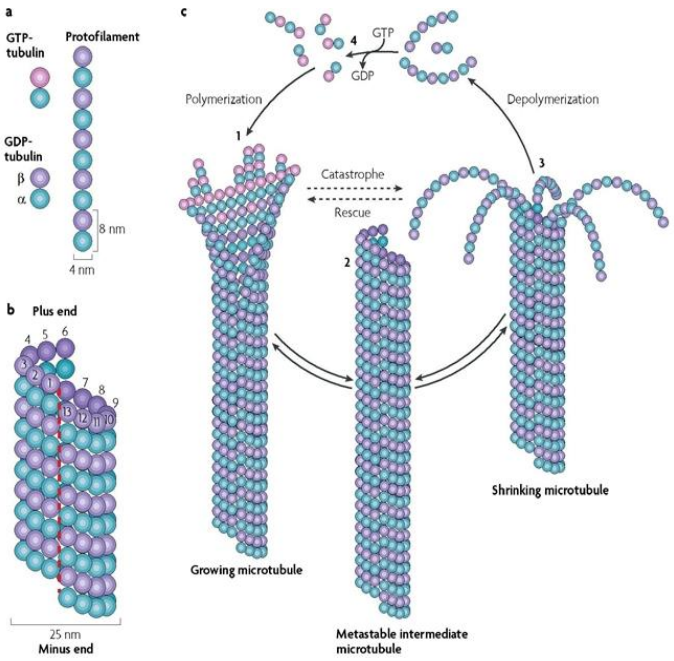


**Figure 5***:* Microtubules are composed of stable α/β-tubulin heterodimers that are aligned in a polar head-to-tail fashion to form protofilaments (a). The cylindrical and helical microtubule wall typically comprises 13 parallel protofilaments in vivo (b). The helical pitch in combination with the longitudinal repeat between α/β-tubulin subunits along a protofilament generates the lattice seam (red dashed line). Assembly–polymerization and disassembly–depolymerization of microtubule (c) is driven by the binding, hydrolysis and exchange of a guanine nucleotide on the β-tubulin monomer. GTP hydrolysis is not required for microtubule assembly per se but is necessary for switching between catastrophe and rescue. Polymerization is typically initiated from a pool of GTP-loaded tubulin subunits (c-1). Growing microtubule ends fluctuate between slightly bent and straight protofilament sheets. GTP hydrolysis and release of inorganic phosphate occurs shortly after incorporation and is promoted by burial and locking of the partially exposed nucleotide as a result of the head-to-tail assembly of dimers. Growing microtubules sheets are believed to maintain a 'cap' of tubulin-GTP subunits to stabilize the straight tubulin conformation within the microtubule lattice. Closure of the terminal sheet structure generates a metastable, blunt-ended microtubule intermediate (c-2), which might pause, undergo further growth or switch to the depolymerization phase. A shrinking microtubule is characterized by fountain-like arrays of ring and spiral protofilament structures (c-3). This conformational change, which is presumably directed by tubulin-GDP, may destabilize lateral contacts between adjacent protofilaments. The polymerization–depolymerization cycle is completed by exchanging GDP of the disassembly products with GTP (c-4). Adapted from [10].

Some chromosomes biorient immediately upon nuclear envelope breakdown and oscillate, but do not tend to stray far from the spindle midzone [11]. The referred minus-end-directed microtubule motor cytoplasmic dynein is thought to capture and pull on microtubule plus-ends at the cortex to influence the spindle positioning and function.

There are three different classes of microtubules within the spindle (**Figure 6**), defined by the position of the microtubule plus-end. The first class is KT-MTs, that extent from the spindle pole to the chromosome, where they contact kinetochores either laterally or with the plus-end embedded directly in the kinetochore disk [3]. The second class of spindle microtubules is astral microtubules. These emanate from the spindle pole and extent away from the cell equator toward the cell periphery. The plus-ends of astral microtubules interact with the cell cortex. This interaction is important for both the positioning of the spindle in the middle of the cell, and in determining the location of the cleavage furrow during cytokinesis [3]. The third class of microtubules in the spindle is interpolar microtubules, which extent from one spindle pole into the central spindle toward the other spindle pole [3].

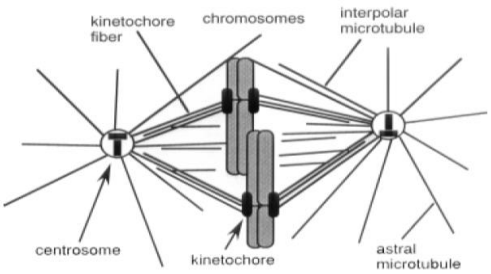


**Figure 6:** Mitotic spindle organization during metaphase. Diagram of a metaphase spindle. Key structural components include centrosomes, chromosomes, kinetochores, astral microtubules, interpolar microtubules, and KT-MTs. Adapted from [3].

The accurate segregation of chromosomes during mitosis and meiosis is essential to ensure the propagation of cells and species. Segregation errors during meiosis lead directly to birth defects, and segregation errors during mitosis in somatic cells contribute to the development and progression of cancer. Thus, the accurate segregation of the genetic material is fundamental to life.

### 1.6. Microtubules and Motor Proteins

All cells are able to perform essential intracellular motility processes. Several mechanisms have evolved to generate the mechanical forces that are required to drive biological motility. A particularly successful and ubiquitous mechanism of biological force production utilizes mechanochemical enzymes – motor proteins. These convert chemical energy, typically in the form of adenosine triphosphate (ATP), into mechanical force. Many cellular and subcellular movements of eukaryotic cells are generated by motor proteins that act upon rigid cytoskeletal fibers. Eukaryotic cells use motor proteins that move along cytoskeletal polymers to transport various intracellular cargos, including membranous organelles, protein complexes and mRNAs.

There are three classes of cytoskeletal motors: myosins, kinesins and dyneins. Motors of the myosin family act upon actin filaments to generate cell surface contractions and other morphological changes, vesicle motility, cytoplasmic streaming, and muscle cell contraction. Members of the dynein and kinesin microtubule-based motor families move vesicles and organelles within cells, cause the beating of flagella and cilia, and act within the mitotic and meiotic spindles to segregate replicated chromosomes to progeny cells. Mitotic motors use at least three distinct mechanisms: cross bridging and sliding microtubules relative to adjacent microtubules or others structures; transporting specific mitotic cargoes along the surface lattice of spindle microtubules; and regulating microtubule assembly dynamics and coupling movement to microtubule growth and shrinkage. In addition, analyses of the functional inter-relationships between multiple mitotic motors have revealed that specific mitotic

movements are not driven by individual motors but, instead, results from shifts in a dynamic balance of complementary and antagonistic forces generated by multiple motors functioning cooperatively.

All of these referred motors can be recognized by the presence of a unique and conserved amino acid sequence that forms the ATP-binding and force producing domain of the molecule. One of the major roles of microtubules is to transport membrane vesicles and organelles through the cytoplasm of eukaryotic cells.

Because microtubules are usually oriented with their minus-end anchored in the centrosome and their plus-end extending toward the cell periphery, different members of the kinesin and dynein families are thought to transport vesicles and organelles in opposite directions through the cytoplasm (**Figure 7**) [12].

Conventional kinesin and other plus-end-directed members of the kinesin family carry their cargo toward the cell periphery, whereas cytoplasmic dyneins and minus-end-directed members of the kinesin family transport materials toward the center of the cell. In addition to transporting membrane vesicles in the endocytic and secretory pathways, microtubules and associated motor proteins position membrane-enclosed organelles (such as the endoplasmic reticulum, Golgi apparatus, lysosomes, and mitochondria) within the cell.

Molecular genetic techniques have revealed novel motor proteins more quickly than our ability to determine their functions. It is therefore not surprising that defects in motor-dependent transport are associated with a large range of diseases, including neurodegeneration, tumorigenesis and developmental defects.

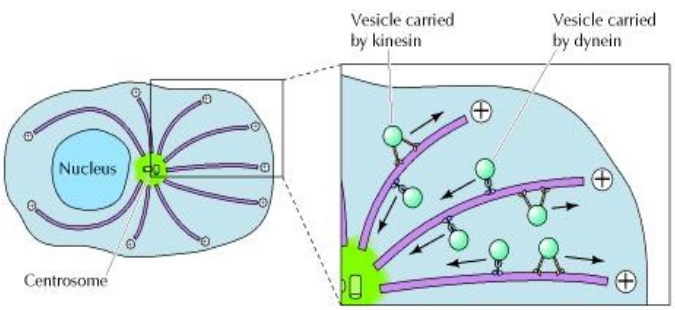


**Figure 7**: Schematic of dynein and kinesin transport of vesicles and organelles in opposite directions through the cytoplasm. Adapted from [12].

# 2. The Motor Protein Dynein

All dyneins discovered to date move towards the microtubule minus-ends, which in most cells are collected into the microtubule organizing center (MTOC) near the nucleus. Kinesin and dynein, the prototypes of microtubule motor proteins, move along microtubules in opposite directions—kinesin mostly moves toward the plus-end and dynein toward the minus-end.

Dynein was originally identified 50 years ago as an ATPase in *Tetrahymena pyriformis* cilia [13], dynein was named by Gibbons and Rowe after the unit of force, the dyne [14]. A cytoplasmic form of dynein was subsequently isolated from brain tissue [15] and shown to drive intracellular transport towards the minus-ends of microtubules [16]. The cytoplasmic dynein 1 heavy chain (which is encoded by DYNC1H1 in humans) is used for almost all of the minus-end-directed transport in the cytoplasm of most eukaryotic cells. Cytoplasmic dynein 2 (encoded by DYNC2H1 in humans) has a specialized role in transporting material along motile and sensory cilia and flagella. This dissertation will focus on Cytoplasmic Dynein 1, and will be mentioned as “dynein”.

Given that dyneins and kinesins both move along microtubules, one might have expected their mechanisms of motility to have more in common with one another than with the actin-based motor, myosin. Nevertheless, crystal structures of myosin and kinesin revealed that – despite moving on different cytoskeletal polymers – these motors share a G protein-related fold and similarities in their core mechanisms [17].

Dynein is a motor that can take μm-scale movements along the microtubules without dissociating [18]. Dynein moves by alternating steps of the dynein heads, a mechanism similar to that of kinesin. This model implies coordination between the two heads, such that one remains bound while the other one moves forward. This stepping behavior of dynein is more variable than that of kinesin, which takes invariant 8 nm-long steps towards the microtubule plus-end. Dynein predominantly takes 8 nm-long steps towards the minus-end, but occasionally takes steps of up to 32 nm, or one, or a few steps backwards towards the plus-ends [18,19]. Dynein can also take steps sideways to an adjacent protofilament [20].

Dynein is currently at the frontier of cell motility research at the molecular level, as its mechanism of movement is much less understood than that of kinesin and myosin. Dyneins belong to the AAA+ superfamily (ATPases associated with diverse activities) [21]. Conventional AAA+ ATPases function as hexameric rings that unfold proteins, dismantle DNA and RNA duplexes and pry apart macromolecular complexes and aggregates [21].

Dynein has a relative molecular mass of 1200 K, composed of six subunits: two copies of dynein heavy chain, dynein intermediate chain, dynein light intermediate chain, and two of each of the three dynein light chains (**Figure 8**). Dynein heavy chain is approximately 500 kDa in size and consists of two distinct domains, the motor domain and the stem (also known as the tail). The motor domain contains six AAA family ATPase units that power dynein's functions and a "stalk" region through which dynein directly binds microtubules. Although most AAA+ ATPases self-assemble into and function as hexameric rings, dynein is unusual in that its six AAA modules are linked in a single polypeptide and are not identical. The AAA domains, along with a coiled-coil extension containing the microtubule -binding domain, form the carboxy-terminal head domain of dynein. The amino-terminal tail of the cytoplasmic dynein heavy chain is involved in its homodimerization and acts as a scaffold for the assembly of five different non-catalytic subunits to form the cytoplasmic dynein complex.

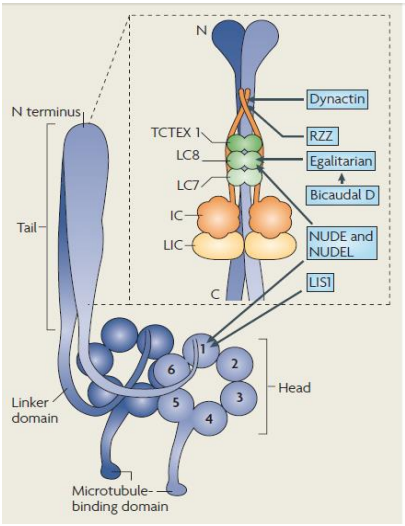


**Figure 8**: The dynein molecule structure and its associating cofactors. Dynein, itself a complex of heavy (HC), intermediate (IC) and light chains, and its cofactors, several dynein adaptor proteins that attach to different dynein subunits (shown in blue boxes). Adapted from [87].

The dynein intermediate chains directly bind dynein light chains and the dynein adaptor molecule, dynactin, and are required for cargo binding, while the dynein light intermediate chains directly bind to the stem region of dynein heavy chain. The dynein light intermediate chains are required for the stability of the dynein complex and for dynein's role in chromosome segregation. There are three dynein light chain families: Tctex1, LC8, and Roadblock. The dynein light chains directly bind to sites on the dynein intermediate chain and cooperate with dynein intermediate chain to bind various cargos.

Although much is known about the structural composition of the dynein complex, relatively little is known about its regulation. While changes in the composition and phosphorylation states of dynein subunits can modulate dynein's activities, it is believed that dynein's functions are largely controlled through interactions with its accessory factors, dynactin and NUD-2/LIS1.

### 2.1. Functions of Cytoplasmic Dynein

Cytoplasmic dynein performs a variety of cellular functions, and these activities seem greatest in metazoan cells, but cytoplasmic dynein is also used to varying extents in fungi, *alveolata*, *stramenopila* and *amoebozoa* [22]. In the yeast

*Saccharomyces cerevisiae*, the sole known role of cytoplasmic dynein is positioning the nucleus during cell division [23], whereas in filamentous fungi [24] and the slime mold *Dictyostelium discoideum* [25] it is also used for vesicle transport.

Dynein concentrates at the nuclear envelope and facilitates nuclear envelope breakdown by pulling nuclear membranes and associated proteins poleward along astral microtubules leading to nuclear membrane detachment [26]. After NEBD, dynein is essential for correct spindle formation [27]. Dynein has been implicated in silencing the SAC by transporting checkpoint proteins from attached kinetochores to the spindle poles, known as “stripping” [28]. In dividing cells, dynein also facilitates chromosome segregation.

The pulling force of dynein is also used during cell division [29]. By hauling on astral microtubules that emanate from the spindle, cytoplasmic dynein can cause the spindle to oscillate or to localize towards one end of the cell. Remarkably, during spindle oscillation in mammalian cells, cortical dynein dynamically redistributes from one side of the cell to the other, dissociating from its cortical receptors when the spindle pole is within ~2 um and accumulating with them when the spindle pole moves further away [30]. In large cells, dynein seems to exert pulling forces on microtubule asters even when the microtubules are not long enough to reach the cell cortex [31]. Recent studies indicate that this can occur as the dynein-driven movement of organelles along microtubules generates sufficient viscous drag to slowly pull the microtubule network in the opposite direction. This model suggests that the pulling force would vary according to microtubule length (as net organelle transport is greater on longer microtubules). In *C. elegans* embryos, length-dependent pulling is proposed to be a key ingredient for aster centering and spacing [32].

At the outer nuclear envelope, dynein has been reported to contribute to nuclear rotation [33] and positioning [34], centrosome separation [35] and the breakdown of the nuclear envelope for open mitosis [26]. At cell division, cytoplasmic dynein helps assemble microtubules into the chromosome-segregating device known as the spindle.

It is thought that when the plus-ends of spindle microtubules have stably engaged with the kinetochores, cytoplasmic dynein is thought to remove spindle-assembly checkpoint proteins by transporting them towards the spindle poles [28]. In mammalian cells, cytoplasmic dynein is also reported to help maintain initial spindle-KT attachments and drive rapid poleward chromosome movements during their alignment at the metaphase plate [37].

### 2.2. Dynein Regulation

In performing its multiple cellular functions, the cytoplasmic dynein motor is subject to complex regulation involving allosteric mechanisms within the dynein complex, as well as numerous extra molecular interactions controlling subcellular targeting and motor activity. Recent work has distinguished high and low load regulatory modes for cytoplasmic dynein, which, combined with a diversity of targeting mechanisms, accounts for a very broad range of functions.

Numerous proteins participate in its recruitment to subcellular sites of action, providing insight into how it contributes to such a diversity of cellular functions. Dynein is composed of multiple subunits, and changes in the composition of these subunits are thought to modulate dynein's activities. Dynein subunits are extensively phosphorylated, and changes in their phosphorylation states can alter dynein's ability to bind cargos and MTs as well as its motor activity.

At least two of these cofactors – dynactin and a complex of the dynein-interacting proteins LIS1 and NudE (or its paralogue NudEL) – additionally regulate cytoplasmic dynein activity, indicating that its mechanochemical behavior is also tailored to specific cellular roles. These regulators alter the behavior of cytoplasmic dynein and are involved in most, if not all, of its cellular functions.

## 3. Dynein Regulators

### 3.1. Lis1 and NudE/L

Dynein behavior is mediated by numerous factors, including the dynactin complex, and also, an additional group of regulatory proteins initially identified in *Aspergillus nidulans*. The *NudF* gene in *A. nidulans* was found to be homologous to human Lissencephaly 1 (*Lis1*). Lis1 (known as LIS-1 in *C. elegans)* is highly conserved from yeast to humans, and the loss of a single copy in humans results in a severe developmental disorder known as classical or type I lissencephaly (smooth brain). Patients with type I lissencephaly display severe retardation and epilepsy [38], and they typically die during early childhood. Lissencephaly is caused by a disruption in neuronal migration during early brain development that results in a drastic reduction in the number of cells within the cerebral cortex. Mouse models have shown that disruption of Lis1 specifically interrupts the migration of nuclei through the leading processes [39].

*In vitro* studies of Lis1 have revealed that it interacts physically with both cytoplasmic dynein and dynactin. The extent to which Lis1 is required for dynein's activity outside of nuclear migration is unclear; however, a growing body of evidence suggests that Lis1 is required for the majority of dynein's cell-cycle functions, since

inhibition of Lis1 disrupts centrosome movements, nuclear envelope breakdown, spindle assembly, and chromosome segregation, all of which are under the control of dynein [39,40]. Furthermore, Lis1 co-localizes with dynein at multiple subcellular sites, including the centrosomes, kinetochores, mitotic cortex, and the leading edge of migrating cells [41,42]. Although Lis1 and dynein tightly co-localize at multiple sites, they may be targeted to these sites at least partially independently of one another, since co-immunoprecipitation studies indicate that only a fraction of dynein and Lis1 are associated *in vivo* [40].

Lis1 has two distinct motifs: a Lis1 homology domain, which promotes self-dimerization, and a WD repeat, located in the C-terminal half of the protein. Lis1 has been shown to directly bind several dynein and dynactin components, including those that regulate its motor and cargo binding activity, through its WD repeat region. *In vitro* biochemical studies have suggested that binding of Lis1 to dynein may stimulate its ATPase activity in a microtubule -dependent manner, thus Lis1 may serve to activate or enhance dynein's motor activity. It is thought that Lis1 modulates dynein motility by interfering selectively with the usual coupling of the ATP hydrolysis and microtubule binding affinity cycles. By electron microscopy and mutational analysis [43], it is shown *in vitro* and yeast cells that Lis1 binds to the AAA3/4 interface of the dynein motor domain via its β-propeller domain. This interaction uncouples the ATP hydrolysis cycle from microtubule binding affinity changes at dynein's MTBD, as demonstrated by a combination of biochemical analysis and fluorescence imaging. When Lis1 is bound, dynein is arrested in a strongly microtubule -bound state, although ATP hydrolysis can still go on. Rather than binding to the main ATPase site within dynein's AAA+ ring or its microtubule-binding stalk directly, Lis1 engages the interface between these elements. Lis1 causes individual dynein motors to remain attached to microtubules for extended periods, even during cycles of ATP hydrolysis that would canonically induce detachment. Thus, Lis1 operates like a "clutch" that prevents dynein ATPase domain from transmitting a detachment signal to its track-binding domain (**Figure 9**). It is still unclear whether Lis1 serves as

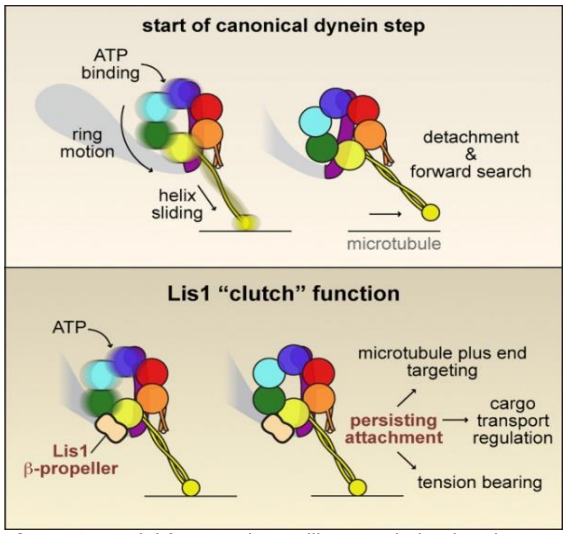


**Figure 9:** Model for Dynein Motility Regulation by Lis1. Top: Model of a canonical dynein step; Bottom: Lis1 mediated motility regulation. For clarity, only one Lis1 β-propeller domain and one dynein heavy chain are shown (both are dimers), and dynein's C-terminal region, which lies on the near face of the ring, is omitted. Adapted from [43].

an obligatory cofactor for all dynein-dependent processes or if it has dynein-independent functions.

In addition to Lis1, *NudE* was also identified in the *A. nidulans* dynein pathway. *NudE* was first identified as a multicopy suppressor of *NudF* [44] and has two mammalian homologues, NudE and NudEL (gene names Nde1 and Ndel1, respectively). Lis1 and cytoplasmic dynein each interact with NudE (known as NUD-2 in *C. elegans)* and its isoform NudEL, which are also involved in brain development and in general LIS1-dynein function. NudE localizes to mitotic kinetochores before dynein, dynactin, and LIS1, and exhibit additional temporal and spatial differences in distribution from the motor protein.

Related roles for Lis1, dynein and NudE have been reported in non-neuronal cells, where these proteins co-localize to kinetochores, centrosomes, cell cortical regions and the nuclear envelope [45–47]. The inhibition of NudE function prevents dynein, dynactin, and Lis1 localization to kinetochores, leading to metaphase arrest and kinetochore mis-orientation [47].

NudE interacts with Lis1 through a predicted N-terminal coiled-coil region [44] and with cytoplasmic dynein through a globular C-terminal domain [48].

NudE helps to recruit Lis1 to the dynein molecule, and abrogates dynein force production, whereas Lis1 alone or with NudE induces a persistent-force dynein state that improves ensemble function of multiple dyneins for transport under high-load conditions (**Figure 10**).

The ability of NudE, Lis1 and dynein to form a triplex complex and the location of interaction sites within the components suggest that NudE recruits Lis1 to the dynein complex, and may help position it close to the motor domain [49].

Single-molecule laser bead trap analysis revealed that Lis1 substantially prolonged dynein stalls under load, leading to a marked increase in the ability of multiple dynein molecules to transport high loads [49] and identifying a previously unrecognized form of cytoplasmic dynein regulation. NudE alone inhibits dynein motor activity in the same ways, although the complete Lis1-NudE-dynein complex showed an increase in the duration of the dynein-microtubule interaction under load [49].

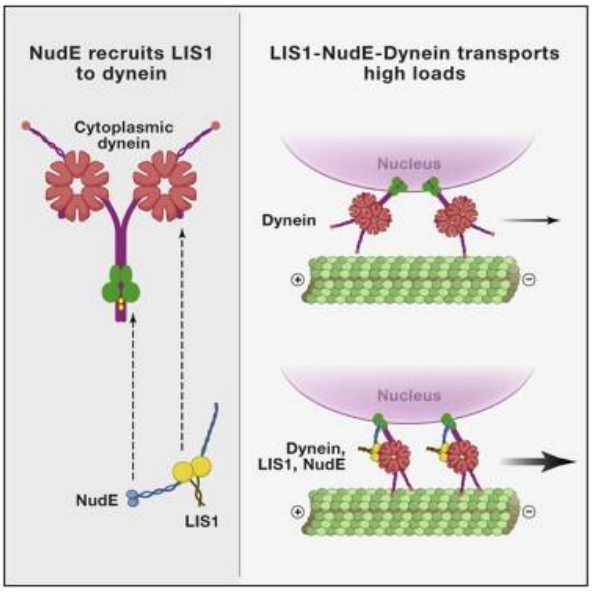


**Figure 10**: Schematic of the supposed function of the complex formed by Lis1-NudE-Dynein [49]. Lis1 with NudE induces a persistent-force dynein state that allows dynein to transport under high-load conditions, whereas them it would soon detach from the microtubules. Adapted from [49].

Recent work indicates that NudE and dynactin compete for overlapping sites within the dynein intermediate chains [50], ensuring that individual dynein molecules cannot be occupied by both regulators. Given this situation, independent mechanisms for dynein cargo recruitment at the nuclear envelope might be required to permit both dynactin and Lis1 regulation.

### 3.2. The Dynactin Complex

The Dynactin Complex was first identified based on its ability to activate dynein-mediated vesicle mobility in an *in vitro* assay. Dynactin associates with dynein through direct binding between p150glued and the intermediate chain of the dynein complex [51,52]. Association of dynactin and dynein is believed to serve two major roles. First, dynactin possesses cargo-binding activity, so it can act as an adaptor protein to link dynein to its cargo [53]. Second, dynactin has been shown to enhance the processivity of dynein by two-fold *in vitro* motility assays [54], i.e. it allows dynein to stay associated with microtubules for a longer period of time by preventing it from diffusing away after dynein detachment [54].

Although dynactin is essential for targeting dynein to cargos, only a fraction of dynactin is associated with dynein within the cell. Dynactin may play a role in anchoring microtubules to the centrosome independently of dynein [55]. During mitosis, rather than acting as a processivity factor, dynactin is thought to recruit dynein to selected sites to perform a particular function [56].

The dynactin complex has a molecular mass of 1 mDa, nearly as high as that of cytoplasmic dynein itself, and it comprises eleven different subunits. Dynactin consists of a 40 nm filament of actin-related protein 1 (ARP-1), decorated by capping proteins at the barbed (+) end, and a subcomplex of ARP-11 and accessory subunits at the pointed minus-end. The working portion of dynactin is its 150 kDa subunit, an orthologue of the *Drosophila melanogaster Glued* gene product [57]. p150 $^{Glued}$ contains a small microtubule -binding CAP-Gly (cytoskeleton-associated protein-glycine-rich)

domain at its N-terminus, followed by two predicted α-helical coiled-coil regions, the first of which binds dynein through its intermediate chains [51],and a C-terminal ARP-1-binding site [58]. The evidence of a role for dynactin cargo recruitment came from overexpression of its 50 kDa 'dynamitin' subunit, which dissociates p150$^{Glued}$ from the ARP-1 filament and causes severe mitotic and subcellular transport defects [52].

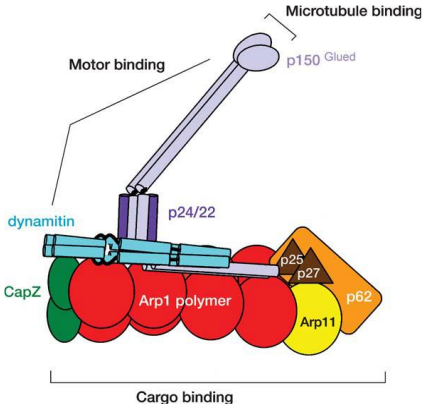


**Figure 11**: Schematic illustrating the location and approximate structural features of dynactin subunits. Adapted from [53].

The dynactin complex is composed of two basic structural units, the rod and the arm. The rod is the site of cargo binding and is composed of seven proteins: ARP-1, ARP-11, Actin, CapZ, p25, p27, and p62. The arm mediates binding to both microtubules and dynein and is composed of p150glued, p50/dynamitin and p24/p22 (**Figure 11**).

The heterotetrameric complex of p62, ARP-11, p25 and p27 is called the pointed-end complex (**Figure 12**). This structure binds neither dynein nor microtubules, and its p62, p27, and p25 subunits are not present in yeasts, indicating that they are dispensable for dynactin's most basic functions [53]. The ARP-11 subunit, which caps one end on dynactin's ARP-1 filament, and p62, which binds ARP-11 and ARP-1, are necessary for dynactin stability. These subunits also allow dynactin to bind to the nuclear envelope prior to mitosis.

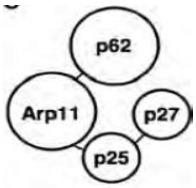


**Figure 12**: Proposed structure of the "pointed-end" complex. Adapted from [59].

The subunits p27 and p25, are thought to be peripheral components that can be removed without any obvious impact on dynactin integrity [59]. The finding that p27 and p25 are interdependent for stability is consistent with the observation that they are binding partners [60]. Nevertheless, in another study, depletion of p62, p25, and p27, led to decreased ARP-1 levels, but did not affect the stability of p150 glued or p50 [56]. Also, although depletion of p27 also leads to decreased ARP-1 levels, albeit a bit less compared with p25 depletion, it was observed only minor defects upon p27 depletion [56].

As expected for cells lacking dynactin, profound spindle defects were seen following ARP-11 RNAi treatment, with many cells exhibiting multipolar spindles. A similar result was obtained for p62 depletion. Cells depleted of p27 and p25 showed normal spindle morphology, suggesting that this dimer is not required for the dynactin-dependent events of mitotic spindle assembly and spindle pole focusing [59].

### 3.3. Cargo-specific cofactors: Bicaudal D, the RZZ complex, and Spindly

Dynein regulators are often referred to as activators because dynein-based motility in cells is repressed in their absence. In addition to dynactin, NudE and Lis1, several other dynein interactors have been identified. This complexity reflects diverse dynein cargo recruitment mechanisms, although contributions of the additional interactors to motor regulation directly or through dynactin and/or NudE-Lis1 are also possible.

The RZZ complex in metazoans is composed of three conserved proteins: ROD (Rough deal, in *C. elegans* the homologue is ROD-1), ZW10 (Zeste white 10) and Zwilch. Together with another recently discovered metazoan protein, Spindly, RZZ docks dynein to the kinetochores. In human cells, dynein-mediated removal of Spindly from microtubule-attached kinetochores, is critical for checkpoint silencing [61]. In addition, RZZ and Spindly (in *C. elegans* the homologue is SPDL-1) might help to regulate the maturation of attachments between microtubules and the kinetochores [62].

Bicaudal D (in *C. elegans* the homologue is BICD-1) is another adaptor of dynein, but unlike dynactin, LIS1 and NudE, it is specific to metazoans. Bicaudal D has been best characterized for its involvement in the dynein-mediated localization of mRNA throughout *D. melanogaster* oogenesis and development [63] and in the transport of Golgi vesicles in mammalian cells [64], but it also contributes to other dynein-mediated processes, including nuclear positioning, lipid droplet transport and microtubule organization [63]. The studies of Bicaudal D suggest that it serves as a modular link between dynein and cargo; the N-terminal coiled coil interacts with dynein, whereas the C-terminal coiled-coil binds cargo-specific factors. In HeLa cells, the N-terminal portion of Bicaudal D is responsible for the recruitment of dynein and dynactin. When the N-terminal fragment of Bicaudal D is artificially tethered to cargoes, it induces their dynein-dependent transport to microtubule-minus ends [65].

# 4. The early *Caernohabditis elegans* embryo as a model system to study cell division

## 4.1. *C. elegans* as an experimental system

Proteins and processes of mitosis are highly conserved in eukaryotes from yeast to man. What is learned in one system is often directly applicable to understanding a process in another system. To understand the function of an individual component and how it interacts with other essential proteins requires that genetics be combined with biochemistry and cell biology. An ideal biological system would therefore require these three types of studies.

The nematode *Caernohabditis elegans* seems appropriate to study the mechanisms of cell division. Besides its availability for strong genetic techniques, *C. elegans* has proven useful for both biochemical [66] and cell biological approaches [67]. In addition, Wormbase, a well-developed database of worm information is available online and includes numerous links to methods resources and user-groups. Genetic crosses are easy and a collection of resources is available through the *Caernohabditis* Genetics Center (CGC). The genome of *C. elegans* is sequenced, consisting in 97 megabases and containing approximately 19000 predicted genes. In systematic screens, all predicted genes have been silenced using RNAi.

The early embryo contains large clear cells, which are well-suited for live imaging, and a rapid and invariant development, which allows for high resolution analysis of mutant phenotypes. *C. elegans* is a free-living soil nematode that is approximately one millimeter long that feeds on bacteria. Under laboratory conditions *C. elegans* is fed *Escherichia coli* bacteria grown on plates or in liquid culture. *C. elegans* has a rapid life cycle of approximately three days (**Figure 13**) at 20ºC and only six chromosomes. *C. elegans* has two sexes: hermaphrodite and male. The two sexes differ in size, morphology and behavior. The sex typically used for laboratory experiments is the hermaphrodite since it produces both sperm and eggs, can self-fertilize and lays approximately 300 eggs. Males arise spontaneously with a low frequency, roughly 1/500. In laboratory, males are used for genetic crosses. About 2000 genes have so far been reported to be essential for viability of *C. elegans*. In the past years *C. elegans* one-cell embryos have appeared as a powerful model system to study cell division.

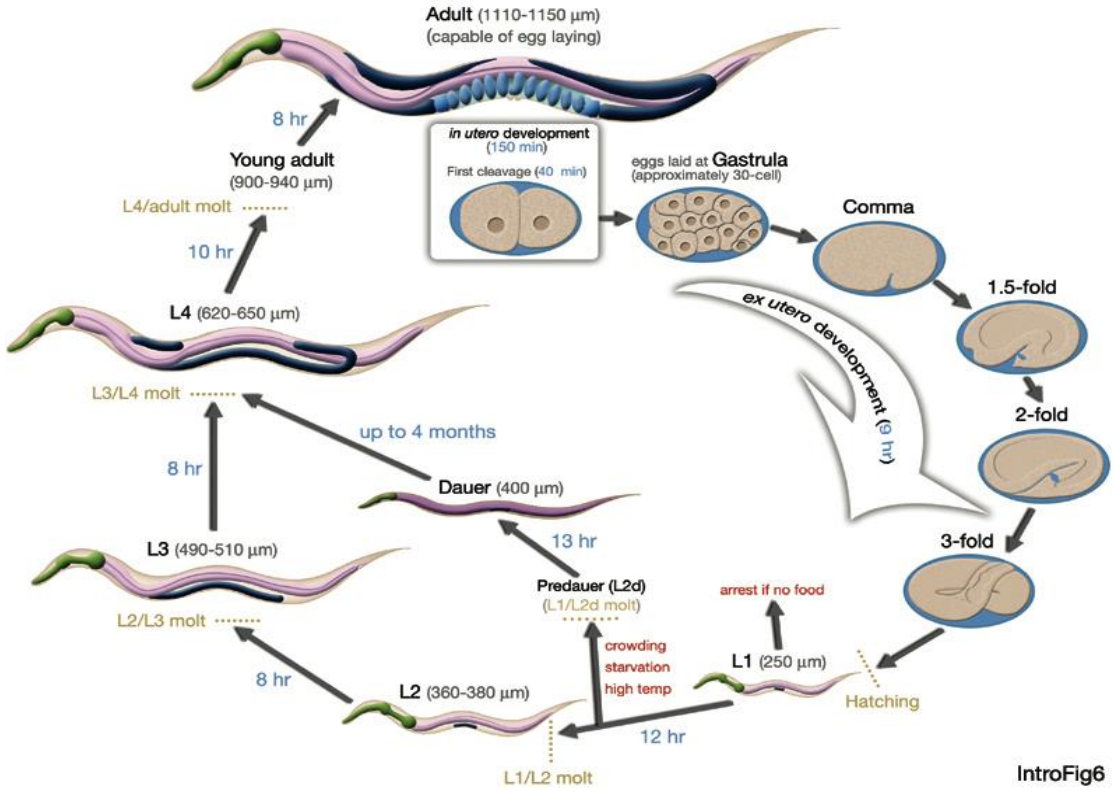


**Figure 13**: *C. elegans* life cycle at 20ºC. Numbers in blue along the arrows indicate the length of time the animal spends at each certain stage. The length of the animal at each stage is marked next to the stage name. Adapted from Worm Atlas.org.

The architecture of the syncial gonad makes it possible to use RNAi to generate oocytes whose cytoplasm is reproducibly depleted of targeted essential gene products via a process that does not depend exclusively on intrinsic protein turnover. Depletion relies on the rate of embryo production instead of protein half-life, the kinetics tend to be similar for different targets. By 36-48 hours after introduction of the dsRNA, newly formed oocytes are typically >95% depleted of the target protein (**Figure 14**).

The depleted oocytes can then be analyzed as they attempt their first mitotic division following fertilization.

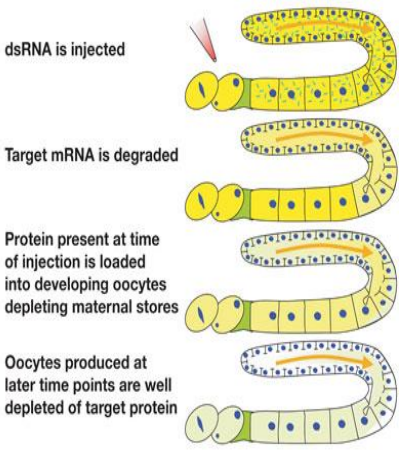


**Figure 14***:* The *C. elegans* gonad and advantages. The gonad is a syncytial tube lined with nuclei in various stages of meiotic prophase. The meiotic nuclei contribute mRNA that is translated to generate the protein that is loaded into the developing oocytes. Introduction of a dsRNA triggers the degradation of the corresponding mRNA. However, the syncytial gonad and connected oocytes still contain the target protein that was present at the time of injection. Maternal stores are depleted by the continual packaging of gonad cytoplasm into developing oocytes. By 36 to 48 hours after introduction of the dsRNA oocytes are typically >95% depleted of the target protein. Adapted from [86].

### 4.1.1. Mos1-mediated single-copy insertion (MosSCI)

Transgenes in *C. elegans* were initially generated by injecting DNA into the germline. The transgenes would typically be overexpressed in somatic cells and silenced in the germline. A technique that is based on the single-copy insertion of transgenes has arisen in the past years; this method consists on the mobilization of a Mos1 transposon that generates a double-strand break in noncoding DNA. The break is repaired by copying DNA from an extra chromosomal template into the chromosomal site. Homozygous single-copy insertions can rapidly be obtained. Single-copy transgenes can be expressed in the female and male germlines. The process of constructing a MosSCI strain is described in literature [68].

## 4.2. The first mitotic division of the *C. elegans* embryo

In the first cell division of *C. elegans*, mature oocytes are fertilized in the spermatheca of an adult hermaphrodite. Mature oocytes are arrested in meiosis I. Fertilization by sperm triggers the completion of meiosis I and II. Three of the haploid products of meiosis are extruded from the egg as polar bodies. The remaining haploid pronucleus contributes the maternal chromosomes to the embryo. The sperm contributes the centrioles and a haploid pronucleus to the egg. The centrioles progressively mature into centrosomes. The embryo is initially symmetric, and a signal from the centrosomes then breaks the symmetry, leading to the formation of two cortical domains, an anterior domain and a posterior domain. After polarity is established, the maternal and the paternal pronucleus migrate towards each other.

Pronuclear migration consists of the movement of the oocyte pronucleus towards the sperm pronucleus and movement of the sperm pronucleus away from the cortex toward the embryo center. Initially, the oocyte pronucleus moves ~12 μm toward the posterior at a slow rate (~3.5 μm/min). As it approaches the sperm pronucleus, the oocyte pronucleus accelerates, moving an additional 10 μm at ~5-10 times its initial rate [69]. The sperm pronucleus begins its migration later than its female counterpart and travels at a slow rate of ~3.5 μm/min until it meets the oocyte pronucleus near the embryo center (~7 μm). Both male and female pronuclear migrations depend on microtubules growing from two centrosomes associated with the male pronucleus.

After pronuclear meeting (PM), the nuclear-centrosome complex moves to the center of the embryo and begins to rotate to align with the long axis of the embryo. Nuclear Envelope Breakdown (NEBD) occurs, and chromosomes begin to align. The mitotic spindle then begins to move toward the embryo posterior during metaphase and asymmetric elongation during anaphase contributes to its posterior displacement.

Since the cleavage furrow bisects the mitotic spindle, this displacement results in an asymmetric first cleavage. The posterior cell (called P1) is smaller than the anterior cell (called AB). The first cell division is shown as a cartoon in **Figure 15**.

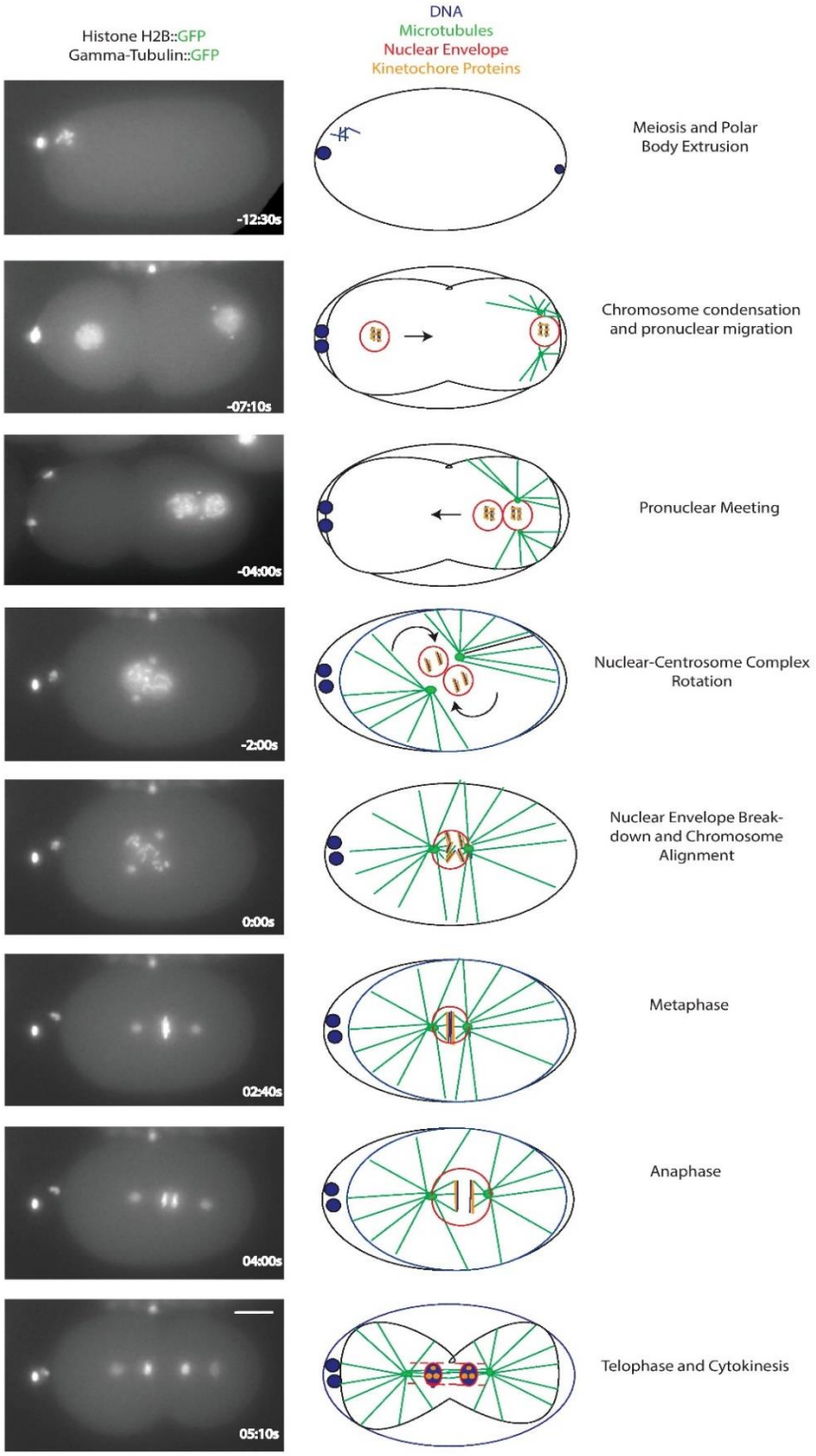


**Figure 15**: The first mitotic division of the *C. elegans* embryo. (Left column). Schematics illustrate the major features of the first division (Right column). Approximate times is in minutes::seconds before/after nuclear envelope breakdown.

# Objectives

It is known that the dynein motor interacts with several proteins that do not belong to the dynein complex itself but are crucial for adapting the motor to its cellular function. The objective of this project is to understand how dynein adaptor proteins, such as the complex formed by NudE/Lis1 and the Dynactin complex regulate dynein function during mitosis. The roles of other known dynein regulators, such as Spindly, Bicaudal-D and proteins of the RZZ complex will also be assessed.

In order to accomplish this, I will use the *Caernohabditis elegans* one-cell embryo as an animal model for cell division. To determine the function of dynein co-factors, RNA-mediated interference (RNAi) will be used to deplete target proteins from one-cell embryos. I will then conduct embryonic lethality tests in order to assess the importance for embryonic development and perform phenotypic analysis through quantitative live-imaging assays. The migration of the female and male pronucleus will provide information about dynein activity at the nuclear envelope, as well as dynein's ability to grab and pull on microtubules. The distance between the centrosomes will provide information about kinetochore-dynein, since a premature separation of the poles before anaphase onset indicates that kinetochore-microtubule attachments are not established efficiently. To assess NUD-2 and LIS-1 importance for Dynein localization to kinetochores, I will take advantage of an assay that allows me to accumulate GFP-tagged Dynein at kinetochores of monopolar spindles in the second mitotic division.

As a whole, I aim to get a better understanding of dynein regulatory mechanisms that ensure the fidelity of chromosome segregation, which is essential for proper cellular function.

# Material and Methods

## 1. Nematode strains and culture conditions

Wild-type *C. elegans* (strain N2) and several mutant worm stocks, as well as *Escherichia coli* OP50 bacteria, were obtained from the *Caenorhabditis* Genetics Center (CGC), a central repository for strains under contract from the NIH National Center for Research Resources (http://biosci.umn.edu/CGC/CGChomepage.htm).

In order to characterize the function of Dynein Cofactors, particularly the complex formed by LIS-1/NUD-2 and the Dynactin complex, but also interactions with BICD-1, SPDL-1 and ROD-1, several strains were acquired or made in order to assess these cofactors functions. The following table lists all strains that were used, but also their respective genotype and construction methods (**Table 1**).

**Table 1**: List of all strains that were required for the study of the function and location of Dynein cofactors, such as the LIS-1/NUD-2 complex and/or the dynactin complex, as well as BICD-1, ROD-1 and SPDL-1. It is specified the name of each strain and what they are expressing, the genotype of each strain, and information about whether the strain was received or constructed in the laboratory, either by MosSCI insertion or by crossing with existing strains. The table is divided in 3 groups: Control, NUD-2/LIS-1 and Dynactin Complex.

| | Strain | Genotype | Received | Constructed |
|---|---|---|---|---|
| **Control** | N2 (wild-type) | - | Yes | - |
| | TH32 strain co-expressing GFP histone H2B and GFP y-tubulin | ((unc-119(ed3) III; ruIs32[pAZ132; *pie-1*/GFP::histone H2B] III; ddIs6 [GFP::tbg-1; unc-119(+)] V). | Yes | - |
| **NUD-2/LIS-1 Complex** | *nud-2 (ok949)* | (R11A5.2(*ok949*) I.) | Yes | - |
| | *nud-2 (ok949)* outcrossed with N2 6 times | The deletion was backcrossed six times into WT and followed by PCR. This aims to eliminate mutations other than the NUD-2 deletion. (R11A5.2(*ok949*) I.) | - | Crossed |
| | NUD-2::mCherry | (unc-119(ed3) III; prtSi37 [pRG200;PNUD-2::NUD-2 CDS::mCherry::StrepTagII:3'UTRNUD-2, cb-unc-119(+)]II) | - | MosSCI |
| | NUD-2::mCherry, *nud-2 (ok949)* outcrossed 6 times. | (unc-119(ed3) III; prtSi37 [pRG200;PNUD-2::NUD-2 CDS::mCherry::StrepTagII:3'UTRNUD-2, cb-unc-119(+)]II) ;(R11A5.2(ok949) I.), | - | Crossed |
| | *nud-2 (ok949)* into TH32 background (GCP39) | (unc-119(ed3) III; *ruIs32*[pAZ132; pie-1/GFP::histone H2B] III; ddIs6 [GFP::tbg-1; *unc-119*(+)] V; R11A5.2(*ok949)* I.) | - | Crossed |
| | *nud-2 (ok949),*, NUD-2::mCherry in TH32 background. | R11A5.2(*ok949*) I.); (unc-119(ed3) III; prtSi37 [pRG200;PNUD-2::NUD-2 | - | Crossed |

| | | | | |
|---|---|---|---|---|
| | | CDS::mCherry::StrepTagII:3'UTRNUD-2, cb-unc-119(+)]II); (unc-119(ed3) III; ruIs32[pAZ132; pie-1/GFP::histone H2B] III; ddIs6 [GFP::tbg-1; unc-119(+)] V; | | |
| | LIS1::GFP | [gfp::Lis1(ojIs10); *unc-119*(+)] | Yes | - |
| | LIS1::GFP, *nud-2 (ok949)* | ([gfp::Lis1(ojIs10); *unc-119*(+)],R11A5.2(ok949) I.) | - | Crossed |
| | LIS1::GFP, H2B::mCherry | [gfp::Lis1(ojIs10); unc-119(+)]; *unc-119(ed3)* III; ltIs37 [pAA64; pie-1/mCherry::his-58; unc-119 (+)] IV | Yes | - |
| **Dynactin Complex** | Actin-related protein 1::mCherry | (unc-119(ed3)III; prtSi9[pRG152; Parp-1::arp-1reencoded::mCherry::StrepTagII; *cb-unc-119*(+)]II). | - | MosCI |
| | DHC::GFP (EU1444) | (orIs17[Pdhc-1::GFP::dhc-1, *unc-119*(+)]) | Yes | - |
| | DHC::GFP, ARP1::mCherry | (unc-119(ed3)III; prtSi9[pRG152; Parp-1::arp-1reencoded::mCherry::StrepTagII; cb-unc-119(+)]II; orIs17[Pdhc-1::GFP::dhc-1, *unc-119*(+)]). | - | Crossed |
| | DHC::GFP, ARP1::mCherry with *nud-2 (ok949)* | (unc-119(ed3)III; prtSi9[pRG152; Parp-1::arp-1reencoded::mCherry::StrepTagII; cb-unc-119(+)]II; orIs17[Pdhc-1::GFP::dhc-1, *unc-119*(+)]; nud-2 *(ok949)*;I) | - | Crossed |
| | DHC::GFP, H2B::mCherry | (orIs17[Pdhc-1::GFP::dhc-1, unc-119(+)]);*unc-119(ed3*) III; ltIs37 [pAA64; pie-1mCherry::his-58; *unc-119* (+)] IV | - | Crossed |
| | DHC::GFP, H2B::mCherry, *nud-2 (ok949)* | (orIs17[Pdhc-1::GFP::dhc-1, unc-119(+)]);unc-119(ed3) III; ltIs37 [pAA64; pie-1/mCherry::his-58*; unc-119* (+)] IV; nud-2 (*ok949*);I) | - | Crossed |

Worms were cultured on agar plates and fed *E. coli* strain OP50 bacteria as described [70]. OP50 is a uracil auxotroph with a slower growth rate than WT *E. coli* and is not resistant to antibiotics [70]. These agar plates have a constant amount of bacteria, which reduces the need for refocusing the microscope when switching from one plate to another. Preparation of plates is as mentioned on WormBook [71].

All strains were maintained in an incubator with temperature set for 20ºC. After injection of RNAi worms were incubated either at 16ºC or 20ºC, depending on the type of depletion that was desired.

# 2. Generation of Transgenic Strains

## 2.1. Mos Single Copy Insertion (MosSCI): Cloning *NUD-2*::mCherry

The *NUD-2* gene was amplified by PCR (**Table 2; Appendix Figure 1**) using 5x HF Buffer, 10 mM dNTPs, 100 mM 5' and 3' primer, template DNA (genomic DNA), Phusion Polymerase and sterile dd$H_2O$. To amplify pUCshort57, the cloning vector, the template was 50 ng/µl from an existing plasmid. From this same plasmid, another PCR was conducted to amplify mCherry. Thermocycler conditions used were as follows, an initial denaturation step of 98ºC for 30s, followed by 30 cycles of a denaturation of 98ºC for 10s, annealing of 55ºC for 30s and an extension of 72ºC with time depending on the extent of the gene product (15-30 sec/kb). An extension of 72ºC for 5 minutes would finalize the product amplification. The thermocyclers used were Biometra® Tpersonal Alfa Gene or Applied Biosystems® Veriti. To check if the PCR worked, 5 µl of the 100 µl PCR reaction was run on a 1% agarose gel, adding 1/5 volume of 6X Loading Dye, and 3 µl of 10 mg/mL Ethidium Bromide. The PCR product was purified using a PCR Clean-Up Kit (NzyGelpure from NzyTech®), and eluted in 32 µL of DNA Elution Buffer.

**Table 2**: List of all primers that were required to assemble the NUD-2::mCherry construct into the cloning vector pUC57 short. The primers are oriented 5'->3' and their purpose if also referred.

| **Primers used to make the construct NUD-2::mCherry in pUC57 short** | |
|---|---|
| **Primers (5'-3')** | Purpose |
| TGTACTGAGAGTGCACCATATGCTCGAGGCTGTTCGACCACCACTG | NUD-2 promoter that overlaps with pUC57_short (oRG716) |
| TTGACAGAGGTAGCCCGTGTCGTTGTAAG | NUD-2 CDS that overlaps with mCherry (oRG717) |
| CGACACGGGCTACCTCTGTCAACGGCGGC | mCherry that overlaps with NUD-2 CDS (oRG718) |
| ATGAAATGTTACTTTTCGAACTGCGGGTG | mCherry that overlaps with NUD-2 3'UTR (oRG719) |
| AGTTCGAAAAGTAACATTTCATTTTTTGGTTTTTC | NUD-2 3' UTR that overlaps with mCherry (oRG720) |
| CAGCTATGACCATGATTACGCCAGATCTAATGATGGACAATACACG | NUD-2 3' UTR that overlaps with pUC57_short (oRG721) |
| GGCGTAATCATGGTCATAG | pUC57 forward (oRG509) |
| CATATGGTGCACTCTCAG | pUC57 reverse (oRG510) |

Then, all the PCRs were assembled together with a recent technique that allows the enzymatic assembly of DNA molecules up to several hundred kilobases, known as the Gibson assembly [72]. The protocol for Enzymatic Assembly is adapted from literature. The PCR reactions must overlap their product with the next by 20 bp.

The bands were purified before proceeding to the assembly, and 15 µL of 1.33x AMM (containing a mix of three enzymes: an exonuclease, a DNA polymerase and a DNA ligase) were added to 5 µL of equimolar mixed overlapping DNA fragments. This reaction was then incubated at 50ºC for 1 hour, and transformed into competent cells (DH5α). To confirm the presence of the insert, colonies were picked into 5 mL of LB

plus the appropriate antibiotic and grown overnight at 37ºC. Then, DNA was purified with the ZymoResearch Miniprep Kit®. A diagnostic digest was conducted using 10X New England Biolabs Buffer, 10X BSA, EcoRI and XhoI, and $ddH_2O$, to confirm if the colonies were positive and had the expected band pattern. 6X DNA Loading Buffer were added to this reaction and run on an agarose gel to check for the presence of the insert. If the restriction enzymes cut in the expected pattern, the plasmid would be sent for sequencing at Macrogen, on tubes containing 500 ng DNA and 25 pmol of sequencing primer (**Table 3**; **Annex Figure 1**).

**Table 3**: List of the primers used to sequence the NUD-2::mCherry, and the purpose of each primer. Primers are written according to 5'->3').

| **Primers used to sequence the construct NUD-2::mCherry in pUC57 short** | |
|---|---|
| **Primers (5'-3')** | Purpose |
| AGCAGACAAGCCCGTC | pUC57 short (oRG594) |
| GGTGGCATGGATGAATTG | C-terminus of mCherry (oRG278) |
| AAACATCCATTTGCGGTAGC | NUD-2 (oRG616) |
| CGACACGGGCTACCTCTGTCAACGGCGGC | mCherry overlap with NUD-2 3'UTR (oRG718) |
| GAAATGCATAGATTACG | 5' UTR and beginning of NUD-2 mCherry (oRG727) |

The sequencing showed that all the fragments were correctly positioned and without mutations. The construct was then transferred to pCFJ151, a vector designed for MosSCI integration on chromosome 2. To accomplish this, a simple restriction reaction with NEB enzymes XhoI and BglII was conducted both on the insert (from pUC57 – **Annex Figure 2**) and on the vector (pCFJ151 – **Annex Figure 3**). The vector was then treated with Calf Intestinal Phosphatase (CIP), in order to prevent self-ligation. The entire restriction digest was run on a 1% agarose gel, cutting out the desired fragment size (both insert and vector were approximately 7 kb). This slice of gel was purified with Zymoclean Gel DNA Recovery Kit (ZymoResearch®). Then, the vector and insert were ligated (**Annex Figure 4**) using 10X DNA ligase buffer and T4 DNA ligase, for 2 hours at 16ºC. A control, containing $ddH_2O$ instead of insert was also prepared, so that the amount of background from uncut and re-ligated vector was known. Then, the ligation was transformed into competent bacteria DH5α. The rest of the protocol until sequencing was done as mentioned above. Diagnostic digest was conducted with NEB restriction enzymes XhoI and BglII, the same enzymes used before, and showed the ligation was successful. A culture of 5 mL LB with Ampicillin antibiotic 100mg/mL was grown overnight at 37ºC. This final construct was also sent to sequence to Macrogen with the same primers as before, after the assembly in pUC57 short, in order to confirm the correct localization of all components (**Table 3**). Then, the 5 mL were miniprepped

with a specific kit, Plasmid Mini Prep Kit (Invitrogen®), and eluted in 50 µL. This DNA was then used to mix with 2X Injection Mix (Invitrogen®) for the MOsSCI technique (**Table 4**). In order to design plasmids and confirm sequencing results SnapGene v2.2.2® was used. All primers were designed using Primer3.

### 2.2. Injecting to make new strains – MosSCI technique

The following table lists all necessary components for the 2X Injection Mix (Table 4). The mix for injection was centrifuged at maximum centrifuge speed during a period of 10 minutes. Then, 0.3 µL were loaded into an injection needle. After this, young adult hermaphrodites, in this case EG2469 strain (that integrates on chromosome 2) were placed with a pick on a thin agarose pad (2%) onto mineral oil, under the Nikon® SMZ745 scope and were massaged until movement ceases. Then, they were injected in the gonad (**Figure 16**) with the injection mix using an Eppendorf® PatchMan NP2 micromanipulator on Zeiss® Axiovert S100 with an Eppendorf® FemtoJet express pump.

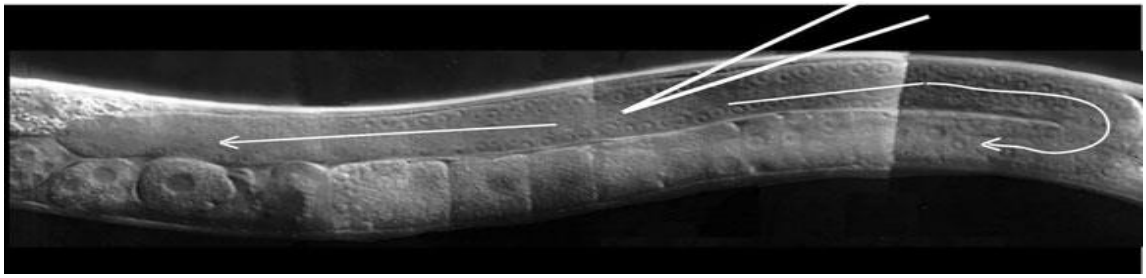

**Figure 16:** Microinjection of the C. elegans gonad. The optimal position of the injection needle in the cytoplasmic core of the distal germ line is depicted. For DNA transformation, injection solution should flow in both directions through both the distal and proximal germ line (arrows) (Adapted from [73]).

The set pump pressure parameters were a pi of 1200 hPa, ti (s) of 0.1 and 50 of pc (hPa). After injection, 3 worms were placed per plate, left to recover on OP50 plates and placed in the 25ºC incubator until starvation. DNA injected into the gonad of a hermaphrodite concatenates to form an extra chromosomal array and is eventually incorporated into the nucleus.

**Table 4**: Components required for the 2X Injection Mix for MosSCI. The following table describes each plasmid that was required and the concentration that is necessary for the Injection Mix.

| Plasmid | Description | Final Concentration |
|---|---|---|
| **pCFJ601** | Peft-3::transposase | 50 ng/ µL |
| | Transgene in pCFJ151 vector | 10-50 ng/ µL |
| **pMA122** | Phsp::peel-1 | 10 ng/ µL |
| **pGH8** | Prab-3::mCherry (Pan-neuronal) | 10 ng/ µL |
| **pCFJ90** | Pmyo-2::mCherry (pharynx-muscle) | 2.5 ng/ µL |
| **pCFJ104** | Pmyo-3::mCherry (body muscle) | 5 ng/ µL |

### 2.3. Obtaining Homozygous MosSCI Strains

The protocol that was followed to obtain transgene homozygous lines is the referred in literature [68]. After gene conversion is induced by the transposase (pCFJ601), using the template DNA with *unc-199,* the only worms able to survive starvation were those carrying the extra-chromosomal array (pGH8, pCFJ90, pCFJ104) or those that integrated the *unc-119* (+) gene, since mutant *unc-119* worms are unable to form dauer larvae during starvation. After the plates were starved the nematodes were heat-shocked, by placing the plates in a 34ºC incubator for 4 hours. This allows Peel-1 toxin (pMA122) to kill the carrying with an extra chromosomal array. After 4-6 hours later the plates were screened for MosSCI insertions under a fluorescent microscope. Insertion animals are typically L1 or dauer animals that move very well and do not have any of the fluorescent co-injection markers (mCherry). Then, 4-5 worms were picked off each plate and moved to a new plate. The insertion was made homozygous by picking single worms to individual plates (5 to 6) and propagating the strain some generations until the population became homozygous. The transgenic strain could then be outcrossed to remove any mutations. This way, worms with specific genes tagged with desired fluorescent markers are created and can then be crossed with other homozygous strains to obtain new strains.

## 3. Genetic Crosses

### 3.1. Crossing Strains with Fluorescent Markers

New strains were obtained by crossing existing strains of different alleles. Then, it is a process of following the plates with the desired alleles and markers until obtaining a homozygous strain. A practical example of this procedure was making a strain co-expressing DHC-1::GFP and ARP-1::mCherry. By crossing the strain DHC::GFP and the ARP1::mCherry strain and observing the resulting generations, worms homozygous for both were obtained, resulting in a new strain.

The screening of fluorescence on worms was done in the fluorescence microscope Axioskop2 (Zeiss).

### 3.2. Crossing Strains using PCR to follow deletion alleles

For crosses involving the *nud-2 (ok949)*, progeny was followed by single worm PCR until a homozygous strain was achieved. In the single worm PCR the primers used were flanking the region of the gene, and amplified different sizes of product. If

the gene was present, the amplified product was greater than if the genome had the deletion. The worm PCR was made to according to the following steps: 1) Worm Lysis, where for a Mix per 10 worms consisted of 5 µL of 20 mg/mL of Proteinase K that were added to 95 µL of 1x Lysis Buffer (constituted by 10 mM Tris pH. 8, 50 mM KCl, 1.5 mM $MgCl_2$). Then, 10 µL were distributed on the lids of PCR tubes and one worm was added to each lid. Bacteria was avoided, since it could cause PCR contamination. Immediately, the solution with the worm was spin down in a minicentrifuge and placed in the thermocycler to undergo 90 minutes at 65ºC, followed by 15 minutes at 95ºC. This allowed the extraction of worm DNA. The controls used were WT and NUD-2 deletion (RB1022).

Next followed the PCR itself. 2 µL of template were used in a PCR Mix of 23 µL. This mix consisted of 16.5 µL of $ddH_2O$, 1.25 µL of each primer, forward and reverse, 2.5 µL of 10X NzyTech Taq Reaction Buffer, 0.5 µL of dNTPs, 0.8 µL of 50 mM $MgCl_2$ and 0.2 µL of NzyTech Taq Polymerase. Then, the solution was submitted to an initial denaturation of 95ºC for 2 minutes, followed by 30 cycles of a 95ºC denaturation for 30 seconds, a annealing of 60ºC for 30 seconds, and an extension of 72ºC for a period 1 minute and 30 seconds. This was followed by a final extension of 5 minutes at 72ºC. Then, 15 µL of each tube were mixed with 2.5 µL of 6X Orange Dye and were run on an agarose gel (1%) with Ethidium Bromide. The resulting bands indicated the presence or absence of the deletion and indicated which plates should be followed.

A practical example is the cross DHC::GFP, with Histone H2B::mCherry and the NUD-2 deletion. To achieve a homozygous line of worms with the deletion, worm PCRs were done in order to follow the plates with the deletion. The fluorescence was followed under the microscope, in order to maintain all markers. After a series of generations a homozygous line was established and the strain was frozen to keep in the collection in the -80ºC chamber.

To follow the NUD-2 deletion, two primers were designed around the NUD-2 gene and one inside the gene (**Table 5**). This way, if a worm was WT, around 2 kb would be amplified (**Figure 17,18**), whereas in the NUD-2 deletion only 0.8 kb was amplified, since the NUD-2 gene is 1.2 kb. Heterozygous worms presents both bands.

**Table 5**:. List of all primers used to screen worms for the presence or absence of NUD-2.

| Primer (5'-3') | Template | Purpose |
|---|---|---|
| AAACATCCATTTGCGGTAGC | Worm Lysis | primer to follow NUD-2 deletion by PCR (616) |
| AATGCTGGCGTTCTCTGTCT | Worm Lysis | primer to follow NUD-2 deletion by PCR (618) |
| GCAAATTGTACACGGGAAT | Worm Lysis | primer to follow NUD-2 deletion by PCR (726) |

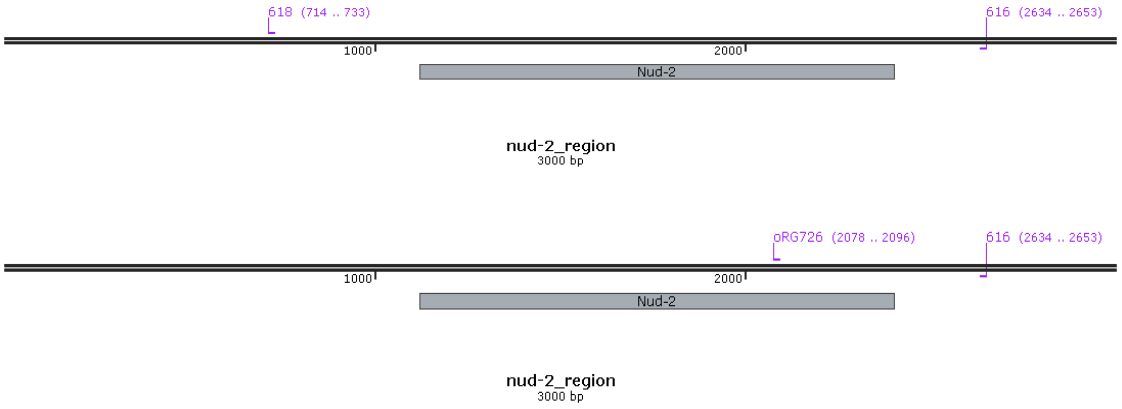


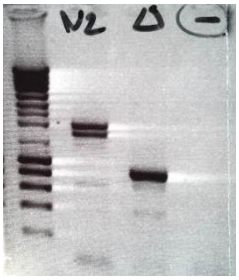

**Figure 17:** Schematic of the NUD-2 gene and primers location. Primers 616 and 618 amplified the gene resulting in a 2 kb product when the worm was WT, and 0.8 kb when the worms lacked the gene. Schematic of the NUD-2 gene and primers 616 and 726 that amplified only when the gene was present, meaning that a product of 575 bp was amplified when the WT locus was present but no product was amplified if the worm had the NUD-2 deletion. **Figure 18:** Example of a gel showing the bands present in Wild-Type (N2), the *nud-2 (ok949),* and a negative control ($H_2O$).

# 4. Assessing Embryonic Lethality

## 4.1. Native Embryonic Lethality Assay

To determine the embryonic lethality of a strain, an embryonic lethality test was conducted. This assay consisted of singling worms that were at the L4 stage to a plate, leaving them to mature into adults. 40 hours after an L4 was placed on a seeded plate, it was an egg-laying adult and was singled out to an individual mating plate. A mating plate is a plate that is only seeded with bacteria in a small area, meaning that the worms laid embryos only where it is seeded, allowing an easier counting of embryos/larvae at the end of the assay. After 8 hours of laying embryos, the hermaphrodites were removed from the plates. After 16 hours, the number of hatched embryos – larvae, and non-hatched embryos were assessed. This assay was conducted at 20ºC.

The percentage of embryonic lethality was assessed by determining the lethality (non-hatched over hatched embryos) per hermaphrodite, and then averaging them. Similarly, 95% Confidence Interval (CI) was determined by assessing the Standard Error (SE) and Standard Deviation (SD) associated per worm.

The lethality associated with *nud-2 (ok949)* was assessed in *nud-2 (ok949)* outcrossed 6 times with WT, in order to remove any mutations other than the deletion.

### 4.2. RNA interference effect on Embryonic Lethality

To determine the effect of depleting the expression of a protein by use of RNAi, an embryonic lethality test was conducted with the difference that on this case the worms at L4 stage were injected with a specific RNAi, either against Dynactin Complex Subunits, NUD-2/LIS-1 Complex, or BICD-1, SPDL-1, or ROD-1, and then the procedure was the same as the one mentioned above.

### 4.3. Production of dsRNA

When selecting a DNA sequence for use as template, we considered if the coding region was an appropriate region from the gene of interest for dsRNA trigger. The sequences should be derived from exons and not introns or promotor regions. We also considered the length, since longer dsRNAs may be more effective since they are fragmented into a greater number of effector siRNA molecules than shorter dsRNAs. PCR products, as well as plasmids can be used as templates for in vitro transcription reactions. These reactions employ a simple bacteriophage RNA polymerase and a DNA template with promotor sequences corresponding to the RNA polymerase (**Figure 19**). To accomplish this, primers were designed to amplify the region of the desired gene, adding the T3 promoter sequence (AATTAACCCTCACTAAAAGG) to the 5' end of one primer and the T7 promoter sequence (TAATACGCTCACTATAGG) to the 5' end of the reverse primer.

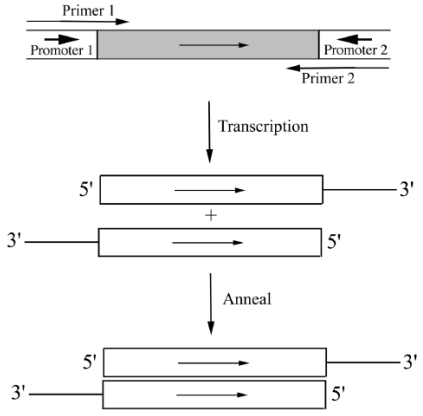


**Figure 19**: PCR-amplified template DNA for RNA soaking and injection experiments. PCR product contains a DNA insert (gray box) flanked by two promoters. The promoter sites can be incorporated into the primer sequence, as indicated. The PCR fragment can be used directly (after cleanup) in an in vitro transcription reaction. A runoff transcript will be produced with either RNA polymerase. If the two promoters are identical, only one in vitro transcription reaction is required to generate dsRNA [74]

First, the gene of interest was amplified by PCR, containing 10x Taq Buffer, 2.5 mM $MgCl_2$, 0.4 mM dNTPs, 0.4 mM of each primer, both for T3 and T7 (**Table 6**), Plasmid DNA (if so, diluted 1:50) or Genomic DNA (100 ng), Taq Polymerase 5U/µL (Nzytech Taq®) and $H_2O$. Thermocycler conditions applied were an initial denaturation of 95ºC for 30s, followed by 35 cycles of a denaturation of 92ºC for 30s, annealing of 58ºC for 30s, and an extension of 72ºC of 1 min per kb, followed by a final extension of 72ºC for 7 minutes. To confirm amplification an agarose gel was run. The PCR reaction was cleaned with DNA Clean

and Concentrator Kit (ZymoResearch), quantified, and then both T3 and T7 Transcription Reactions (Ambion®) were prepared, consisting in a mix of rNTPs, 10x T3/T7 Buffer, Template DNA, and T3 or T7 enzyme mix accordingly added. These two tubes incubated at 37ºC for a minimum of 5 hours. Next, DNAse was added and incubated for 15 minutes. The resulting RNA reactions were clean with MegaClear Kit®. In order to anneal both sense and antisense ssRNA, 30µL of Eluted T3 ssRNA were combined with 30 µL of Eluted T7 ssRNA and with 30µL of 3X Soaking Buffer (32.7 mM $Na_2HPO_4$, 16.5 mM $KH_2PO_4$, 6.3 mM NaCl, 14.1 mM $NH_4Cl$). This reaction was incubated 68ºC for 10 minutes and then at 37ºC for 30 minutes. To confirm the annealing between the ssRNAs, an agarose gel was run. Then, the dsRNA concentration was measured on NanoDrop®. Finally, the RNA was divided in aliquots and kept in a collection at -80ºC.

**Table 6:** List of all the constructed dsRNA and primers required for the *in vitro* transcription. The template used for each amplification are also described, as well as the target of each dsRNA.

| Constructed RNA interference | Primers Used | | Template Used | Targets |
|---|---|---|---|---|
| | T3 (5'-3') | T7 (5'-3') | | |
| **ARP-1** | AATTAACCCTCACTAA AGGCCCTTAACAATC GGAACAGC | TAATACGACTCACTAT AGGACGACGTCATCG CCAATC | Plasmid containing arp-1 cDNA | Targets Arp-1 |
| **ARP-11** | AATTAACCCTCACTAA AGGTCTTGCCAATCG TTTTCTG | TAATACGACTCACTAT AGGATTGGATGTGCC GGAGAA | Plasmid containing arp-11 cDNA | Targets Arp-11 |
| **p62 (dnc-4)** | AATTAACCCTCACTAA AGGCTTTGGTCAGCA TGAACTCC | TAATACGACTCACTAT AGGAATCAACTTGGT GAGGTGACG | Plasmid containing p62 cDNA | Targets Dynactin-4 |
| **p25 (dnc-5)** | AATTAACCCTCACTAA AGGGCGATAGCTCGT TGTTTCG | TAATACGACTCACTAT AGGACTACGATGAGA CGGAATGG | Plasmid containing p25 cDNA | Targets Dynactin-5 |
| **p27 (dnc-6)** | AATTAACCCTCACTAA AGGTTATTGTGCAGC AGAAGCAGA | TAATACGACTCACTAT AGGCCATCGCCAGTA GTGCAA | Plasmid containing p27 cDNA | Targets Dynactin-6 |
| **LIS-1** | AATTAACCCTCACTAA AGGTCGGAGAGGCAA AAAGAAGA | TAATACGACTCACTAT AGGCTCGAACCCAAT TTTCGTGT | cDNA | Targets Lis1 |
| **NUD-2** | AATTAACCCTCACTAA AGGATGGATTTGTCT GAGGATCAA | TAATACGACTCACTAT AGGTTAAGCCCGTGT CGTTGTAA | cDNA | Targets NUD-2 |
| **BICD-1** | AATTAACCCTCACTAA AGGTCTTCCTCTGCA GCCATTTT | TAATACGACTCACTAT AGGTGGAGAAGCTTC GTCAGGAT | cDNA | Targets BICD-1 |

### 4.4. Embryonic Lethality Assay injecting RNA interference

#### 4.4.1. Full Depletion

Previously to inject dsRNA, an aliquot was thawed and centrifuged 10 minutes at maximum centrifuge speed, to pellet any debris. For these lethality tests, WT worms at L4 stage were injected with dsRNA and left recovering and growing for 40 hours. Then, all adult hermaphrodite worms were singled out to individual plates, and left laying embryos. After 8 hours, the mothers were removed, and 16 hours after that, the number of larvae versus embryos were assessed. This type of experience was conducted at 20ºC.

#### 4.4.2. Partial Depletion

A partial depletion can also be achieved by means of RNAi injection. In order to conduct a partial depletion, hermaphrodites at L4 stage were injected with the desired dsRNA, and placed at 16ºC for 24 hours. After this time they started laying embryos and worms were singled out to individual plates. After 17 hours the worms were removed from their individual plates, and 7 hours later they were re-used to test a full depletion, by singling them out again and leaving them to lay embryos for 17 hours. After this period of time, the hermaphrodites were removed. After 16 hours, the number of larvae versus embryos was assessed. This type of experience was conducted at 20ºC. This way, from a single injected worm it was possible to obtain a partial (24 hours) depletion, and a full depletion (48 hours) with a dsRNA. This was conducted to determine synergistic effects between: LIS1/NUD-2, NUD-2/ROD-1, NUD-2/SPDL-1 and NUD-2/BICD-1.

## 5. Assessing Protein Function by Loss-of-Function Phenotype induced by RNAi

### 5.1. Injections

In order to infer the function of dynein cofactors, worms co-expressing GFP::histone H2B and GFP::γ-tubulin were injected at the L4 stage with the desired dsRNA. After 48 hours at 20ºC, adult hermaphrodites were dissected to isolate embryos for live imaging.

### 5.2. Sample preparation and Microscopy

Embryos were dissected from adult hermaphrodites on a specific and tested media, either Egg Salts 0.7x (1X Egg Salts: 118 mM NaCl, 40 mM KCl, 3.4 mM $MgCl_2$, 3.4 mM $CaCl_2$, 5 mM HEPES pH 7.4) or M9 (42 mM $Na_2HPO_4$, 22 mM $KH_2PO_4$, 86 mM NaCl, 1 mM of $MgSO_47H_2O$ per liter) and transferred with a mouth pippete to a 2% agarose pad.

These two different media were used with different purposes. Egg Salts 0.7x is the standard medium where worms were dissected in order to assess the first mitotic division from the early stages of division, because this medium enables embryos without a defined eggshell to remain viable and proceed with mitosis. On the other hand, M9 only allows embryos with a formed eggshell to survive. This medium was used to film for short periods of time, usually from NEBD to late AO with the goal of assessing pole-pole distance.

The embryos were then gathered with the help of an eyelash, and a coverslip 18*18 mm was placed on top, to allow filming under the inverted Widefield Microscope Zeiss® Axiovert 200M. After adjusting the Köhler illumination and using the objective of 63x, 7 slices of 1.5 µm were recorded, with an interval of 10 s between z-Stacks, 100 ms of Exposure, a Binning of 2x2, and a Camera Gain of 3. Channel Alexa 488 was used with power at 30%, and for Differential Interference Contrast (DIC) Transmission Light Channel with DICIII Condenser was used. Fluorescence was controlled with Zeiss FluoArc, the stage was controlled with Prior NanoScanZ, ABS = 12.5V, using also Prior ProScan III. The shutter used was Uniblitz ® Model VCM-D1 Shutter Driver. The temperature was controlled with Okolab box, and set at 20ºC during filming.

Alternatively, some experiments were filmed with a Zeiss Axio Observer: *bicd-1* and *spdl-1* RNAi in the *nud-2 (ok949)* background. The camera was a Hamamatsu Digital Camara C11440 Onca Flash 4.0 and the piezo stage was a WSB PiezoDrive 08. The time-lapse movie acquirement was the same as mentioned for Axiovert 200M, but the fluorescence channel 488 was set at 10% laser intensity and 50 ms exposure.

### 5.3. Image Analysis

Video recordings were analyzed with Fiji® Image J. Image processing, Image J is a free image processing software developed by Wayne Rasband at the NIH. It can be downloaded at http://imagej.nih.gov/ij/s

Quantitative analysis of the first mitotic division was made with the plugin MTrackJ. The positions of the two pronucleus and the centrosomes along the anterior-

posterior axis of the embryo were determined for each time-lapse image sequence. First, the embryo egg shell, visualized by DIC, was used as a reference to set the anterior-posterior axis. The image was then rotated so that the long axis of the embryo (i.e the anterior-posterior axis) was horizontal, thus corresponding to the x-axis. The coordinates (X,Y) of each structure were then obtained by tracking the middle of the GFP-labeled structures (nucleus with diffuse Histone H2B::GFP or centrosome with gamma-Tubulin::GFP). The displacement along the x axis of each image was then calculated using the most anterior point of the eggshell as a reference point, and the distance was normalized to embryo length. In addition to the displacement along the anterior-posterior axis, I also determined the distance between the two centrosomes over time. Frames at which defined events in mitosis occurred, such as pronuclear meeting, nuclear envelope breakdown and anaphase onset, were noted and used as a reference to align the tracks of individual embryos. Then, the mean, standard deviation, standard error were obtained according to literature [75].

To determine the speed of female pronuclear migration, the mean of pronuclear migration data on control embryos aligned relative to pronuclear meeting (PM) was obtained (**Figure 20**). Then, looking at individual data and the graphical representation, a slow and a fast phase could be distinguished: slow phase (-230 to -50 seconds) and fast phase (-50 to 0 seconds). The data of each embryo was then analyzed between these time points, and individual means were obtained. This mean was in % per second, and was converted in μm/minute assuming a 55 μm mean embryo length. After conversion, the average of these means was assessed, and it represents the mean velocity of either the slow or fast phase, accordingly. The 95% CI was also determined.

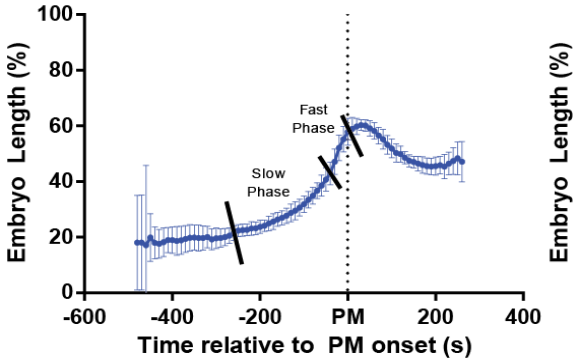


**Figure 20:** Graphical representation of the female pronuclear migration of control embryos and of how the speed of migration is calculated. The slow and the fast phase are defined by the black lines. Slow phase (-230, -50s); Fast Phase (-50,0s). Graphs are normalized to embryo length (%) along time. All graphical representations are aligned relatively to PM, refereed at X=0.

The data was analyzed and plotted on Microsoft Office Excel 2013 and Graph Pad 5®. A confidence interval of 95% was used for error bars of the mean of each situation evaluated, considering at least 10 embryos per experiment [75].

# 6. Protein Localization

## 6.1. One Cell Embryo

To determine the localization of proteins of interest in the one cell embryo the same technique was used for dissection of adult hermaphrodites. The embryos were filmed since the early prophase until anaphase onset under the 60X objective of the Andor Revolution XD® Spinning Disk Confocal Microscope, using an automatic Lambda SC Smart Shutter™ Controller, CSU22 Confocal Scanner Unit from Yokogawa Camera, X-Cite® Series 120 Q, an Olympus IX2-UCB Fluorescent Light Controller, a stage temperature controller, The Cube, from Life Imaging Services set at 20ºC, Prior NanoScan, Prior ProScan II, and a Precision Control Box 100 Series from Andor Technology. The Microscope was installed with the IQ Andor 2 software. Strains (DHC::GFP with H2B::mCherry), (DHC::GFP, H2B::mCherry in the *nud-2 (ok949))* and (LIS1::GFP with H2B::mCherry) were acquired with Andor Revolution Nikon Eclipse Ti, with ASI MS-2000 Piezo pE-100. The camera is CSU-X Yokogawa. The software used for acquisition is also a new version, IQ Andor 3.

The laser power and exposition were variable and dependent of the strain being filmed, since the tagged proteins could have different levels of expression (Table 7).

**Table 7:** Laser intensities, exposures and Z-stack conditions used for all strains filmed under Andor Revolution XD® Spinning Disk Confocal Microscope.

| Strain | Laser 488 | | Laser 568 | | Stacks |
|---|---|---|---|---|---|
| | Intensity | Exposure | Intensity | Exposure | |
| **DHC::GFP, ARP1::mCherry Without/with NUD-2 deletion** | 50% | 150 ms | 100% | 150 ms | 9 µm (1.5 µm*7 slices) each 10 seconds |
| **LIS1::GFP, without/with NUD-2 deletion** | 100% | 250 ms | - | - | 9 µm (1.5 µm*7 slices) each 10 seconds |
| **NUD-2 deletion, NUD-2::mCherry in TH32 background** | 30% | 100 ms | 100% | 500 ms | 8 µm (2 µm*5 slices) each 15 seconds |
| **TH32** | 25% | 100 ms | - | - | 9 µm (1.5 µm*7 slices) each 10 seconds |
| **NUD-2 deletion in TH32 background** | 25% | 100 ms | - | - | 9 µm (1.5 µm*7 slices) each 10 seconds |
| **DHC::GFP, H2B::mCherry** | 80% | 50 ms | 90% | 50 ms | 11 µm (1 µm*12 slices) each 15 seconds |
| **DHC::GFP, H2B::mCherry, NUD-2 deletion** | 80% | 50 ms | 90% | 50 ms | 11 µm (1 µm*12 slices) each 15 seconds |
| **LIS1::GFP, H2B::mCherry** | 100% | 50 ms | 90% | 50 ms | 11 µm (1 µm*12 slices) each 15 seconds |

### 6.2. Monopolar spindle assay in the second embryonic division

In order to determine if a protein accumulates at unattached kinetochores, a Zyg-1 assay was performed. Zyg-1 is a gene required for centriole replication, therefore, *zyg-1(RNAi)* prevents centriole replication. The first division is unaffected because the sperm contributes two centrioles, but in the second division there is only one centrosome per cell, which results in the formation of a monopolar spindle in the second division (**Figure 21**). This way, we can determine if a fluorescently-tagged protein is accumulated on kinetochores.

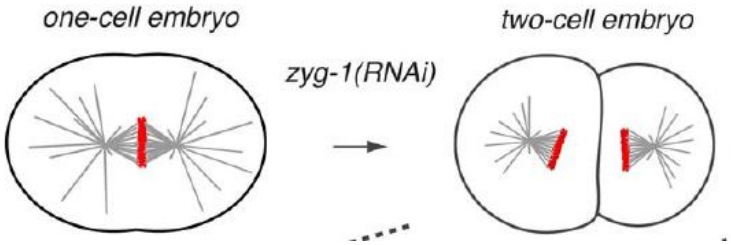


**Figure 21**: Establishment of a monopolar spindle due to the effect of *zyg-1* RNA interference on the second mitotic division of *C. elegans*. During the second division the RNAi prevents centriole replication, and consequently the chromosomes align at the metaphase plate, but cannot be equally split into two daughter cells since only one spindle pole is available. The microtubules can only attach on one side of the metaphase plate, and therefore the spindle cannot properly form. Chromosomes wait for the microtubule attachment to the kinetochore but eventually the cell gives up and chromosomes decondense, leading to multinucleated cells.

All the settings used for the two-cell embryo were the same as the ones mentioned in the one-cell embryo (**Table 7**). These two-cell embryos were filmed just before NEBD to late anaphase onset.

In ImageJ Fiji, after rotating the embryos so that the long axis corresponds to the X axis, and the anterior end is on the left, embryos are analyzed. To determine if the accumulation of proteins resides at the attached or unattached kinetochore, a line scan can be obtained by drawing a 5 px wide line that runs through the aligned kinetochores. After normalization to the highest value, it can be compared to the line scan that represents chromosomes, H2B::mCherry, and this way determine at what side/sides it accumulates. This assay can be done in one-cell embryos and two-cell embryos injected with *zyg-1 RNAi*.

To determine the protein expression levels we took advantage of the Zyg-1 assay. First, and per embryo, a time point is chosen after NEBD, when the chromosomes are tightly aligned on the monopolar spindle (this time is flexible). Then, a 5-pixel-wide line scan was drawn at the same image position in the H2B::mCherry and DHC::GFP channels. The peak of H2B::mCherry fluorescence was used to define pixel 0. In the DHC::GFP line scan, 6-pixel-wide regions on either side of pixel 0 were

searched to identify the peak DHC-1 signal. Because of the asymmetric “cloud” of non-kinetochore signal, background estimation was performed by drawing a small square of defined dimensions, 8 pixels to the left of the kinetochore. Measuring this squares gives the average background intensity that can then be subtracted from the peak intensity. This result is reported as a measure of the kinetochore-localized signal. The protocol is adapted from [76].

# Results

### NUD-2/LIS-1 and Dynein/Dynactin co-localize during the first embryonic division

To characterize the role of the dynein cofactor NUD-2 in the early *C. elegans* embryo, I generated a worm strain stably expressing NUD-2::mCherry. This strain was created by the MosSCI technique that allows single copy insertions. The transgene is being expressed from its endogenous promotor and 3´UTR (**Figure 22**).

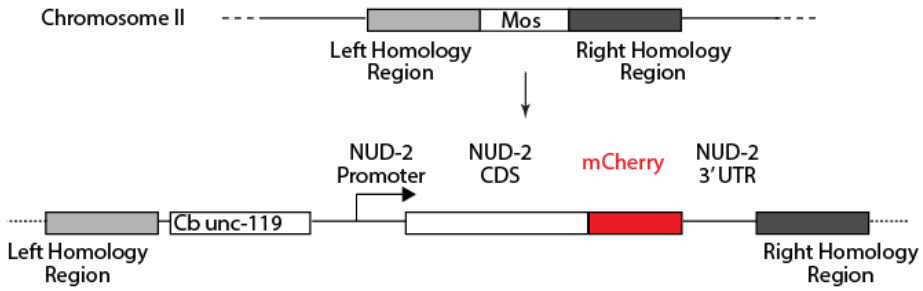


**Figure 22:** Schematic of the construction technique of the NUD-2::mCherry strain. This construct was integrated into the Chromosome II using the Mos-1 mediated single-copy insertion (MosSCI) [77]. This technique inserts transgenes as single copies at a defined chromosomal locus.

Live imaging revealed that NUD-2::mCherry is expressed in the one-cell embryo. NUD-2::mCherry accumulated in the Nucleus prior to NEBD, in the Nuclear Envelope, and in the Spindle (**Figure 23**).

To determine the localization of LIS-1, which is predicted to form a complex with NUD-2, I used an existing strain expressing LIS-1::GFP. LIS-1 localized to the Nuclear Envelope, in the Nucleus just prior to NEBD, in the Cytoplasm and in the Spindle (**Figure 23**). NUD-2 and LIS-1 do not appear to localize in the centrosomes. These results demonstrate that NUD-2 co-localizes with its binding partner LIS-1 during the first embryonic division of *C. elegans*.

Since LIS-1 is reported to interact with Dynein and Dynactin, the localization of these proteins was assessed. The motor protein dynein mostly co-localizes with dynactin during the first mitotic division of the *C. elegans* embryo. Before NEBD both dynactin and dynein localize to the nuclear envelope, and in the centrosomes. Nevertheless, only dynactin is localized inside the nucleus. After NEBD, they both localize to the Spindle (**Figure 23**). Both dynein and dynactin are seen in the cytoplasm.

Since NUD-2/LIS-1 and Dynactin are Dynein regulators, they were expected to co-localize in most subcellular components. All four proteins co-localize in the Nuclear

Envelope, in the Nucleus, in the cytoplasm and in the spindle. Nevertheless, only Dynein and Dynactin are seen in the centrosomes (**Figure 23**).

Considering that the dynein complex is subject to a tight regulation that modulates localization, the localization of dynein/dynactin in the absence of NUD-2 will be assessed, to get further insight into the NUD-2 function. In order to accomplish this, a strain consisting of DHC-1::GFP carrying the *nud-2(ok949)* allele was obtained and the localization and intensity of Dynein were assessed. Also, an ARP1::mCherry strain will also be crossed into the strain carrying the *nud-2(ok949)*, to give insights about the localization of Dynactin in the absence of NUD-2.

A strain consisting of LIS-1::GFP;H2B::mCherry was recently crossed and will be injected with *nud-2* (RNAi), in order to assess LIS-1 location and function without its binding partner NUD-2.

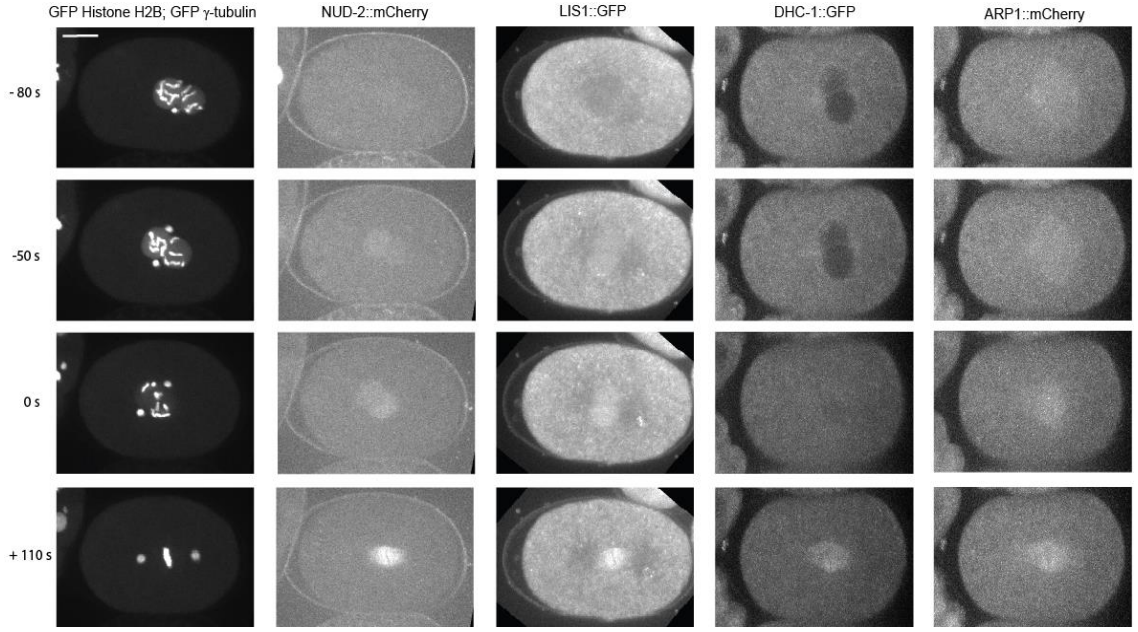


**Figure 23**: Localization of LIS-1 and NUD-2 during the first mitotic division. Stills of time-lapse movies of the first mitotic division of the *C. elegans* embryo filmed under the Spinning Disk Confocal Microscope. A representative video was chosen per experiment. **A**. Control strain that is expressing Histone H2B::GFP, γ-Tubulin::GFP, therefore allowing the visualization of the centrosomes and the chromosomes, in several mitotic events: PM (-80 seconds), Prior to NEBD (-50 seconds), NEBD (0 seconds) and AO (+ 110 seconds). **B**. Strain expressing NUD-2 tagged with mCherry, which shows that NUD-2 localizes to the Nucleus, Nuclear Envelope, Spindle and Cytoplasm. **C**. Strain expressing the LIS1 protein tagged with a green fluorescent marker shows that LIS-1 localizes to the Nuclear Envelope, Nuclei prior to NEBD, Spindle and Cytoplasm. **D.** Stills of DHC-1 fused with GFP. DHC-1 is required for Dynein structure and functioning, therefore crucial for its assembly, functioning, and location. **E.** Stills of ARP-1, the backbone of Dynactin, without which it also cannot properly localize and therefore function. Stills are aligned to NEBD (0 s). Bar corresponds to 10 μm.

To determine whether NUD-2 functionally contributes to embryogenesis, we used a strain carrying the *nud-2(ok949)* allele, generated by the International *C. elegans* Gene Knockout Consortium (www.celeganskoconsortium.omrf.org). Previous

work showed that nud-2*(ok949)* likely corresponds to a null allele [78]. I first performed an embryonic lethality test, (**Figure 24**) by determining the percentage of progeny that is able to complete embryogenesis. In worms lacking NUD-2 10% of embryo progeny fails to develop into larvae. The NUD-2::mCherry transgene rescued the lethality associated with the NUD-2 deletion, which shows that the fusion protein is functional. These results reveal that the NUD-2 is functionally important for embryonic development.

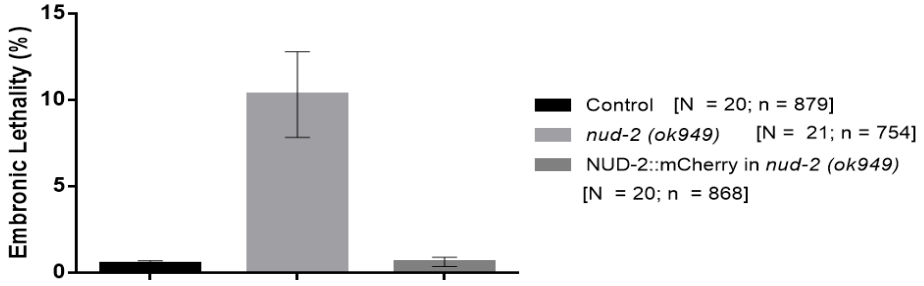


**Figure 24**: Graphical representation of the embryonic lethality present in Control (Wild-Type N2), *nud-2(ok949),* and NUD-2::mCherry in the *nud-2(ok949) strain.* Control = 0.5%, *nud-2(ok949)* = 10%, NUD-2::mCherry in *nud-2(ok949)* = 0.6%. Error bars represent the mean with a 95% Confidence Interval (CI). N = Number of Worms; n = Number of Progeny.

## Dynein and Pronuclear Migration

### NUD-2

### The migration of the female pronucleus is affected in the absence of NUD-2

To determine whether the enhanced embryonic lethality observed in worms lacking NUD-2 could be a result of defects during embryonic cell division, I followed the movement of chromosomes and centrosomes in the one-cell embryo by live imaging. For this purpose I crossed the *nud-2(ok949)* strain with a strain co-expressing H2B Histone::GFP and γ-Tubulin::GFP. In the wild-type, the oocyte pronucleus moves towards the sperm pronucleus, and after pronuclear meeting, the nuclear-centrosome complex moves from the embryo posterior towards the center of the embryo. This female pronucleus usually moves at two different rates: a slow rate of approximately 3.5 μm/min and a fast rate of 5-10 times its initial rate.

The *nud-2(ok949)* strain was filmed on the Fluorescence Microscope Axiovert 200M and results show that the migration of the female pronucleus on worms depleted of NUD-2 is slower compared to Control (**Figure 25-A, B**). This is seen by the individual traces, which spread more on worms depleted of NUD-2, suggesting that some of these NUD-2 depleted worms are more sensitive to the absence of the protein than others. The embryos start migrating closer to the posterior and take the same time

as control embryos to reach the male pronucleus. This leads to a slower mean of the migration of the female nucleus.

A third strain, that restores NUD-2 to *nud-2(ok949)* strain by use of a transgene NUD-2::mCherry was also filmed and analyzed. Results show that restoring NUD-2 recovers the slower female nucleus migration phenotype (**Figure 25-C**), proving that absence of NUD-2 leads to this particular phenotype, and that the transgene is functional.

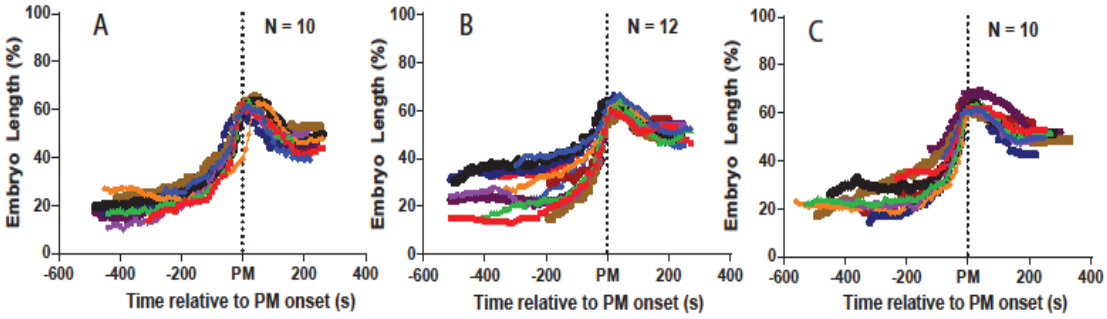


**Figure 25**: Schematic of the one-cell embryo pronuclear migration and Graphical representation of Individual traces of the Female Pronuclear Migration in *nud-2(ok949)* embryos. Embryos are expressing H2B Histone::GFP and γ-Tubulin::GFP (Control) **A**), *nud-2(ok949)* (**B**), and NUD-2::mCherry into *nud-2(ok949)* (**C**). Graphs are normalized to embryo length (%) along time. All graphical representations are aligned relatively to Pronuclear Meeting (PM), refereed at X=0.

## The velocity at which the female nucleus migrates is decreased in worms depleted of NUD-2

To assess more details of the female pronucleus, the velocity of migration was determined. In wild-type, the female pronucleus it is described to move at a slow rate of ~3.5 μm/min, when it starts migrating towards the male pronucleus localized to the posterior end. As it approaches the sperm pronucleus, the oocyte pronucleus accelerates, moving ~5-10 times its initial rate.

In worms lacking NUD-2, the slow phase of the female pronuclear migration in worms depleted of NUD-2 appears to be generally slower than the control, with an average of 2.4 μm/min, even though it is not statistically significant (student-t test, two-tailed p=0.0878). More examples could make the difference significant and will be obtained. The transgenic strain that restores NUD-2 has an average speed of 2.7 μm/min, and appears to partially recover the speed to control levels, with 3.1 μm/min (**Figure 26-A**).

As for the speed of the fast phase of female pronuclear migration, it remained similar in all three situations, and the differences were not statistically significant (**Figure 26-B**).

These results indicate that the slow rate of the female pronuclear migration is affected when worms are depleted of NUD-2, leading to a slower migration.

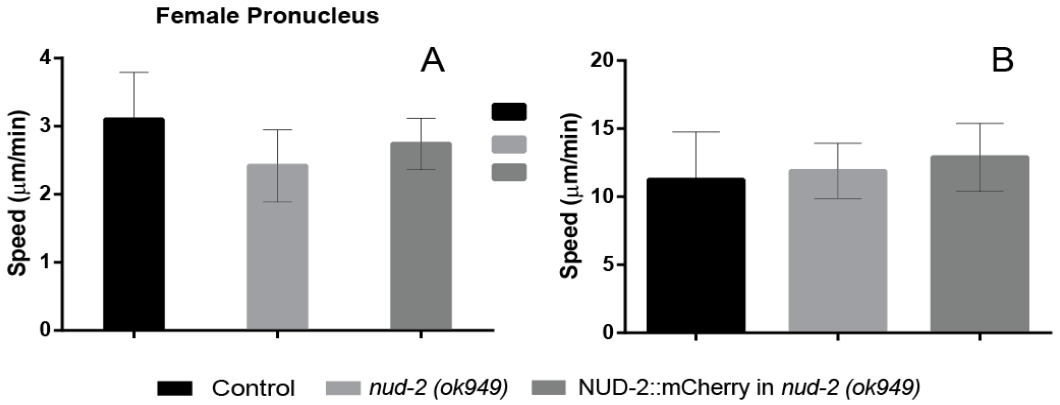


**Figure 26**: Graphs representing the speeds of pronuclear migration in Control, *nud-2(ok949)* and NUD-2::mCherry in *nud-2(ok949)* of embryos in the H2B Histone::GFP and γ-Tubulin::GFP background. **A**. Speed of the slow phase of the Female Pronucleus, respectively, 3.1, 2.4 and 2.7 μm/min) **B**. Speed of the fast phase of the Female Pronucleus, respectively, 11.3, 11.9 and 12.9 μm/min. Time is relative to PM. Error bars represent the mean with a 95% CI.

## Absence of NUD-2 leads to a displacement of the male pronucleus to the posterior side of the embryo

To uncover more phenotypes that could derive from depleting embryos of NUD-2, the migration of the male nucleus was assessed. In the wild-type, the male pronucleus travels from the posterior end towards the female pronucleus. After the pronucleus meet, both travel to the center of the embryo.

It is visible that the male nucleus travels less toward the center of the embryo after PM than control (**Figure 27-A**). Again, results show that the fusion protein is functional, since the mean of NUD-2::mCherry in *nud-2(ok949)* worms is similar to Control (**Figure 27-B**). These results suggest that NUD-2 is required for the correct male pronuclear migration.

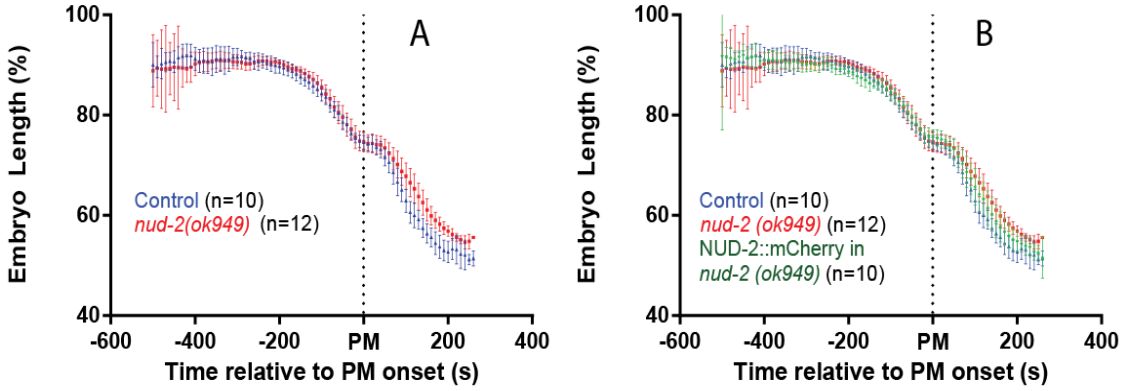


**Figure 27**. Graphs representing the mean of all three situations: Control, *nud-2(ok949)*, and transgene NUD-2::mCherry into the *nud-2(ok949)*, all in H2B Histone::GFP and γ-Tubulin::GFP background. The graphs are aligned according to

time relative to pronuclear meeting (PM), refereed at X=0, and are normalized by embryo length. Error bars represent the mean with a 95% CI.

## NUD-2 and LIS-1

### NUD-2 is synergistic with LIS-1

NUD-2 and LIS-1 are in a complex and are therefore expected to interact and contribute to dynein function in mitosis. In wild-type embryos, NUD-2/LIS-1/Dynein allow the transport of heavy-cargo along the microtubules. In order to assess synergistic effects between LIS-1 and NUD-2, a partial and full depletion (**Figure 28**) were conducted on WT and *nud-2(ok949)* worms, by injecting them with *lis-1 (*RNAi).

Results show that the lethality of WT worms injected with *lis-1* (RNAi) is just above 50% after 24 hours, while in worms depleted of NUD-2 the lethality is already 100% (**Figure 28**). After 48 hours the *lis-1* (RNAi) is fully lethal on both strains. This result confirms that there is synergy between these two proteins.

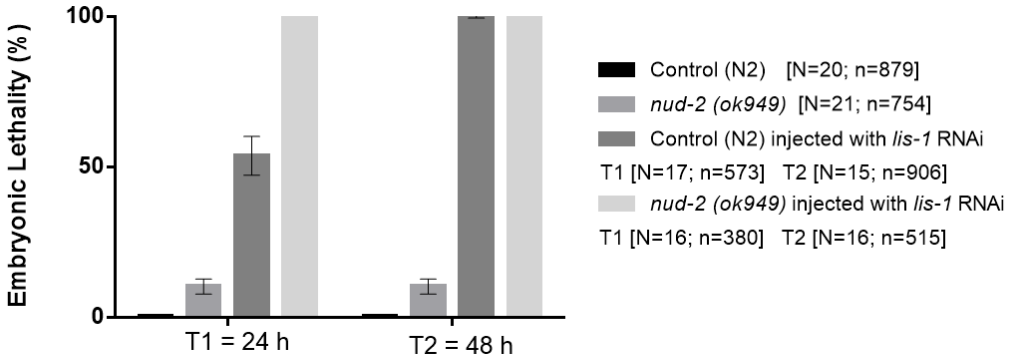


**Figure 28**: Graphical representation of the embryonic lethality present in WT and *nud-2 (ok949)* worms after a partial (24h) and full (48h) depletion of LIS-1. Embryonic lethality is shown in percentage. Respectively, top to bottom, 0.5%; 10%; 54%, 100%; and 100%, 100%. Error bars represent the mean with a 95% CI.

### NUD-2 and LIS-1 are required for Pronuclear Migration

To confirm the results obtained in the lethality test, and determine which mitotic events were affected, the phenotype was assessed in the same conditions of partial and full depletion, but in worms expressing Histone H2B::GFP and Gamma-Tubulin::GFP (control) and worms expressing these markers in the *nud-2(ok949)* background. This allows visualization of chromosomes and centrosomes throughout the time-lapse movie.

Focusing on the 24 hour time point that corresponds to a partial depletion, in control worms injected with *lis-1* (RNAi), the phenotype appears to be less severe than in the *nud-2(ok949)* background; there is pronuclear migration and pronuclear meeting,

(**Figure 29, Colum 2**). After 48 hours, the *lis-1* (RNAi) phenotype is the same as seen in the partial depletion of LIS-1 in the *nud-2(ok949)*, where centrosomes do not separate and detach from the male nucleus, and there is no pronuclear migration (Column 3). The *nud-2 (ok949)* embryos pronuclear migration and meeting occur normally and at the correct time (**Figure 29, Column 4**), but when injected with *lis-1* (RNAi), there is no pronuclear meeting (**Figure 29, Column 5)**.

These results show that LIS-1 and NUD-2 interact and are required for pronuclear migration.

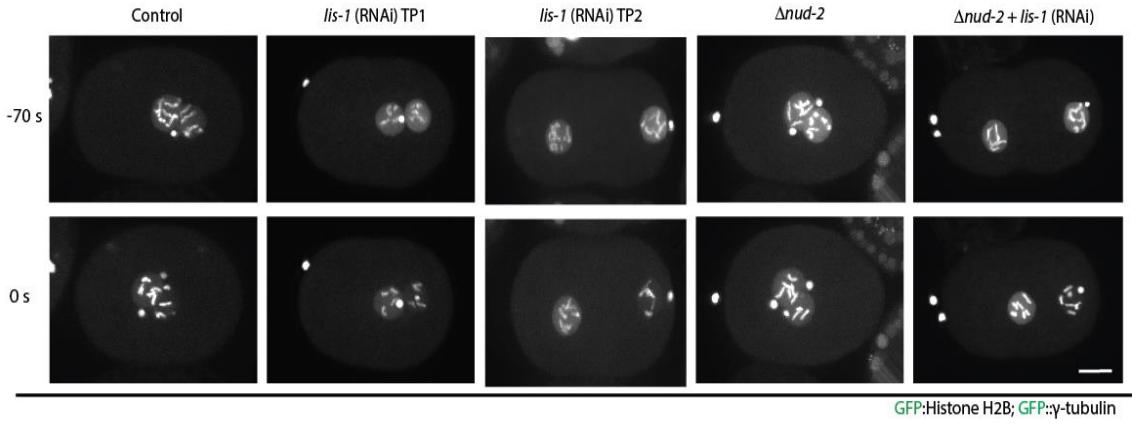


**Figure 29**: Several stills of time-lapse movies of *nud-2(ok949*), *nud-2(ok949)* injected with *lis1 (*RNAi*)*, and control worms injected with *lis-1* (RNAi). All stills are aligned relatively to NEBD (0 seconds). Bar corresponds to 10 µm.

## NUD-2 and SPDL-1

### Embryonic Lethality tests reveal a synthetic lethal interaction between NUD-2 and SPDL-1

NUD-2 is a sensitive background to observe interactions with other proteins in mitosis. To determine if NUD-2 interacts with SPDL-1, an assay similar to the one conducted with LIS-1 and NUD-2 was conducted (**Figure 30**). Results indicate that a partial depletion of SPDL-1 in *nud-2(ok949)* worms (Time Point 1 = 24h) is fully lethal, whereas in WT worms the lethality is set at 43%.

Regarding the full depletion of SPDL-1 (Time Point 2 = 48h), both strains injected with *spdl-1* are 100% embryonic lethal.

These results suggest that there is an increased embryonic lethality when worms depleted of NUD-2 are depleted of SPDL-1, indicating synergy between the two proteins.

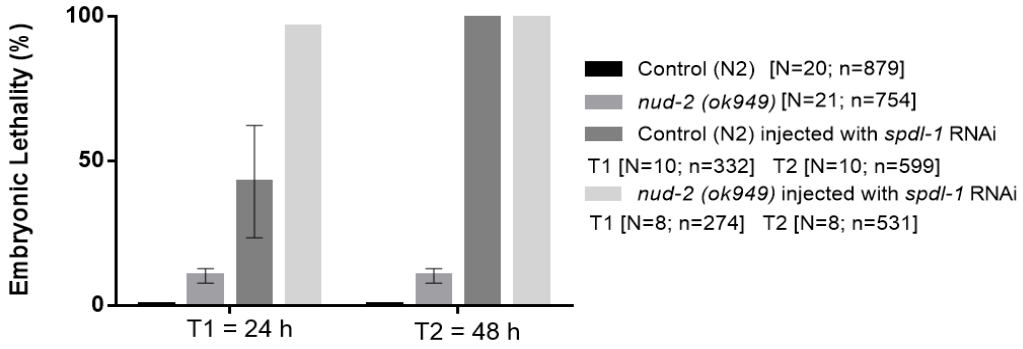


**Figure 30**: Graphical representation of the embryonic lethality present in WT and *nud-2(ok949*) worms after a partial (24h) and full (48h) depletion of SPDL-1. Embryonic lethality is shown in percentage. Respectively, from top to bottom, 0.5%; 10%; 43%, 100%; 97%, 100%. Error bars represent the mean with a 95% CI.

## SPDL-1 does not affect Pronuclear Migration in *nud-2(ok949)*

When taking into consideration the synergistic effect between NUD-2 and SPDL-1 shown in the lethality test (**Figure 31**) I decided to determine if dynein was affected during pronuclear migration. In order to do this, I injected *nud-2(ok949)* with *spdl-1(RNAi)* and assessed the first mitotic division.

The pronucleus in control embryos depleted of SPDL-1 manage to migrate and meet (**Figure 31, Column 2**). When depleting SPDL-1 in a strain already depleted of NUD-2, the phenotype does not seem to worsen, since the pronucleus still manage to migrate and meet, therefore indicative of no interactions between NUD-2/SPDL-1 during pronuclear migration (**Figure 31, Column 4**).

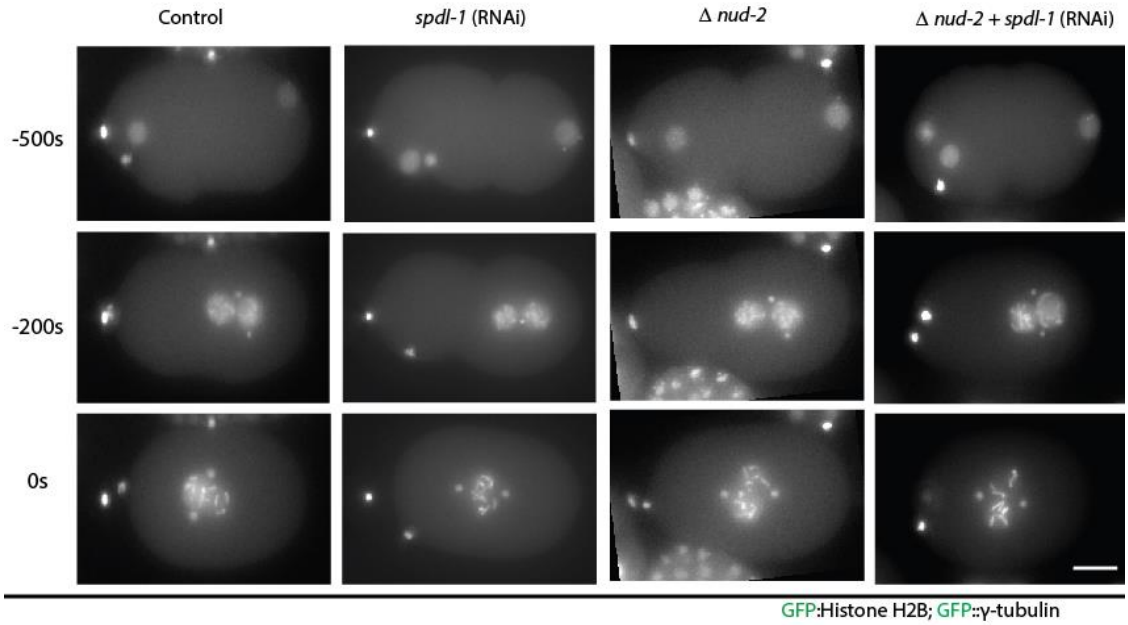


**Figure 31**: Several stills of time-lapse movies of control and *nud-2(ok949)* embryos depleted of SPDL-1. Distinct mitotic events are shown: Early Embryo (-500 s), PM (-200 s), NEBD (0 s). All are aligned relatively to NEBD (0 seconds). Bar corresponds to 10 µm.

Quantification of the first mitotic division enabled to determine that both the female and male pronucleus overlap with embryos lacking NUD-2, which means that SPDL-1 and NUD-2 do not interact or further affect dynein function in pronuclear migration (**Figure 32-A,B**).

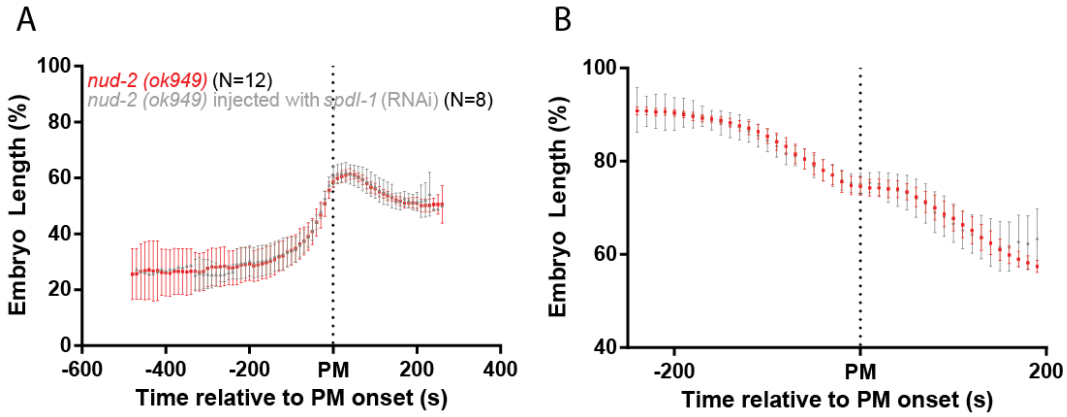


**Figure 32**: Graphical representations comparing *nud-2(ok949)* (Control) with *nud-2(ok949)* injected with *spdl-1* RNAi. This aims at comparing if the two proteins interact with each other in the early *C. elegans* embryo. **A**.Mean of the Female Pronuclear Migration. **B**.Mean of the Migration of the Male Pronuclear Migration. Graphs are aligned either relatively to PM and are normalized to embryo length.

Altogether, these results indicate that SPDL-1 and NUD-2 probably affect dynein function at the kinetochores.

## NUD-2 and BICD-1

### BICD-1 depletion partially suppresses Embryonic Lethality of *nud-2(ok949)* embryos

BICD-1 is reported to be essential for the activation and the recruitment of dynein. In order to determine possible synergetic effects between the NUD-2 and BICD-1 effect on dynein-dependent processes during the first mitotic division, an embryonic lethality assay was conducted on the sensitized *nud-2 (ok949)* background (**Figure 33**).

Results indicate that a partial depletion of BICD-1 in *nud-2 (ok949)* worms (Time Point 1 = 24h) has a 3% while the *nud-2 (ok949)* strain has a 10% embryonic lethality. Regarding the full depletion of BICD-1 (Time Point 2 = 48h), in *nud-2 (ok949)* worms, the embryonic lethality is set at 4% (**Figure 33**).

These results suggest that BICD-1 depletion rescues the *nud-2 (ok949)* associated embryonic lethality.

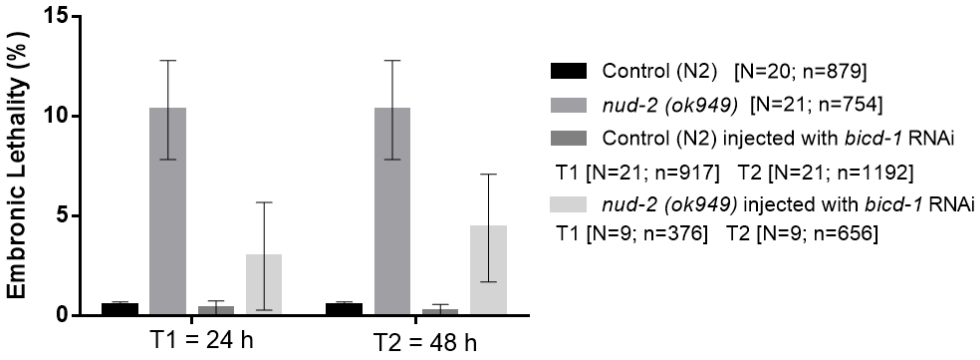


**Figure 33**: Graphical representation of the embryonic lethality present in WT and *nud-2(ok949)* worms after a partial (24h) and full (48h) depletion of BICD-1. Embryonic lethality is shown in percentage. Respectively, top to bottom, 0.5%; 9%; 0.4%, 0.2%; 3%, 4%. Error bars represent the mean with a 95% CI.

## BICD-1 depletion partially rescues the Pronuclear Migration defects observed in *nud-2(ok949)*

Since the lethality tests reveal that BICD-1 rescues the *nud-2(ok949)* embryonic lethality, I decided to assess if Pronuclear Migration was also being rescued.

In order to do this, *nud-2(ok949)* worms were injected with *bicd-1* (RNAi) and filmed while undergoing their first mitotic division.

The individual traces of migration of the female nucleus is similar to WT (**Figure 34-A,B,C**), and not to *nud-2(ok949).* The male pronucleus fully overlaps with *nud-2(ok949)* embryos (**Figure 34-D**).

These results suggest that the female pronucleus migration is partially recovers when *nud-2(ok949)* are injected with *bicd-1* (RNAi).

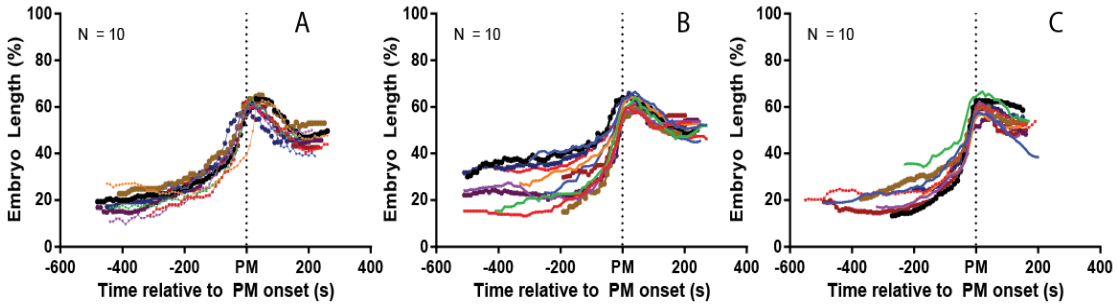


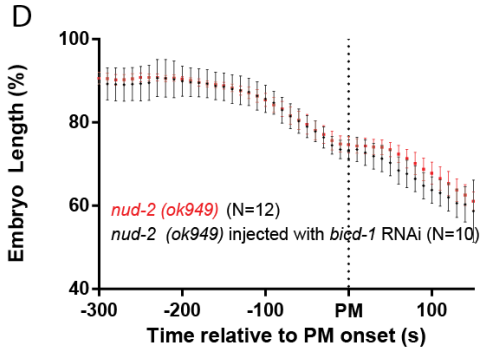


**Figure 34:** Graphical representations comparing *nud-2(ok949)* (Control) with *nud-2(ok949)* injected with *bicd-1* RNAi. This aims at comparing if the two proteins interact with each other in the early *C. elegans* embryo. **A.** Individual traces of Control**. B**. Individual traces of *ok949***. C.** Individual traces of *ok949 + bicd RNAi*. Graphs are aligned either relatively to PM or NEBD and normalized to embryo length. Error bars represent the mean with a 95% CI.

## Dynactin Complex

### Dynactin subunits contribute differentially to embryogenesis

Dynactin is an adaptor between Dynein and cargo. Dynactin is composed of several subunits whose functions in mitosis are still unclear. I therefore aimed at determining the percentage of progeny that is able to complete embryogenesis by conducting an embryonic lethality test.

Results show that worms depleted of distinct Dynactin subunits have different embryonic lethality's (**Figure 35**). In worms lacking ARP-1, ARP-11 or p62, 100% of embryo progeny fails to develop into larvae.

Of the "pointed-end" complex, what is noticeable is that depleting p25 leads to 89% embryonic lethality, while p27 - its partner – leads to a lethality is around 35%. To further complete this assay, a double depletion of both p25 and p27 was also conducted, and results show that it leads an embryonic lethality of almost 100%.

These results indicate that Dynactin subunits probably have different functions in mitosis, particularly the p27 subunit.

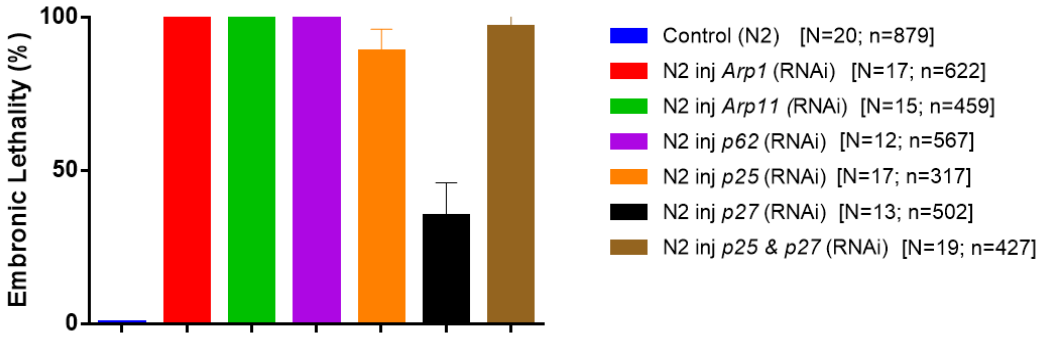


**Figure 35**: Graph representing the embryonic lethality present in WT worms and WT worms injected with RNAi against all the "pointed-end" complex dynactin subunits, and Arp-1, the backbone of dynactin. Embryonic Lethality is displayed in percentage, respectively, from top to bottom: 0.5%, 100%, 100%, 100%, 89%, 35%, 97%.

### Dynactin subunits ARP-1, ARP-11 or p62 are essential for Dynactin stability and function

After determining the Dynactin subunits that were required for viability I decided to observe the phenotype of the embryo undergoing the first mitotic division without particular Dynactin subunits.

Depletion of one of these three dynactin subunits leads to a very similar phenotype in most cases; the centrosomes do not separate and end up detaching from the male nucleus, and there is a slow migration of both the male and the female pronucleus. Also, premature NEBD occurs.

Consequently, no anaphase takes course, leading to a multinucleated embryo (**Figure 36**). In the cases where the centrosomes separate, the centrosomes end up drifting through the cell, and the same mentioned phenotypes occur.

These results indicate that these three Dynactin subunits are essential for maintaining Dynactin integrity and its function.

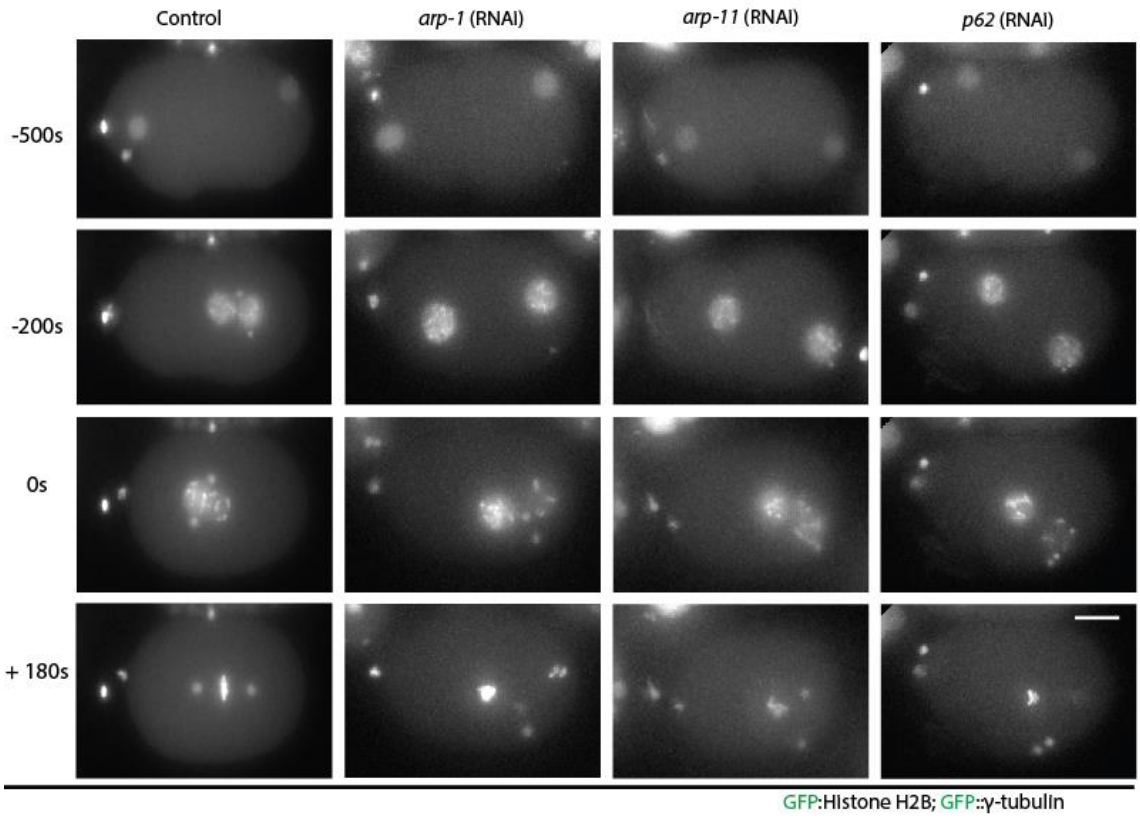


**Figure 36**: Comparing Control with ARP-1, ARP-11 and p62 depletions. Stills of time-lapse movies of the first mitotic division of the *C. elegans* embryo filmed under the Axiovert 200M Microscope. A representative video was chosen per situation. **A.** Control strain that is expressing Histone H2B::GFP, γ-Tubulin::GFP, therefore allowing the visualization of the centrosomes and the chromosomes, in distinct mitotic events: Early Embryo (-500 s), PM (-200 s), NEBD (0 s) and AO (+180 s). **B.** Control injected with *arp-1* RNAi, the backbone of dynactin. **C**. Control injected with *arp-11* RNAi, an essential pointed-end subunit for dynactin stability. **D**. Control injected with *p62* RNAi, another essential pointed-end subunit required for dynactin stability. All the stills are aligned to NEBD (0 seconds). Bar corresponds to 10 µm.

## Dynactin subunits p25 and p27 may have different functions in mitosis

The “pointed-end” dynactin subunits p25 and p27 have been associated with cargo specification. I aimed at determining each subunit function of this dimer. In order to do this I injected control worms with *p25* and/or *p27* RNAi and filmed the first mitotic division.

Depletion of one of these two dynactin subunits lead to a phenotype different from any other studied dynactin subunits depletion; when embryos are depleted of p25, both the male and the female pronucleus migrate slower than control, and NEBD occurs normally. Also, the centrosomes separate and do not detach from the male nucleus.

Nevertheless, spindle rotation appears affected, and chromosome alignment and segregation are severely affected (**Figure 37, Column 2**).

When embryos are depleted of p27 the migration of the male and female pronucleus are similar to control, and NEBD occurs at the correct time. The centrosomes separate normally, and remain attached to the male nucleus. Anaphase shows some mistakes such as lagging chromosomes and missegregation (**Figure 37, Column 3, Data not shown**).

Lastly, a double depletion of these two subunits lead to a similar phenotype to that of p25 depletion on its own. Pronuclear migration is slower, but pronuclear meeting occurs, as well as NEBD. The chromosomes do not properly align and there are problems with segregation (**Figure 37, Column 4**).

These results further support that Dynactin subunit p27 may play a different and important role in Dynein function in mitosis.

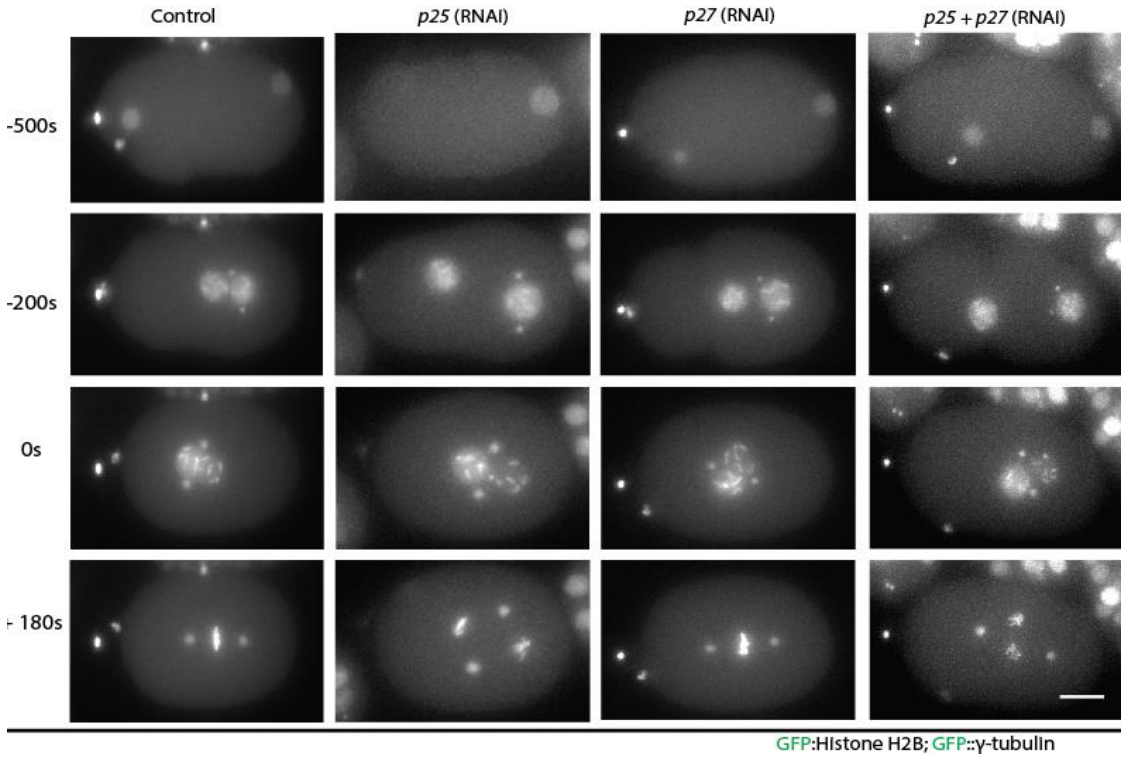


**Figure 37**: Comparing Control with p25, p27 and p25/p27 depletion. Stills of time-lapse movies of the first mitotic division of the *C. elegans* embryo filmed under the Axiovert 200M Microscope. A representative video was chosen per situation. **A**. Control strain that is expressing Histone H2B::GFP, γ-Tubulin::GFP, therefore allowing the visualization of the centrosomes and the chromosomes, in distinct mitotic events: Early Embryo (-500 s), PM (-200 s), NEBD (0 s) and AO (+180 s). **B**. Control injected with *p25* RNAi. **C**. Control injected with *p27* RNAi. **D.** Control injected with both *p25* and *p27* RNAi. All the stills are aligned to NEBD (0 seconds). Bar corresponds to 10 µm.

The individual traces of the migration of the female nucleus indicate that the depletion of p27 does not affect pronuclear migration (**Figure 38-A,B**). This suggests that p27 is not required for dynein function in pronuclear migration.

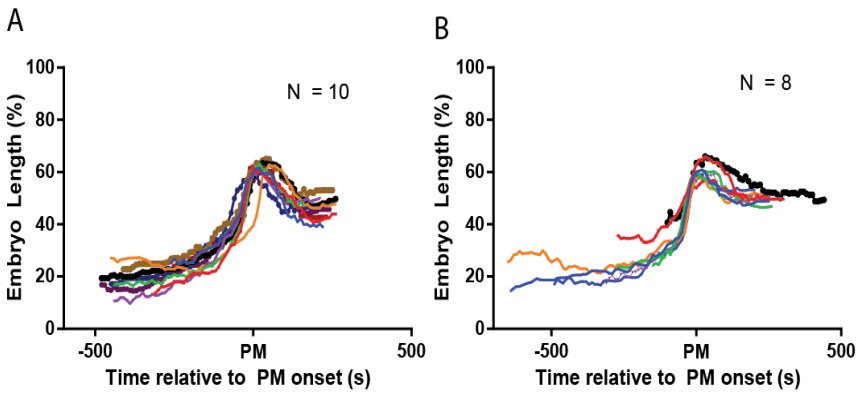


**Figure 38:** Comparing the Individual traces of the Female Pronuclear Migration in control embryos **(A)** and control injected with *p27* RNAi **(B)**. Graphs are normalized to embryo length (%) along time. All graphical representations are aligned relatively to PM (PM), refereed at X=0.

The phenotype of p27 depletion is milder than p25 or p25/p27 double depletion and may therefore give more insights about the function with dynein. Both female and male pronucleus migrate as control (**Figure 39-A, B**).

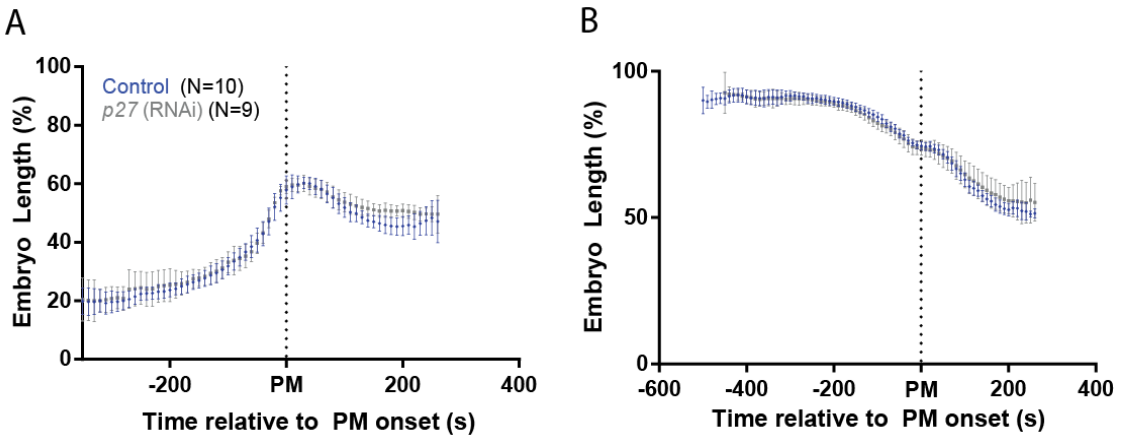


**Figure 39:** Graphical representations comparing strains Control and Control injected with *p27 RNAi*. This aims at comparing if the two proteins interact with each other in the early *C. elegans* embryo. Graphs are aligned either relatively to PM and are normalized to embryo length. Error bars represent the mean with a 95% CI.

## Dynein at the Kinetochore

### NUD-2

**Before the start of Pronuclear Migration the centrosomes of embryos depleted of NUD-2 separate slower than control**

After observing that *nud-2(ok949)* embryos present a slower pronuclear migration I decided to determine if there was any effect on early centrosome separation, which is dynein-dependent and highly stereotypical on wild-type. The distance over time between the two centrosomes that form near the male nucleus was therefore tracked.

This would give insight about the requirement of NUD-2 for dynein function in centrosome separation.

It appears that the centrosomes of embryos depleted of NUD-2 separate slower than Control (student-t test, two-tailed p=0.0853) or NUD-2 restored worms (student-t test, two-tailed p=0.1036) but it is not statistically significant and therefore more examples are required (**Figure 40**).

This suggests that NUD-2 is required for the correct separation of the centrosomes in the early stages of the first mitotic division of the *C. elegans* embryo, essential for female pronuclear migration.

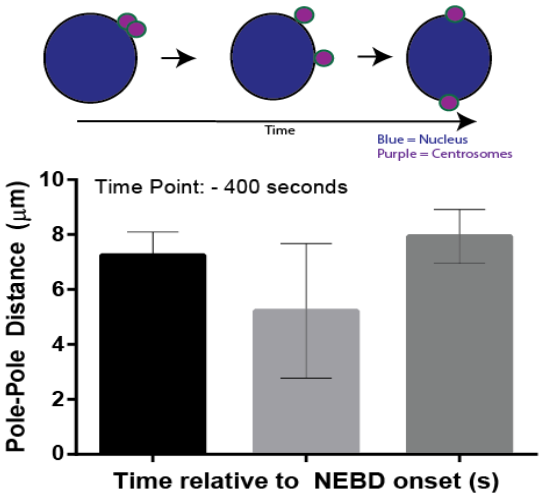


**Figure 40: Top:** Schematic of the dynein-dependent early centrosome separation. **Bottom:** Graph representing the mean distance between the two centrosomes before PM in the Male Nucleus in Control, *nud-2(ok949)*, and NUD-2::mCherry in *nud-2(ok949)*. All data is aligned to NEBD onset, and time point -400 seconds before NEBD was chosen to represent the early centrosome separation. There are three experiments in consideration: Control in Black (N=8), *nud-2(ok949)*, in Light Grey (N=8), and NUD-2::mCherry in *nud-2(ok949)*, in Dark Grey (n=4). Error bars represent the mean with a 95% CI.

These results might explain the slower migration of the female pronucleus towards the male pronucleus, considering that the microtubules that grow from the centrosomes are not able to reach the female nuclear envelope as fast as control centrosomes, where dynein grabs and pulls the microtubules, resulting in the movement of the nucleus towards the center of the embryo.

### NUD-2 and ROD-1

### NUD-2 or ROD-1 deletion lead to a similar premature centrosome separation

Since *nud-2(ok949)* has an effect on pronuclear migration and early centrosome separation, I decided to assess inter-centrosome distance during the first mitotic division.

Dynein at the kinetochores is important for stable KT-MT attachments. On control embryos, centrosomes gradually separate until anaphase leads to the separation of the chromosomes. In *nud-2(ok949)* embryos I observed that during chromosome segregation, just before anaphase onset, a “bump” is visible on the graphical

representation of embryos depleted of NUD-2 (**Figure 41-A**), indicating a premature pole separation.

In our lab, the RZZ complex function in kinetochore-dynein is also being studied, and ROD-1 is known to be a Dynein recruiter to kinetochores. Using as comparison an RNAi already tested by another person, *rod-1* RNAi, results show that lack of NUD-2 leads to a premature pole separation with the same severity as ROD-1 depletion. This bump corresponds to the separation of the poles due to unstable kinetochore-microtubule attachments before anaphase.

On the second graph (**Figure 41-B**) it is visible that the strain that restores NUD-2 into the NUD-2 deletion strain fully overlaps with control values and no longer shows premature pole separation. This indicates that fusion protein is functional and that dynein at the kinetochores is probably affected when NUD-2 is not present.

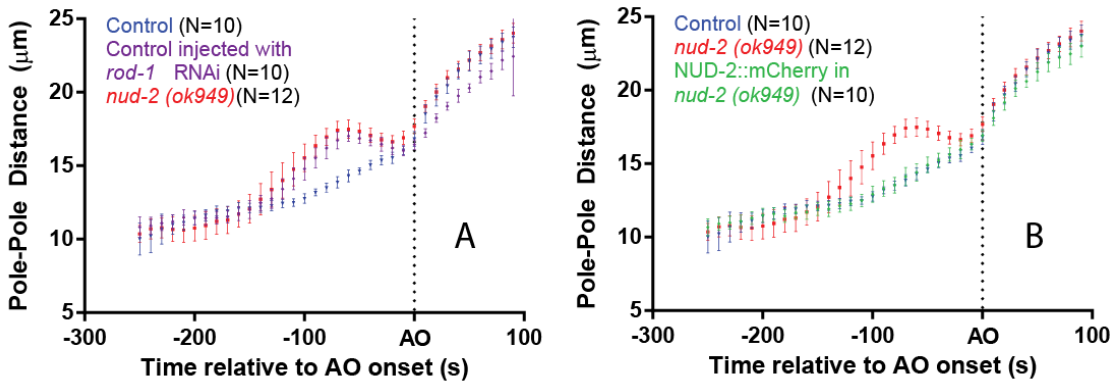


**Figure 41**: Centrosome separation in Control, *nud-2(ok949)*, *rod-1* RNAi, and NUD-2::mCherry in *nud-2(ok949)* strains. Graphs representing the distance between the two poles before Anaphase Onset, and aligned in time to the same event. Control in Blue, *nud-2(ok949)* in Red, Control depleted of ROD-1 in Purple, and NUD-2::mCherry in the *nud-2(ok949)* in Green. **A**. Comparison between control, *nud-2(ok949)* and TH32 injected with *rod-1* RNAi. **B**. Comparison between control *nud-2(ok949)* and NUD-2::mCherry in the *nud-2(ok949)* background. Error bars represent the mean with a 95% CI.

Considering that NUD-2 and ROD-1 both cause a similar phenotype in centrosome separation, a partial and full depletion were conducted on WT and *nud-2(ok949)* worms, by injecting them with *rod-1* RNAi.

Results show that the lethality of WT worms injected with *rod-1* RNAi is 79% after 24 hours, the same seen in worms depleted of NUD-2 and ROD-1 **(Figure 42**). After 48 hours, a full depletion, *rod-1* RNAi is 100% lethal in both strains. As a control, the lethality of WT worms was assessed and is 0.5%. The lethality of strains depleted of NUD-2 was also assessed and is set at around 10%.

This suggests that there is no synthetic lethal relationship between ROD-1 and NUD-2.

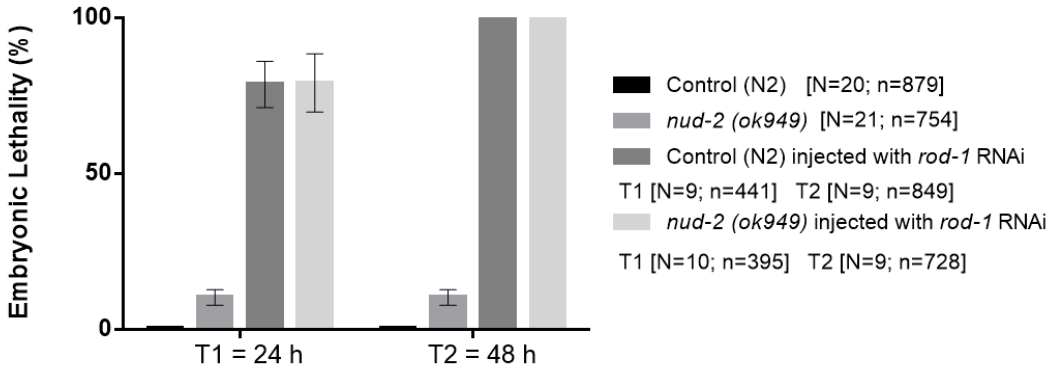


**Figure 42**: Graphical representation of the embryonic lethality present in WT and *nud-2(ok949)* worms after a partial (24h) and full (48h) depletion of ROD-1. Embryonic lethality is shown in percentage. Respectively, top to bottom, 0.5%; 10%; 79%, 100%; 79%, 100%. Error bars represent the mean with a 95% CI.

## NUD-2 and LIS-1

### NUD-2 accumulates at both attached and unattached kinetochores, unlike Dynein, Dynactin and LIS-1 that accumulate only at unattached kinetochores

To determine if Dynein/Dynactin and LIS-1/NUD-2 accumulate at unattached kinetochores I generated monopolar spindles. Injecting embryos with *zyg-1* RNAi prevents centriole replication which has consequences after the first mitotic division. The second division is then unable to separate the chromosomes since it only has one centrosome instead of two, therefore forming a monopolar spindle, where the chromosomes are attached to only one spindle pole. This assay allows to determine if the tagged proteins accumulate at the attached or unattached kinetochores.

In control, Dynein/Dynactin are known to accumulate at unattached kinetochores, since when the microtubules connect to the kinetochore Dynein leaves kinetochores by moving along microtubules towards spindle poles.

The results show that Dynein and Dynactin accumulate at unattached kinetochores (**Figure 43-A**). NUD-2 accumulates at attached and unattached kinetochores (**Figure 43-B**). This assay also shows that LIS-1 accumulates at the kinetochores (**Figure 43-C**), as does Dynein and Dynactin.

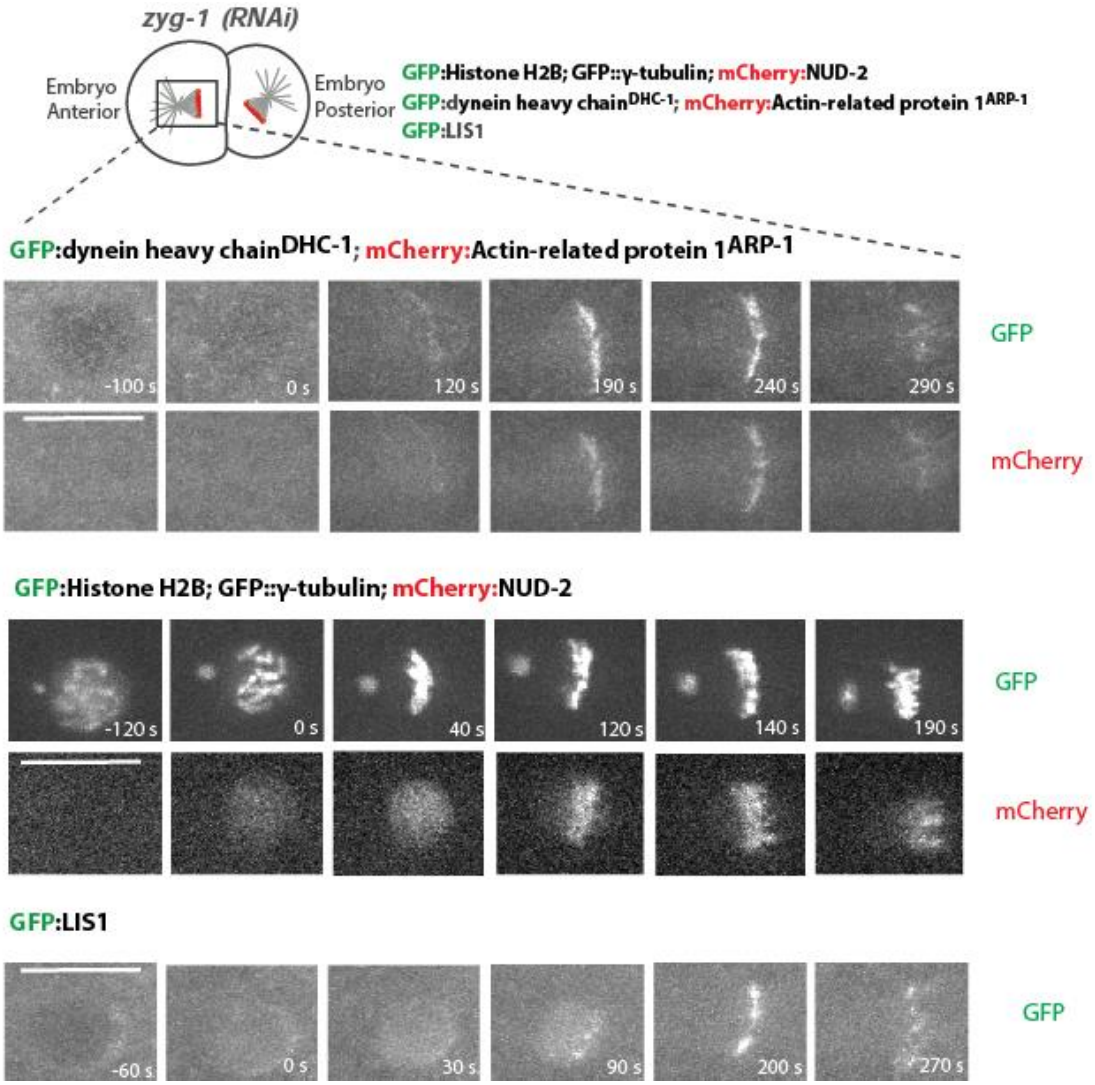


**Figure 43**: Several stills from representative time-lapse movies of the monopolar spindle obtained in the second mitotic division by injection of *zyg-1* RNAi: DHC-1::GFP;ARP1::mCherry, NUD-2::mCherry; Histone H2B::GFP, and LIS1::GFP. All examples are aligned to NEBD that corresponds to 0 seconds. Bar corresponds to 10 µm.

Since the premature pole separation seen when embryos lack NUD-2 is indicative of problems with Dynein at the kinetochore, I decided to determine if the accumulation or function of Dynein/Dynactin, and LIS-1 is affected in the absence of NUD-2. This will allow to determine if Dynein and Dynactin manage to locate and properly function in the absence of NUD-2.

In order to do this I crossed Histone H2B::mCherry with DHC-1::GFP, and then crossed this strain with the *nud-2(ok949).* This strain will allow me to quantify Dynein at the kinetochore with and without NUD-2, giving insight about NUD-2 requirement for Dynein localization/function.

It was visible that Dynein accumulation at the kinetochores on the monopolar spindle formed during the second division of the *C. elegans* embryo was decreased when NUD-2 was absent (**Figure 44-A**). Quantification of DHC-1 Kinetochore

Fluorescence Intensity revealed that in the absence of NUD-2 Dynein at the kinetochores decreased by almost 3-fold (**Figure 44-B**).

These results show that NUD-2 contributes to Dynein recruitment to kinetochores.

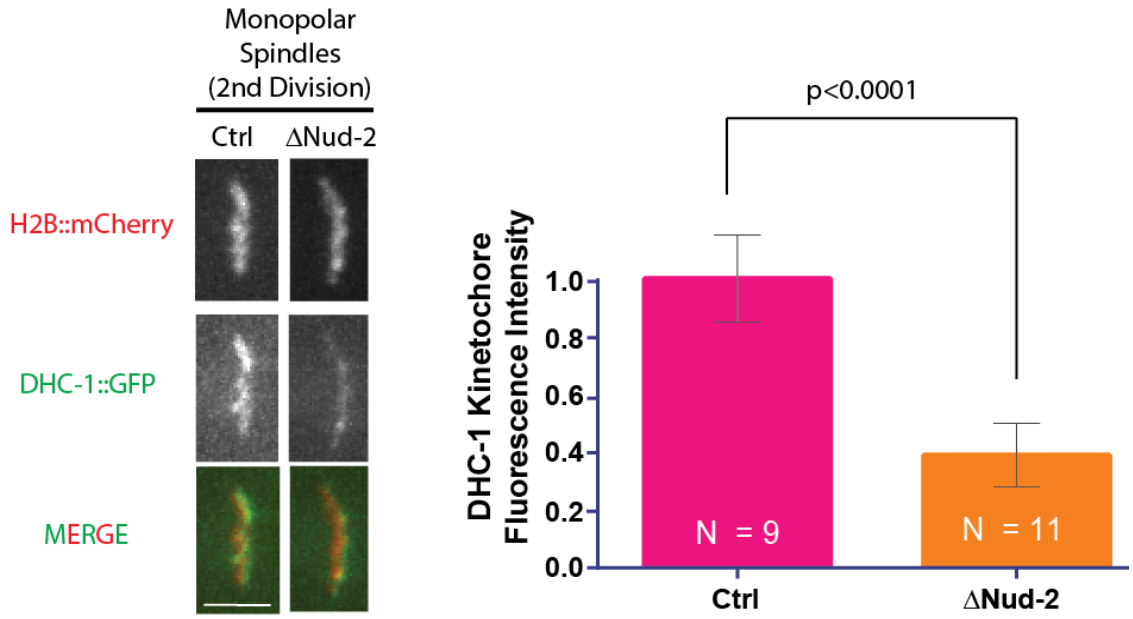


**Figure 44**: Analysis of DHC-1 localization on monopolar spindles generated by ZYG-1 depletion in the presence and absence of NUD-2. **A**. H2B::mCherry and DHC-1::GFP false-colored, was crossed into a *nud-2(ok949)* strain. **B.** Graph on the right shows DHC-1 fluorescence intensity measured. N is the number of embryos imaged and error bars represent the 95% confidence interval of the mean. The p-value of an unpaired t-test shows that this difference is considered to be extremely statistically significant (p<0.0001). Bar = 5 μm.

## The 10% embryonic lethality associated with *nud-2 (ok949)* lethality is probably due to errors in chromosome segregation

After determining that NUD-2 is functionally important for embryonic development, and that embryos lacking NUD-2 present non-lethal defects in pronuclear migration and severe non-lethal premature centrosome separation, the 10% embryonic lethality remained unexplained.

In order to determine if the lethality was due to problems in chromosome segregation I assessed the first mitotic division from NEBD to AO, to observe the presence lagging chromatin (**Figure 45-A**). I observed that in the control the chromosomes normally separated without lagging chromatin, whereas when embryos where depleted of NUD-2 there were cases of severe lagging chromatin (**Figure 45-A,B**).

When assessing the percentage of anaphases with lagging chromatin I determined 0% of control embryos present lagging chromatin whereas in embryos lacking NUD-2 the percentage was 20% (**Figure 45-C**).

These results suggest that the embryonic lethality present in the *(nud-2 ok949)* is most likely due to miss-segregation of chromosomes.

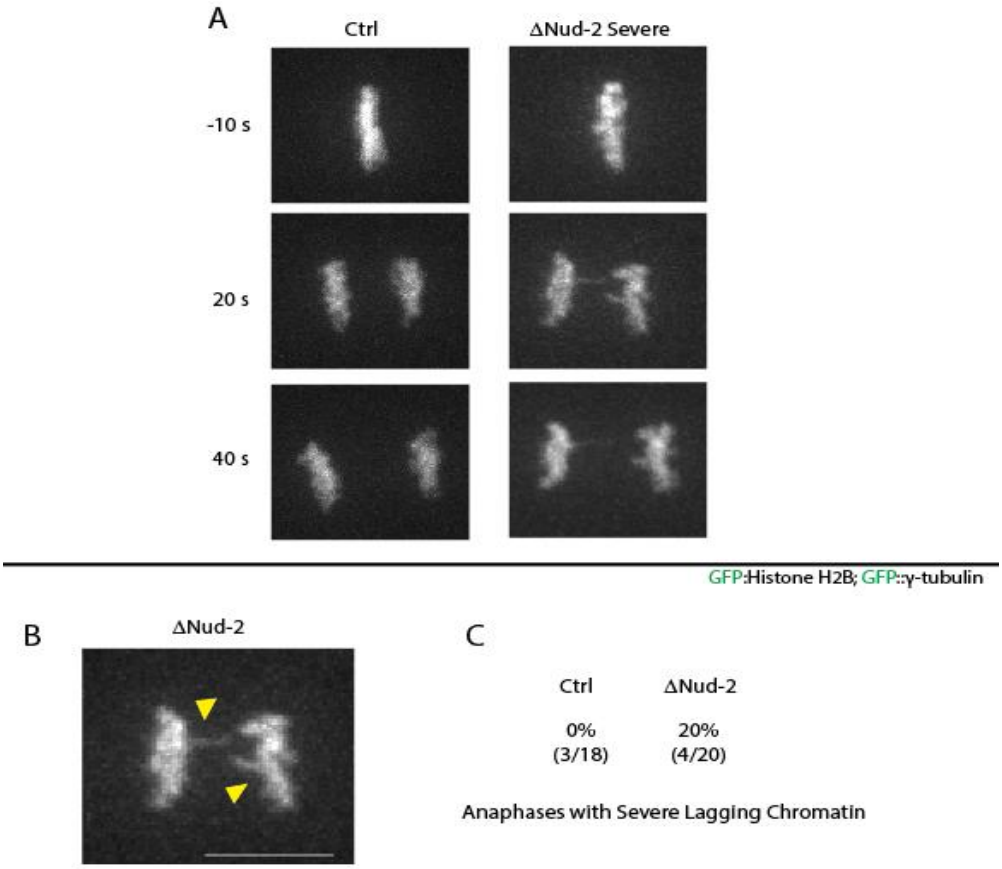


**Figure 45**: Schematic of chromosome segregation in control and *nud-2 (ok949)* embryos. **A**. Phenotypes seen in Control and embryos lacking NUD-2 for the indicated conditions through time. Embryos are aligned to NEBD (0 s). **B.** Amplified example of a severe miss-segregation in *nud-2 (ok949).* **C.** Number of embryos that have lagging chromatin in the control and in the *nud-2 (ok949)* background.

## NUD-2 and BICD-1

### BICD-1 partially rescues *nud-2 (ok949)* phenotype at the kinetochores

Since the embryonic lethality test reveal that BICD-1 recovers the *nud-2 (ok949)* embryonic lethality, and considering that pronuclear migration is also partially rescued by the RNAi, I decided to look at pole-separation that gives information about kinetochore-dynein.

The graphical representation of the distance between the centrosomes, shows that *nud-2 (ok949)* worms injected with *bicd-1* RNAi have a smaller premature pole separation caused by the *nud-2 (ok949)* alone (**Figure 46**).

The results of BICD-1 depletions suggest that a lack of BICD-1 partially suppresses the *nud-2 (ok949)* phenotype, both in pronuclear migration and in centrosome separation.

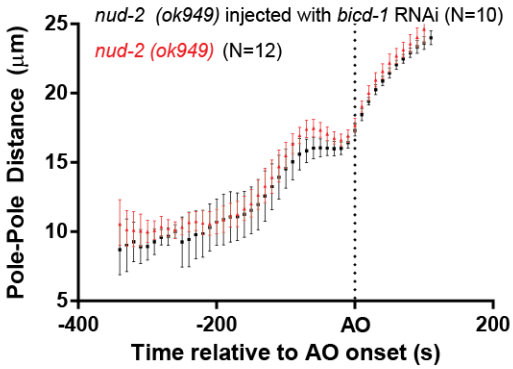


**Figure 46**: Centrosome separation in *nud-2(ok949)* and *nud-2(ok949)* injected with *bicd-1* (RNAi). Graphs representing the distance between the two poles before Anaphase Onset, and aligned in time to the same event. Error bars represent the mean with a 95% CI.

## Dynactin Complex

### Lack of p25 and p27 leads to severe segregation problems

The dynactin subunits p25 and p27 are thought to be required for cargo specification. Also, the embryonic lethality test revealed that they are not as essential for viability as the other dynactin subunits. Therefore, their phenotype was examined during the first mitotic division to determine any effects of dynein-dependent functions.

### Depletion of p27 leads to a premature pole separation

Since the depletion of subunit p27 leads to a relatively low embryonic lethality when comparing to the depletion of other Dynactin subunits, the corresponding phenotype was assessed. Similar to what happens in ROD-1 or NUD-2 depletion, *p27* RNAi, also leads to a premature pole separation (**Figure 47)**, which indicates that Dynein function at the kinetochores is affected. Specifically, it indicates that the KT-MT attachments are not correctly established.

The severity of the *p27* (RNAi) premature pole-separation is variable but appears to be very similar or worse than ROD-1 depletion (that is 100% embryonic lethal). Results therefore suggest that p27 may have an important role in kinetochore-dynein in mitosis.

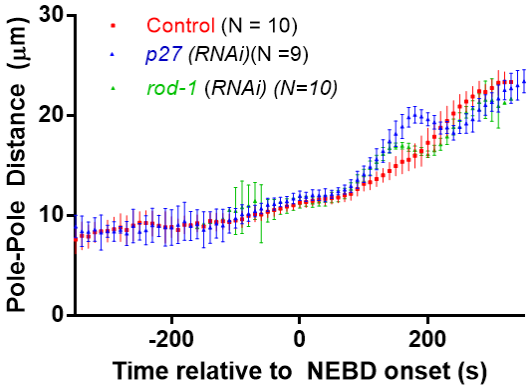


**Figure 47**: Graphical representations comparing the Control, *p27 RNAi* and *rod-1 RNAi*. Graphs is aligned either relatively to Nuclear Envelope Breakdown and is normalized to embryo length. Error bars represent the mean with a 95% CI.

# Discussion

### NUD-2 contributes to cell division in the *C. elegans* embryo

In *C. elegans* LIS-1 is known to be required for all dynein-dependent processes [39,40,79], and consequently, cell viability.

I determined the requirement of its binding partner NUD-2 for embryo survival and for dynein-dependent cell division processes. Depleting NUD-2 lead to 10% embryonic lethality (**Figure 24**). After determining that this protein is partially required for viability, quantitative live-imaging assays were conducted in order to determine the nature of the defects causing the lethality.

Looking into the phenotype of NUD-2 depletion, it was noticeable that both the female and male pronuclear migration was slower (**Figure 25-27**). This could be explained by taking into consideration that LIS-1 with NUD-2 induce a persistent-force dynein state that allows dynein to transport under high-load conditions [49]. Similar to what occurs when LIS-1 is depleted, perhaps without NUD-2 dynein is less capable of maintaining the attachments to microtubules, and therefore has difficulty in transporting heavy cargo, such as a nucleus.

Looking at the early centrosome separation of embryos depleted of NUD-2, it is noticeable that centrosomes separate slower than in wild type embryos (**Figure 40**). This delay in centrosome separation during prophase could also contribute to the slower migration of both nuclei. Dynein located on the nuclear envelope of the female pronucleus pulls on microtubules that grow from the centrosomes attached to the male pronucleus. This provides the forces for nuclear migration. When centrosome separation is delayed, a smaller proportion of microtubules will grow from the male pronucleus towards the anterior side of the embryo where the female nucleus is located, resulting in smaller force production for the movement of either pronucleus.

NudE is proposed to recruit Lis1 to dynein, and so it is likely that the defects in pronuclear migration I observed in embryos lacking NUD-2 are caused by the inability of LIS-1 to properly interact with dynein. If LIS-1 is indeed defective in interacting with dynein in the absence of NUD-2, one would predict that embryos lacking NUD-2 would be highly sensitive to a lowering of LIS-1 levels. Indeed, I observed a significant enhancement of lethality when I partially depleted LIS-1 in the *nud-2 (ok949)* strain compared to LIS-1 partial depletions alone. Live imaging experiments revealed that the pronuclear migration defect was severely enhanced in the NUD-2 null background when LIS-1 was partially depleted. These results are in agreement with the model that

one role of NUD-2 is to mediate the LIS-1-dynein interaction. It will be important to directly determine how the absence of NUD-2 affects the localization of LIS-1, particularly on the nuclear envelope where dynein is assumed to generate forces important for centrosome separation and pronuclear migration. I am currently generating a strain expressing GFP::LIS-1 that can be crossed into the *nud-2 KO* strain to address this question.

**NUD-2 has a role in recruiting dynein to mitotic kinetochores**

The premature spindle pole separation in prometaphase (not to be confused with centrosome separation in prophase) seen in embryos lacking NUD-2 is as severe as that seen when the RZZ complex protein Rough Deal (ROD-1) is depleted (**Figure 41**), which is responsible for dynein recruitment to mitotic kinetochores. Premature spindle pole separation is indicative of defective kinetochore-microtubule attachments, which counteract cortical forces that pull on the centrosomes. My results show that NUD-2, like the RZZ complex, is involved in recruiting dynein to kinetochores. However, while depletion of ROD-1 completely abolishes dynein recruitment, kinetochores lacking NUD-2 still have 30% of wild type dynein levels. The pole tracking data demonstrate that the residual dynein at kinetochores in the *nud-2 KO* strain is equally deficient in resisting tension as kinetochore fully depleted of dynein in ROD-1 depletions.

Why then does NUD-2 depletion lead to relatively low embryonic lethality, whereas ROD-1 depletion results in 100% embryonic lethality? One possible explanation is that dynein's role at kinetochores is not limited to force production to resist tension, which is what the pole tracking assay is measuring. For example, dynein could also be involved in orienting the sister kinetochores towards the spindle poles such that merotelic attachments are avoided (one sister kinetochore attached to both poles). Merotelic attachments results in lagging chromosomes in anaphase, because the sister kinetochore is pulled to both poles simultaneously. Indeed, ROD-1 depleted embryos typically have lagging chromosomes in anaphase. I also filmed chromosome segregation in embryos lacking NUD-2 and observed a significant increase of lagging anaphase chromosomes compared to controls. However, the segregation defect was milder than in ROD-1 depleted embryos. This could explain the differences in lethality between the *nud-2 KO* strain and ROD-1 depletions and perhaps indicates that the residual dynein at kinetochores in embryos lacking NUD-2 is sufficient to partially avert merotelic attachments.

I suspect that the lack of NUD-2 at kinetochores also depletes its binding partner LIS-1 from kinetochores. This hypothesis remains to be tested. Interestingly,

NUD-2::mCherry accumulated at both attached and unattached kinetochores, whereas dynein, dynactin and LIS-1 accumulated exclusively at unattached kinetochores. This suggests that NUD-2 interacts with a kinetochore receptor whose localization to kinetochores does not depend on microtubule attachment status. This receptor remains to be identified.

**NUD-2 and SPDL-1 do not affect Dynein function during Pronuclear Migration and NEBD**

The coiled-coil protein Spindly acts downstream of the RZZ Complex at kinetochores to recruit dynein. Similar to what I observed with LIS-1, I found that partially depleting Spindly from embryos lacking NUD-2 resulted in increased lethality compared to partial Spindly depletion on their own. To determine the cause of the synthetic lethal interaction, I performed live imaging experiments. This revealed that Spindly depletion in embryos lacking NUD-2 does not exacerbate the pronuclear migration defect, which supports the notion that Spindly function is limited to kinetochores. Therefore, the likely explanation for the synthetic lethal interaction between Spindly and NUD-2 is their common role in recruiting dynein to kinetochores: because dynein levels are already lowered by 60% in the absence of NUD-2, embryos are highly sensitive to lowering the levels of Spindly, dynein's other kinetochore receptor.

**BICD-1 does not contribute to cell division in the *C. elegans* embryo**

Bicaudal D is an ubiquitous dynein co-factor, but, unlike Lis1, NudE, and Dynactin, it is specific to metazoans. The studies of Bicaudal D suggest that it serves as a modular link between dynein and cargo, and is involved in dynein recruitment. Since Bicaudal D is known to contribute to nuclear positioning and spindle organization [80], I tested whether the *C. elegans* homolog BICD-1 contributes to pronuclear migration or mitotic spindle assembly in the one-cell embryo. I reasoned that depleting BICD-1 in embryos lacking NUD-2 would be the most promising approach to uncover any potential role of BICD-1 in these processes. The *nud-2* KO strain was thus injected with *bicd-1* (RNAi) (**Figure 33, 34**). Embryonic lethality tests showed a slight but significant rescue of the lethality in the *nud-2 KO* strain injected with *bicd-1* dsRNA. In agreement with the partial rescue of lethality, I also observed a partial rescue of the pronuclear migration defect and the premature pole-pole separation defect.

Interestingly, the fact that BICD-1 depletion is able to partially rescue the defects in the *nud-2 KO* strain suggests that BICD-1 may negatively impact dynein

function in the absence of NUD-2. It will be interesting to test whether BICD-1 depletion also partially rescues the defects of LIS-1 depletions and to determine whether BICD-1 co-localizes with dynein in the one cell embryo.

**Dynactin and Dynein colocalize during the first Mitotic Division**

Dynactin is an essential part of the cytoplasmic dynein motor that enhances motor processivity and serves as an adaptor that allows dynein to bind to cargoes. Dynein function *in vivo* depends upon Dynactin and it is therefore expected that these two complexes colocalize in the cell.

A strain co-expressing both Dynein and Dynactin subunits fused to GFP and mCherry, respectively, allowed me to confirm that these two complexes colocalize at the Nuclear Envelope, the Centrosomes, the Spindle and the Cytoplasm [26,27].

**The Dynactin Subunits Arp1, p62 and Arp11 are essential for Dynein Function**

Considering that the Arp-1 filament is the backbone of the dynactin structure, depletion of Arp-1 was expected to result in a loss of dynein functions that are dynactin dependent.

Indeed, *arp-1* RNAi produced severe phenotype in all the assays used to assess dynein function in mitosis that was indistinguishable from dynein inhibitions. Depletion of the Arp11 subunit, which caps one end on dynactin's Arp1 filament, and p62, which binds Arp11 and Arp1, also severely perturbed the mitotic functions of dynein, such as nuclear rotation [33] and positioning [34], centrosome separation [35] and nuclear envelope breakdown[26]. The three dynactin subunits, Arp1, Arp11 and p62 are therefore essential for dynactin function, and consequently for dynein function. Consistently, their individual depletion leads to 100% embryonic lethality (**Figure 35**). In other organisms, Arp11 and p62 are required for the stability of the dynactin complex. This would explain the penetrant phenotype of Arp11 and p62 depletion. To test whether this is the case for the *C. elegans* dynactin complex will require monitoring dynactin subunit levels by western blot after depletion of Arp11 and p62.

**Dynactin subunits p25 and p27 might play a role in the recruitment of Dynein to the kinetochores**

The subunits p25 and p27 are not observed in yeast and are thought to be dispensable for dynactin's most basic functions [53]. Studies in *Drosophila* S2 cells and human cells suggest that p27 and p25 contribute to, and perhaps specify, the association of dynactin with dynein cargoes [53]. The same studies suggest that the

heterodimer p25/p27 can be removed without impacting dynactin stability and most, dynein-based motile phenomena.

In this study, I found that depleting *C. elegans* embryos of p25 lead to a very high embryonic lethality of nearly 90% (**Figure 35**). Depletion of p25 affected spindle positioning and chromosome segregation, and pronuclear migration was severely delayed (**Figure 37**), perhaps indicating that p25 has a specific role in the targeting of dynein to kinetochores.

Depletion of p27 was less lethal, with an embryonic lethality around 35% (**Figure 35**). The phenotype in the first mitotic division was similar to the one seen in *p25*-depleted embryos, but less chromosome segregation errors occurred (**Figure 37**). Less severe defects of p27 depletion compared to p25 depletion were also observed in another study [56]. In the same publication, authors describe that the depletion of p25 and p27 lead to reduced Arp1 levels. Contradictorily, in another study authors state that depletion of either p25 or p27 resulted in the loss of both subunits but that dynactin structure remained intact [59]. According to the proposed subunit interactions of the pointed-end complex [59], it is plausible that depletion of p25 ends up depleting p27 also. This would explain the increased severity p25 depletion compared to and p27 depletions.

Since p25 and p27 are proposed to function as a complex, the phenotype of the double depletion was assessed. The embryonic lethality now reached 100%, which is higher than individual depletion of p25 or p27. Live imaging showed that the phenotype in one cell embryos was slightly worse in double depletions than in p25 depletions. This indicates that co-depleting p25 and p27 may be preferable over single depletions for functional studies of the complex. Despite the penetrant embryonic lethality, the phenotype of co-depleting p25 and p27 did not achieve that of the dynactin null phenotype. This may indicate a more specific role of the p25/p27 complex in dynactin function, or it could be due to a partial de-stabilization of the dynactin complex. Monitoring of dynactin subunits levels by western blot will be required to exclude the latter possibility.

### Conclusion and Future Perspectives

The function of several dynein cofactors in mitosis was identified, which will allow future studies to resolve how the distinct mitotic functions of dynein are differentially regulated by its co-factors.

In the future, and to address if LIS-1 localization is affected in the absence of its binding partner NUD-2, we could tag the endogenous LIS-1 with GFP, by means of a new technique that allows to edit the *C. elegans* genome using the clustered, regularly

interspersed, short palindromic repeats (CRISPR) RNA-guided Cas9 nuclease and homologous recombination [81]. Then, LIS-1 localization and recruitment to KTs would be evaluated when LIS-1 is depleted of its binding partner NUD-2.

Recent yeast-two hybrid results reveal that NUD-2 interacts with HCP-1 the homolog of the mammalian centromere protein-F (CENP-F)). This is in agreement with the model that supports a major function of Cenp-F in linking the Ndel1/Nde1/Lis1/Dynein pathway to kinetochores [82]. Therefore, it is expected that when HCP-1 is depleted, the NUD-2 levels at the kinetochores decrease substantially.

Moreover, to determine the cause of the synthetic lethal interaction between NUD-2 and LIS-1 and also NUD-2 and SPDL-1, live imaging experiments could be conducted. The first interaction would reveal if the pronuclear migration defects are exacerbated, which would show that NUD-2 is required for LIS-1 targeting to Dynein, and the second interaction will support the notion that SPDL-1 function is limited to kinetochores.

Recent studies in *Xenopus* egg extracts suggest that Lis1 and Dynactin alternatively engage with dynein to allow the motor to promote spindle assembly [83]. This is consistent with a model in which DIC and Lis1-binding sites in amino acids 1-201 of NudE facilitates Lis1 recruitment to dynein by providing a multivalent interaction. We will assess in *C. elegans* if NUD-2 binds LIS-1 and the DYCI-1 (Dynein Intermediate Chain) through Y2H assays. We will also make a LIS-1 and DYCI-1 antibody to perform Western Blots that will reveal the protein levels of each of these four proteins (NUD-2, LIS-1, Dynein and Dynactin), in the absence of another.

Considering the separation-of-function mutants that affect either the DIC or the Lis1 binding in the *Xenopus* egg extracts study [83], we will determine if the residues are conserved in *C. elegans* and we will conduct several assays to determine if the model that these authors suggest is applicable, *in vivo,* to the *C. elegans* model. These assays consist of embryonic lethality tests, synthetic embryonic lethality tests, loss-of-function phenotype characterization through live-imaging assays, protein accumulation at the kinetochores, biochemistry and others.

This will give insight on NUD-2/LIS-1 and Dynein/Dynactin regulation and interaction *in vivo* which remain uncharacterized.

# References

1. Nasmyth, K. Disseminating the genome: joining, resolving, and separating sister chromatids during mitosis and meiosis. *Annu. Rev. Genet.* **35,** 673–745 (2001).
2. Stevens, D., Gassmann, R., Oegema, K. & Desai, A. Uncoordinated Loss of Chromatid Cohesion Is a Common Outcome of Extended Metaphase Arrest. *PLoS One* **6,** e22969 (2011).
3. Compton, D. A. Spindle assembly in animal cells. *Annu. Rev. Biochem.* **69,** 95–114 (2000).
4. Gordon, D. J., Resio, B. & Pellman, D. Causes and consequences of aneuploidy in cancer. *Nat. Rev. Genet.* **13,** 189–203 (2012).
5. Maiato, H., DeLuca, J., Salmon, E. D. & Earnshaw, W. C. The dynamic kinetochore-microtubule interface. *J. Cell Sci.* **117,** 5461–77 (2004).
6. Doxsey, S., McCollum, D. & Theurkauf, W. Centrosomes in cellular regulation. *Annu. Rev. Cell Dev. Biol.* **21,** 411–34 (2005).
7. Reinsch, S. & Gönczy, P. Mechanisms of nuclear positioning. *J. Cell Sci.* **111 ( Pt 1,** 2283–95 (1998).
8. Gönczy, P., Pichler, S., Kirkham, M. & Hyman, A. A. Cytoplasmic dynein is required for distinct aspects of MTOC positioning, including centrosome separation, in the one cell stage *Caenorhabditis elegans* embryo. *J. Cell Biol.* **147,** 135–50 (1999).
9. Mitchison, T. & Kirschner, M. Dynamic instability of microtubule growth. *Nature* **312,** 237–242 (1984).
10. Akhmanova, A. & Steinmetz, M. O. Tracking the ends: a dynamic protein network controls the fate of microtubule tips. *Nat. Rev. Mol. Cell Biol.* **9,** 309–22 (2008).
11. Kapoor, T. M. & Compton, D. A. Searching for the middle ground: mechanisms of chromosome alignment during mitosis. *J. Cell Biol.* **157,** 551–6 (2002).
12. Microtubule Motors and Movements. (2000). at <http://www.ncbi.nlm.nih.gov/books/NBK9833/>
13. Gibbons, I.R. Studies on the protein components of cilia from *Tetrahymena pyriformis*. S. *Proc. Natl. Acad. Sci. U. S. A.* **50,** 1002–10 (1963).
14. Gibbons, I. R. & Rowe, A. J. Dynein: A Protein with Adenosine Triphosphatase Activity from Cilia. *Science* **149,** 424–6 (1965).

15. Paschal, B. M., Shpetner, H. S. & Vallee, R. B. MAP 1C is a microtubule-activated ATPase which translocates microtubules *in vitro* and has dynein-like properties. *J. Cell Biol.* **105,** 1273–82 (1987).
16. Schroer, T. A., Steuer, E. R. & Sheetz, M. P. Cytoplasmic dynein is a minus end-directed motor for membranous organelles. *Cell* **56,** 937–946 (1989).
17. Vale, R. D. & Milligan, R. A. The way things move: looking under the hood of molecular motor proteins. *Science* **288,** 88–95 (2000).
18. Mallik, R., Carter, B. C., Lex, S. A., King, S. J. & Gross, S. P. Cytoplasmic dynein functions as a gear in response to load. *Nature* **427,** 649–52 (2004).
19. Gennerich, A. & Vale, R. D. Walking the walk: how kinesin and dynein coordinate their steps. *Curr. Opin. Cell Biol.* **21,** 59–67 (2009).
20. Reck-Peterson, S. L. *et al.* Single-molecule analysis of dynein processivity and stepping behavior. *Cell* **126,** 335–48 (2006).
21. Neuwald, A. F., Aravind, L., Spouge, J. L. & Koonin, E. V. AAA+: A class of chaperone-like ATPases associated with the assembly, operation, and disassembly of protein complexes. *Genome Res.* **9,** 27–43 (1999).
22. Wickstead, B. & Gull, K. Dyneins across eukaryotes: a comparative genomic analysis. *Traffic* **8,** 1708–21 (2007).
23. Moore, J. K., Stuchell-Brereton, M. D. & Cooper, J. A. Function of dynein in budding yeast: mitotic spindle positioning in a polarized cell. *Cell Motil. Cytoskeleton* **66,** 546–55 (2009).
24. Egan, M. J., McClintock, M. A. & Reck-Peterson, S. L. Microtubule-based transport in filamentous fungi. *Curr. Opin. Microbiol.* **15,** 637–45 (2012).
25. Koonce, M. P. Dictyostelium, a model organism for microtubule-based transport. *Protist* **151,** 17–25 (2000).
26. Salina, D. *et al.* Cytoplasmic dynein as a facilitator of nuclear envelope breakdown. *Cell* **108,** 97–107 (2002).
27. Vaisberg, E. A., Koonce, M. P. & McIntosh, J. R. Cytoplasmic dynein plays a role in mammalian mitotic spindle formation. *J. Cell Biol.* **123,** 849–58 (1993).
28. Howell, B. J. *et al.* Cytoplasmic dynein/dynactin drives kinetochore protein transport to the spindle poles and has a role in mitotic spindle checkpoint inactivation. *J. Cell Biol.* **155,** 1159–72 (2001).
29. McNally, F. J. Mechanisms of spindle positioning. *J. Cell Biol.* **200,** 131–40 (2013).
30. Collins, E. S., Balchand, S. K., Faraci, J. L., Wadsworth, P. & Lee, W.-L. Cell cycle-regulated cortical dynein/dynactin promotes symmetric cell division by differential pole motion in anaphase. *Mol. Biol. Cell* **23,** 3380–90 (2012).

31. Mitchison, T. *et al.* Growth, interaction, and positioning of microtubule asters in extremely large vertebrate embryo cells. *Cytoskeleton (Hoboken).* **69,** 738–50 (2012).
32. Kimura, K. & Kimura, A. Intracellular organelles mediate cytoplasmic pulling force for centrosome centration in the *Caenorhabditis elegans* early embryo. *Proc. Natl. Acad. Sci. U. S. A.* **108,** 137–42 (2011).
33. Levy, J. R. & Holzbaur, E. L. F. Dynein drives nuclear rotation during forward progression of motile fibroblasts. *J. Cell Sci.* **121,** 3187–95 (2008).
34. Tsai, J.-W., Bremner, K. H. & Vallee, R. B. Dual subcellular roles for LIS1 and dynein in radial neuronal migration in live brain tissue. *Nat. Neurosci.* **10,** 970–9 (2007).
35. Van Heesbeen, R. G. H. P., Raaijmakers, J. A., Tanenbaum, M. E. & Medema, R. H. Nuclear envelope-associated dynein cooperates with Eg5 to drive prophase centrosome separation. *Commun. Integr. Biol.* **6,** e23841 (2013).
36. Foley, E. A. & Kapoor, T. M. Microtubule attachment and spindle assembly checkpoint signalling at the kinetochore. *Nat. Rev. Mol. Cell Biol.* **14,** 25–37 (2013).
37. Varma, D., Monzo, P., Stehman, S. A. & Vallee, R. B. Direct role of dynein motor in stable kinetochore-microtubule attachment, orientation, and alignment. *J. Cell Biol.* **182,** 1045–54 (2008).
38. Reiner, O. *et al.* Isolation of a Miller-Dieker lissencephaly gene containing G protein beta-subunit-like repeats. *Nature* **364,** 717–21 (1993).
39. Tsai, L.-H. & Gleeson, J. G. Nucleokinesis in neuronal migration. *Neuron* **46,** 383–8 (2005).
40. Tai, C.-Y., Dujardin, D. L., Faulkner, N. E. & Vallee, R. B. Role of dynein, dynactin, and CLIP-170 interactions in LIS1 kinetochore function. *J. Cell Biol.* **156,** 959–68 (2002).
41. Dujardin, D. L. & Vallee, R. B. Dynein at the cortex. *Curr. Opin. Cell Biol.* **14,** 44–49 (2002).
42. Dujardin, D. L. *et al.* A role for cytoplasmic dynein and LIS1 in directed cell movement. *J. Cell Biol.* **163,** 1205–11 (2003).
43. Huang, J., Roberts, A. J., Leschziner, A. E. & Reck-Peterson, S. L. Lis1 acts as a “clutch” between the ATPase and microtubule-binding domains of the dynein motor. *Cell* **150,** 975–86 (2012).
44. Efimov, V. P. & Morris, N. R. The LIS1-related NUDF protein of *Aspergillus nidulans* interacts with the coiled-coil domain of the NUDE/RO11 protein. *J. Cell Biol.* **150,** 681–8 (2000).

45. Liang, Y. *et al.* Nudel modulates kinetochore association and function of cytoplasmic dynein in M phase. *Mol. Biol. Cell* **18,** 2656–66 (2007).
46. Hebbar, S. *et al.* Lis1 and Ndel1 influence the timing of nuclear envelope breakdown in neural stem cells. *J. Cell Biol.* **182,** 1063–71 (2008).
47. Stehman, S. A., Chen, Y., McKenney, R. J. & Vallee, R. B. NudE and NudEL are required for mitotic progression and are involved in dynein recruitment to kinetochores. *J. Cell Biol.* **178,** 583–94 (2007).
48. Niethammer, M. *et al.* NUDEL is a novel Cdk5 substrate that associates with LIS1 and cytoplasmic dynein. *Neuron* **28,** 697–711 (2000).
49. McKenney, R. J., Vershinin, M., Kunwar, A., Vallee, R. B. & Gross, S. P. LIS1 and NudE induce a persistent dynein force-producing state. *Cell* **141,** 304–14 (2010).
50. McKenney, R. J., Weil, S. J., Scherer, J. & Vallee, R. B. Mutually exclusive cytoplasmic dynein regulation by NudE-Lis1 and dynactin. *J. Biol. Chem.* **286,** 39615–22 (2011).
51. King, S. J., Brown, C. L., Maier, K. C., Quintyne, N. J. & Schroer, T. A. Analysis of the dynein-dynactin interaction in vitro and in vivo. *Mol. Biol. Cell* **14,** 5089–97 (2003).
52. Echeverri, C. J., Paschal, B. M., Vaughan, K. T. & Vallee, R. B. Molecular characterization of the 50-kD subunit of dynactin reveals function for the complex in chromosome alignment and spindle organization during mitosis. *J. Cell Biol.* **132,** 617–33 (1996).
53. Schroer, T. A. Dynactin. *Annu. Rev. Cell Dev. Biol.* **20,** 759–79 (2004).
54. King, S. J. & Schroer, T. A. Dynactin increases the processivity of the cytoplasmic dynein motor. *Nat. Cell Biol.* **2,** 20–4 (2000).
55. Quintyne, N. J. & Schroer, T. A. Distinct cell cycle-dependent roles for dynactin and dynein at centrosomes. *J. Cell Biol.* **159,** 245–54 (2002).
56. Raaijmakers, J. A., Tanenbaum, M. E. & Medema, R. H. Systematic dissection of dynein regulators in mitosis. *J. Cell Biol.* **201,** 201–15 (2013).
57. Holzbaur, E. L. *et al.* Homology of a 150K cytoplasmic dynein-associated polypeptide with the *Drosophila* gene *Glued*. *Nature* **351,** 579–83 (1991).
58. Holleran, E. A. *et al.* beta III spectrin binds to the Arp1 subunit of dynactin. *J. Biol. Chem.* **276,** 36598–605 (2001).
59. Yeh, T.-Y., Quintyne, N. J., Scipioni, B. R., Eckley, D. M. & Schroer, T. A. Dynactin's pointed-end complex is a cargo-targeting module. *Mol. Biol. Cell* **23,** 3827–37 (2012).

60. Eckley, D. M. *et al.* Analysis of dynactin subcomplexes reveals a novel actin-related protein associated with the arp1 minifilament pointed end. *J. Cell Biol.* **147,** 307–20 (1999).
61. Gassmann, R. *et al.* Removal of Spindly from microtubule- attached kinetochores controls spindle checkpoint silencing in human cells. 957–971 (2010). doi:10.1101/gad.1886810.The
62. Gassmann, R. *et al.* A new mechanism controlling kinetochore-microtubule interactions revealed by comparison of two dynein-targeting components: SPDL-1 and the Rod/Zwilch/Zw10 complex. *Genes Dev.* **22,** 2385–99 (2008).
63. Swan, A., Nguyen, T. & Suter, B. Drosophila Lissencephaly-1 functions with Bic-D and dynein in oocyte determination and nuclear positioning. *Nat. Cell Biol.* **1,** 444–9 (1999).
64. Hoogenraad, C. C. *et al.* Mammalian Golgi-associated Bicaudal-D2 functions in the dynein-dynactin pathway by interacting with these complexes. *EMBO J.* **20,** 4041–54 (2001).
65. Hoogenraad, C. C. *et al.* Bicaudal D induces selective dynein-mediated microtubule minus end-directed transport. *EMBO J.* **22,** 6004–15 (2003).
66. Aroian, R. V, Field, C., Pruliere, G., Kenyon, C. & Alberts, B. M. Isolation of actin-associated proteins from *Caenorhabditis elegans* oocytes and their localization in the early embryo. *EMBO J.* **16,** 1541–9 (1997).
67. Hyman, A. A. Centrosome movement in the early divisions of *Caenorhabditis elegans*: a cortical site determining centrosome position. *J. Cell Biol.* **109,** 1185–93 (1989).
68. Frøkjaer-Jensen, C. *et al.* Single-copy insertion of transgenes in *Caenorhabditis elegans. Nat. Genet.* **40,** 1375–83 (2008).
69. O'Connell, K. F. The centrosome of the early *C. elegans* embryo: inheritance, assembly, replication, and developmental roles. *Curr. Top. Dev. Biol.* **49,** 365–84 (2000).
70. Brenner, S. The genetics of *Caenorhabditis elegans*. *Genetics* **77,** 71–94 (1974).
71. Maintenance of *C. elegans.* at <http://www.wormbook.org/chapters/www_strainmaintain/strainmaintain.html#bib2>
72. Gibson, D. G. *et al.* Enzymatic assembly of DNA molecules up to several hundred kilobases. **6,** 12–16 (2009).
73. WormBook. at <http://www.wormbook.org/>

74. Kurreck, J. Methods in Molecular Biology Vol. 265: RNA Interference, Editing, and Modification. Edited by Jonatha M. Gott. *ChemBioChem* **5,** 1719–1720 (2004).
75. Cumming, G., Fidler, F. & Vaux, D. L. Error bars in experimental biology. *J. Cell Biol.* **177,** 7–11 (2007).
76. Moyle, M. W. *et al.* A Bub1-Mad1 interaction targets the Mad1-Mad2 complex to unattached kinetochores to initiate the spindle checkpoint. *J. Cell Biol.* **204,** 647–57 (2014).
77. Frøkjaer-Jensen, C. *et al.* Single-copy insertion of transgenes in *Caenorhabditis elegans. Nat. Genet.* **40,** 1375–83 (2008).
78. Fridolfsson, H. N., Ly, N., Meyerzon, M. & Starr, D. A. UNC-83 coordinates kinesin-1 and dynein activities at the nuclear envelope during nuclear migration. *Dev. Biol.* **338,** 237–50 (2010).
79. Cockell, M. M., Baumer, K. & Gönczy, P. lis-1 is required for dynein-dependent cell division processes in *C. elegans* embryos. *J. Cell Sci.* **117,** 4571–82 (2004).
80. Fumoto, K., Hoogenraad, C. C. & Kikuchi, A. GSK-3beta-regulated interaction of BICD with dynein is involved in microtubule anchorage at centrosome. *EMBO J.* **25,** 5670–82 (2006).
81. Dickinson, D. J., Ward, J. D., Reiner, D. J. & Goldstein, B. Engineering the *Caenorhabditis elegans* genome using Cas9-triggered homologous recombination. **10,** (2013).
82. Vergnolle, M. A. S. & Taylor, S. S. Cenp-F links kinetochores to Ndel1/Nde1/Lis1/dynein microtubule motor complexes. *Curr. Biol.* **17,** 1173–9 (2007).
83. Wang, S., Ketcham, S. A., Schön, A., Goodman, B. & Wang, Y. Nudel / NudE and Lis1 promote dynein and dynactin interaction in the context of spindle morphogenesis. (2013). doi:10.1091/mbc.E13-05-0283
84. Sharp, D. J., Rogers, G. C. & Scholey, J. M. Microtubule motors in mitosis. *Nature* **407,** 41–7 (2000).
85. Musacchio, A. & Hardwick, K. G. The spindle checkpoint: structural insights into dynamic signalling. *Nat. Rev. Mol. Cell Biol.* **3,** 731–41 (2002).
86. Cell division; Worm Book. at <http://www.wormbook.org/chapters/www_celldivision/celldivision.html>
87. Kardon, J. R. & Vale, R. D. Regulators of the cytoplasmic dynein motor. *Nat. Rev. Mol. Cell Biol.* **10,** 854–65 (2009).
88. http://aricsgeneticsstudyguide.weebly.com/cell-cycle-and-mitosis.html

# ANNEX

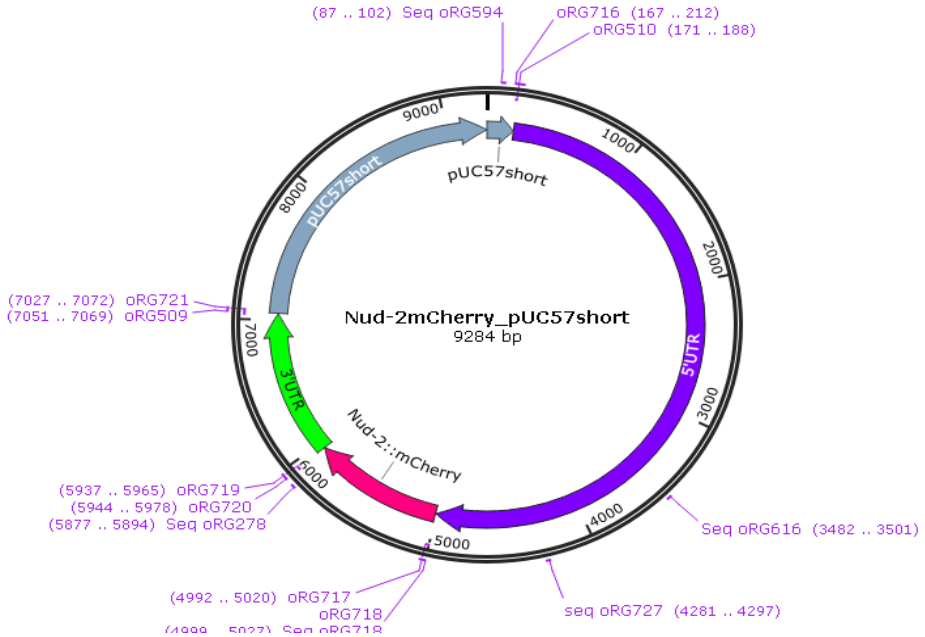


**Figure 1:** Digital circular map of the NUD-2::mCherry construct. In purple the 5' UTR, followed by pink NUD-2::mCherry, green 3'UTR and blue pUC57 short. The location of each primer listed in table 2 and 3 is also visible. Primers used to sequence are here defined as Seq oRG"X".

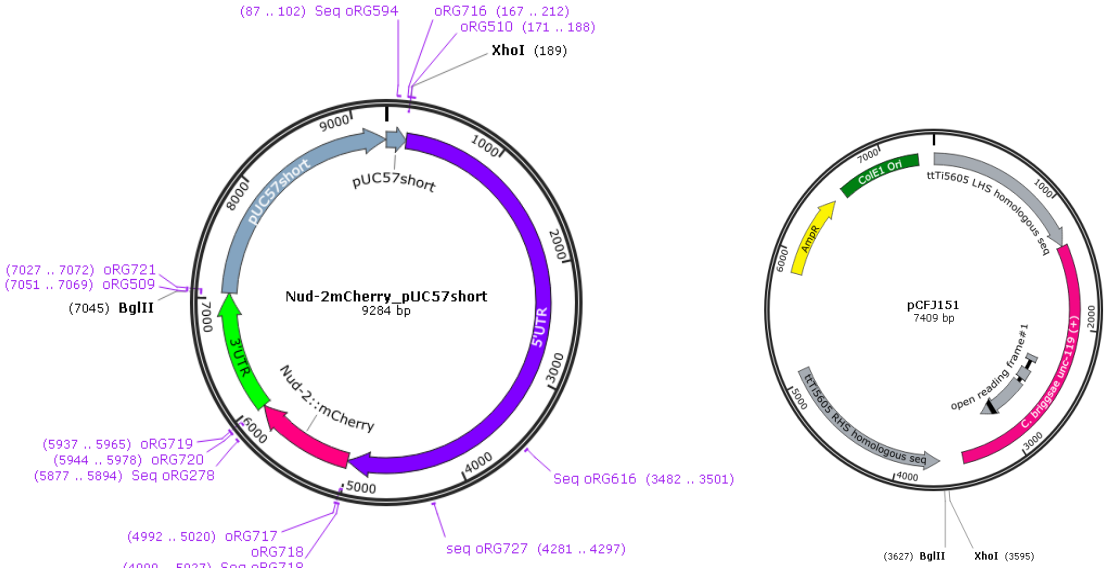


**Figure 2 and Figure 3**: Circular maps of both the cloning vector and the final vector for MosSCI integration on chromosome 2 are displayed, as well as the enzyme restriction sites for XhoI and BglII. These enzymes were required to transfer the NUD-2::mCherry construct into the pCFJ151 vector. Some characteristics of the final vector are also

visible such as homologous sequences for homologous recombination of the Mos Transposase, in gray, and *C. briggsae* unc-*119* (+) gene, that is a positive marker for successful integration.

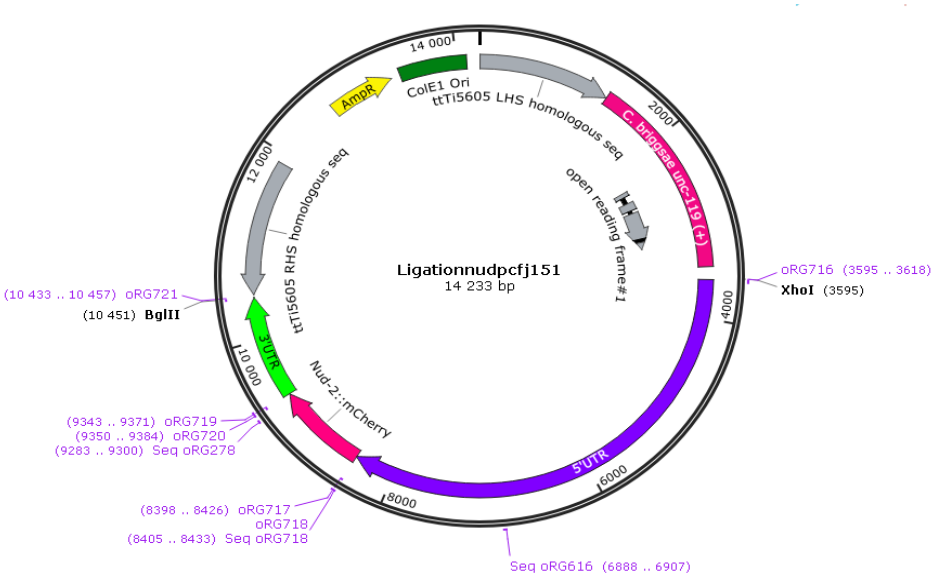


**Figure 4** Circular map of the construct NUD-2::mCherry in the final vector, after ligation, and in the final vector pCFJ151.